1998

Surface structures of Al-Pd-Mn and Al-Cu-Fe icosahedral quasicrystals

Zhouxin Shen
Iowa State University

INFORMATION TO USERS

This manuscript has been reproduced from the microfilm master. UMI films the text directly from the original or copy submitted. Thus, some thesis and dissertation copies are in typewriter face, while others may be from any type of computer printer.

The quality of this reproduction is dependent upon the quality of the copy submitted. Broken or indistinct print, colored or poor quality illustrations and photographs, print bleedthrough, substandard margins, and improper alignment can adversely affect reproduction.

In the unlikely event that the author did not send UMI a complete manuscript and there are missing pages, these will be noted. Also, if unauthorized copyright material had to be removed, a note will indicate the deletion.

Oversize materials (e.g., maps, drawings, charts) are reproduced by sectioning the original, beginning at the upper left-hand corner and continuing from left to right in equal sections with small overlaps. Each original is also photographed in one exposure and is included in reduced form at the back of the book.

Photographs included in the original manuscript have been reproduced xerographically in this copy. Higher quality 6" x 9" black and white photographic prints are available for any photographs or illustrations appearing in this copy for an additional charge. Contact UMI directly to order.

UMI

A Bell & Howell Information Company
300 North Zeeb Road, Ann Arbor MI 48106-1346 USA
313/761-4700 800/521-0600

Surface structures of Al-Pd-Mn and Al-Cu-Fe icosahedral quasicrystals

by

Zhouxin Shen

A dissertation submitted to the graduate faculty

in partial fulfillment of the requirements for the degree of

DOCTOR OF PHILOSOPHY

Major: Physical Chemistry

Major Professor: Patricia A. Thiel

Iowa State University

Ames, Iowa

1998

Graduate College

Iowa State University

This is to certify that the Doctoral dissertation of

Zhouxin Shen

has met the dissertation requirements of Iowa State University

Signature was redacted for privacy.

Major Professor

Signature was redacted for privacy.

For the Major Program

Signature was redacted for privacy.

For the Graduate College

TABLE OF CONTENTS

GENERAL INTRODUCTION

Quasicrystals were discovered in 1982 by Shechtman [1,2] and his coworkers. After the first discovery of Al_6Mn icosahedral quasicrystal [1], hundreds of new alloys have been observed to form quasicrystalline phases. Now it is clear that quasicrystals are not at all a rarity but in fact are quite common. Quasicrystals are typically binary and ternary metallic alloys and most of them are Al rich alloys. Quasicrystals can be classified into different categories according to different properties such as stability (metastable and stable), symmetry (icosahedral, decagonal) etc.

The discovery of quasicrystals created quite a lot controversy mainly because of their forbidden rotational symmetry according to conventional crystallography. Quasicrystals are structures with long-range aperiodic order and crystallographically forbidden rotational symmetries (e.g., fivefold, eightfold, tenfold, and 12-fold rotation axes). These alloys have nearly perfect long-range structure order, which becomes apparent as sharp diffraction patterns, with the absence of translational symmetry in their structures. The International Union of Crystallography has recently broadened the definition of "crystals" to "any solid having essentially discrete diffraction diagrams." [3] In this sense, quasicrystals could be referred to simply as "crystals". However, the term "quasicrystal" is still used to serve a useful function in distinguishing these unusual materials from the conventional periodic crystals.

Although enormous efforts have been made to determine the atomic structure of quasicrystals, no universally-accepted exact structure of a quasicrystal has been determined

yet. One of the most popular structural models of the icosahedral Al-Pd-Mn quasicrystal was proposed by Janot and Boudard. [4,5]. The basic structural unit of the model is a pseudo-Mackay icosahedron (PMI). The PMI consists of three centrosymmetric shells of atoms, with a total of 51 atoms, and with an overall diameter about 10Å. These PMI pack into large, self-similar icosahedra, and so on. Chemical bonds are strong within the PMI, and intercluster bonds are weaker.

Another interesting factor about quasicrystals is that many of their physical properties are quite unusual by the standards of common metals. Quasicrystals are very hard materials compared to normal metals. For example, the Vickers' hardness of icosahedral (i)- Al-Cu-Fe is 800-1000 [6,7], which is comparable to the hardness of silica (750-1200) [8] and much harder than its individual components (70-200 for low-carbon steel, 40-105 for copper, and 25-45 for aluminum [8]). The quasicrystal also exhibits a low coefficient of friction and it has relative "non-stick" character. [9,10] These properties lead naturally to speculation that quasicrystals may be useful in abrasive environments such as engines where hardness and low friction are needed.

Although metallic, quasicrystals are poor thermal and electrical conductors. For example, the thermal conductivity of i-Al-Cu-Fe is about two magnitudes lower than its individual components and is comparable to yttria-doped zirconia. [6] This makes quasicrystal a potential candidate for thermal barrier materials. There are other potential applications of quasicrystals including sensors, cookware, and hydrogen storage. [6,9,11-15]

Some of the above interesting and useful properties of quasicrystals, such as low friction coefficient and low surface energy, involve surface phenomena. This motivates fundamental studies of structure, composition, and chemical reactivity of their surfaces.

Although quasicrystals were discovered 16 years ago and many bulk properties of quasicrystals have been studied and understood, the surface science of quasicrystals is still a completely new field. There are some very basic issues about quasicrystal surfaces that have yet to be resolved, such as the very nature of the surfaces themselves and the effects of various surface preparation techniques. With the availability of large single grains of quasicrystalline alloys, such as the icosahedral phase of Al-Pd-Mn, the study of surface structures and chemistry by techniques such as scanning tunneling microscopy (STM) [16-20], low-energy electron diffraction (LEED) [18,21-24] and x-ray photoelectron spectroscopy (XPS) [25,26] has become one of the most active areas in quasicrystal research over the past 3-4 years. A basic understanding of the intrinsic surface structure and composition of quasicrystalline alloys can be gained from such work.

The structure of clean crystalline surfaces is commonly discussed in terms of the terrace-step-kink (TSK) model, in which atomically flat, low-Miller-index terraces are separated by steps with kinks. Many STM studies have revealed TSK features on crystalline surfaces. STM studies on decagonal Al-Co-Cu [16] and icosahedral Al-Pd-Mn [17] also revealed TSK-type features. Both studies suggested that quasi-periodicity was retained at the surfaces and that the surfaces consisted of rather flat terraces separated by crooked steps. Dynamical LEED analysis [23] of i-Al-Pd-Mn fivefold surface has shown that the surface consists of a mixture of closely similar, relaxed, bulklike terminations (terraces).

However different surface preparation methods may result in totally different surface structure and morphology of quasicrystals. In the above STM and LEED experiments, surfaces were prepared by sputtering and annealing in ultrahigh vacuum. Surface compositions can be shifted from bulk values during both processes. For the example of i-Al-Pd-Mn, the surface becomes Pd rich and Al depleted during Ar^+ sputtering due to the mass difference of Al and Pd atoms. Annealing at proper temperature will restore the surface composition close to bulk value. But if the annealing temperature is too high (above 1000K), preferential evaporation of Mn and Al will begin to happen and result in a Pd rich surface again [31]. The alternative route of cleaving in-situ has also been investigated by STM [20]. The cleaved surface is significantly rougher than the sputter-annealed surface and does not show TSK features. Cleaving in-situ will retain the surface composition to the bulk value and produce clean surfaces. But the effect of cleaving to the surface structure is still unknown, even for simple metals. Both STM studies have been interpreted in terms of fundamental concepts of bulk quasicrystalline structure proposed by Janot and Boudard [4,5].

In this dissertation, we report on the surface structure of i-Al-Pd-Mn twofold, threefold, fivefold and i-Al-Cu-Fe fivefold surfaces. Our LEED studies indicate the existence of two distinct stages in the regrowth of all four surfaces after Ar^+ sputtering. In the first stage, upon annealing at relatively low temperature: 500K-800K (depending on different surfaces), a cubic phase appears. The cubic LEED patterns transform irreversibly to unreconstructed quasicrystalline patterns upon annealing to higher temperatures, indicating that the cubic overlayers are metastable. Based upon the data for three chemically-identical, but symmetrically-inequivalent surfaces, a model is developed for the relation between the cubic overlayers and the quasicrystalline substrate. The model is based upon the related

symmetries of cubic close-packed and icosahedral-packed materials. These results may be general among Al-rich, icosahedral materials. STM study of Al-Pd-Mn fivefold surface shows that terrace-step-kink structures start to form on the surface after annealing above 700K. Large, atomic ally-flat terraces were formed after annealing at 900K. Fine structures with fivefold icosahedral symmetry were found on those terraces. Data analysis and comparison of our STM images and structure model of icosahedal Al-Pd-Mn [4,5] suggest that the fine structures in our STM images may be the pseudo Mackay (PMI) clusters which are the structure units of the structure model. Based upon our results, we can conclude that quasicrystalline structures are the stable structures of quasicrystal surfaces. In other words, quasicrystalline structures extend from the bulk to the surface. As a result of the effort reported in this dissertation, we believe that we have increased our understanding of the surface structure of icosahedral quasicrystals to a new level.

Dissertation Organization

Five papers are included in this dissertation. The first paper, "Structure and Stability of the Twofold Surface of Icosahedral Al-Pd-Mn by Low Energy Electron Diffraction and X-ray Photoemission Spectroscopy", appears in Volume 78 of Physical Review Letters on pages 1050-1053, 1997. The second paper, "The 5-Fold Surface of Quasicrystalline Al-Cu-Fe: Preparation and Characterization with LEED and AES", appears in Volume 385 of Surface Science on pages L923-L929, 1997. Paper III, "Crystalline surface Structures Induced by Ion Sputtering of Al-rich Icosahedral Quasicrystals", has been submitted to Physical Review B. Paper IV, "A comparison of the Three high-symmetry Surfaces of Al-Pd-Mn Quasicrystals", is going to be submitted to Surface Science. Paper V, "STM Study of

an Icosahedral Al-Pd-Mn quasicrystal Fivefold Surface", is going to be submitted to Physical Review Letters. General conclusions follow the last paper and references cited in this general introduction follow the appendix. The appendix documents a newly developed computerized Auger system.

STRUCTURE AND STABILITY OF THE TWOFOLD SURFACE OF ICOSAHEDRAL Al-Pd-Mn BY LEED AND XPS

A paper published in Physical Review Letters

Z. Shen, C.J. Jenks, J. Anderegg, D.W. Delaney, T.A. Lograsso, P.A. Thiel and A.I. Goldman

PACS numbers: 61.44 Br, 68.35 Bs, 61.14 Hg

Abstract

We have used Low-Energy Electron Diffraction (LEED) and X-ray Photoemission Spectroscopy (XPS) to investigate the structure of the twofold surface of icosahedral Al-Pd-Mn. The regrowth of the surface by annealing, after sputtering, took place in two distinct stages. The first stage was the appearance of a fine-grained surface phase with icosahedral, or near-icosahedral symmetry. For higher annealing temperatures (above 800K) a bulk terminated face-centered icosahedral (FCI) surface was observed. The composition of the unreconstructed FCI surface was identical to the bulk. The XPS measurements, correlated with LEED, were consistent with the hypothesis that the narrow Mn $2p_{3/2}$ peak, observed in previous studies of Al-Pd-Mn alloys, can be used as a signature of the icosahedral phase in the Al-Pd-Mn family of intermetallics.

With the availability of large single grains of quasicrystalline alloys, such as the icosahedral phase of Al-Pd-Mn, several experimental probes have been newly applied to the study of quasicrystalline structures. Over the past two years, the study of surface structures and chemistry by techniques such as scanning tunneling microscopy (STM)[1-3] low-energy electron diffraction (LEED)[4-7], and x-ray photoelectron spectroscopy [8,9] has emerged as one of the most active areas in quasicrystal research. The heightened interest in quasicrystalline surfaces has been motivated, in part, by reports of intriguing properties such as oxidation resistance[10-12], low surface friction [13,14], superior wear resistance and other attractive tribological characteristics[13]. All of these properties are ultimately related to the physics and chemistry of the surface on an atomic scale. Therefore, a basic understanding of the intrinsic surface structure of quasicrystalline alloys is prerequisite to understanding how these surfaces interact with their environment.

There are some very basic issues about quasicrystalline surfaces that have yet to be resolved or even addressed. The very nature of the surfaces themselves, as well as the effects of various surface preparation techniques, are the subject of debate. For example, STM measurements on a sample of Al-Pd-Mn prepared by sputtering and annealing in ultra-high vacuum have revealed well-defined relatively flat terraces with quasicrystalline order within the plane of the surface[2]. In contrast, STM measurements of surfaces of Al-Pd-Mn prepared by in-situ cleavage revealed significant atomic-scale roughness[3]. These latter measurements provide some support for a cluster-based approach to quasicrystalline structure advocated by several groups in recent years [15], and have raised concerns regarding the effects of ion bombardment and high temperature annealing upon the surface since selective evaporation and sputtering can significantly change the surface stoichiometry. Indeed, as pointed out by Ebert et al., quasicrystalline phases are complex chemically ordered phases whose surface structure need not be the same as in the bulk [3].

In this letter, we directly address these issues through XPS and LEED measurements conducted on a sample of icosahedral Al-Pd-Mn oriented with a twofold axis perpendicular to the surface. After sputtering the surface with argon, no LEED pattern was observed and we found substantial depletion of the aluminum at the surface. After annealing the sample at temperatures above 800K, a well-ordered, bulk terminated quasicrystalline surface with the same composition as the bulk was recovered. At intermediate annealing temperatures, however, the surface is best characterized as a fine-grained, disordered structure that is either quasicrystalline or a crystalline approximant of the icosahedral phase. We also found that XPS measurements of the width of the Mn $2p_{3/2}$ peak can provide a good indication of the presence of the face-centered icosahedral (FCI) phase at the surface, as proposed in previous work [9].

The LEED experiments were performed in a stainless-steel ultrahigh vacuum chamber (base pressure < 3×10^{-11} Torr) also equipped with provisions for Auger Electron Spectroscopy (AES), ion sputtering and annealing. Supporting measurements by X-ray Photoemission Spectroscopy (XPS) were performed in a second chamber under the same conditions as the measurements described below, albeit at a higher base pressure (upper limit 4×10^{-10} Torr).

Our sample, a flat wafer approximately 12 mm x 15 mm x 2 mm in size, was cut from a single grain of a boule, grown via the Bridgman method[16] using a starting composition of $Al_{72}Pd_{19.5}Mn_{8.5}$, and oriented by the x-ray Laue technique so that a two-fold axis was normal ($\pm 0.2^{o}$) to the surface. Inductively-coupled plasma atomic-emission spectroscopy (ICP-AES) analysis of a small piece adjacent to our sample indicated a bulk composition of $Al_{71}Pd_{19.8}Mn_{9.2}$. The phase purity was verified by scanning electron and Auger microscopies to within 0.5%. For further details regarding our methods of quasicrystalline sample preparation, we refer the reader to reference 17.

After polishing and characterization, the sample was fixed onto a thin Ta plate (20 mm x 25 mm) using two Ta strips. The sample could be resistively heated and liquid-nitrogen cooled via the Ta plate. A thermocouple (W-5%Re/W-26%Re) was spot-welded on the

tantalum plate for real-time control of the sample temperature. To confirm the sample temperature measured by the thermocouple, an infrared thermometer (IR-gun) was also used. The difference between the IR-gun reading of the sample temperature and thermocouple reading was less than 20K. After initial cleaning cycles by ion bombardment and annealing, LEED data at several temperature steps were taken after sputtering for 40 minutes at room temperature and annealing at the desired temperature for 2 - 4 hours. Unless indicated otherwise, all of the LEED data was collected at temperatures at or below 120K.

After sputtering, but prior to annealing at temperatures above 600K, no LEED pattern from the twofold surface was observed. Furthermore, AES measurements indicated that the surface composition was $Al_{62\pm4}Pd_{32\pm3}Mn_{6\pm1}$, well away from both the known stoichiometry for the FCI phase of Al-Pd-Mn and the composition of the bulk sample. The shift in composition upon sputtering is entirely consistent with expected losses of Al and Mn, relative to Pd, for Ar^+ sputtering. We also point out that the lineshape of the Mn $2p_{3/2}$ peak measured by XPS under these conditions was quite broad (see Fig. 1). This last point is notable since recent XPS measurements on clean, well-ordered, fivefold surfaces of Al-Pd-Mn suggest that the sharpness of the Mn peak may be used as an indicator of the presence of quasicrystalline order at the surface of the sample[9].

After re-sputtering the sample and annealing at approximately 600K, a LEED pattern exhibiting twofold symmetry (Figure 2) was observed. The diffraction spots, however, are quite broad and the pattern itself clearly does not correspond to the LEED pattern expected for a bulk terminated twofold FCI surface (see discussion below). The breadth of the peaks suggests that the in-plane domain size for this phase is on the order of approximately 30 Angstroms. Anticipating the discussion below, twofold, threefold and fivefold axes have been superimposed on the pattern and show that, at best, the structure may be characterized as a highly disordered and distorted icosahedral phase. We shall refer to this pattern as "rhombic" because rhombi are apparent in the LEED pattern at certain energies as shown in Fig. 2. The

surface composition after the 600K anneal was measured, by AES, to be $Al_{68\pm2}Pd_{27\pm2}Mn_{5\pm2}$, closer to, but still well away from the bulk composition. Furthermore, the lineshape of the Mn $2p_{3/2}$ peak, measured by XPS, under these conditions remained quite broad (Figure 1).

After sputtering and annealing at temperatures above 800K, the LEED pattern changed dramatically in several ways. First of all, as shown in Figure 3a (taken after a 900K anneal), the diffuse spots of Figure 2 were replaced by a new sharp LEED pattern, also with twofold symmetry, but in a rectangular rather than rhombic pattern. In addition, faceting of the surface was observed, especially close to the edges of the sample, at temperatures above 700K. The faceting is evidenced by Figure 4 which shows two new (0,0) spots in addition to the twofold (0,0) spot (normally positioned at the center of the screen but moved here by sample rotation). The LEED patterns associated with the new (0,0) beams have threefold and fivefold symmetry. We point out that the faceting observed here is consistent with a higher surface energy for the twofold surface relative to surfaces perpendicular to the three- and fivefold directions.

After annealing the sample at 900K the rectangular LEED pattern dominated the surface scattering except at the edges of the sample. AES measurements showed that the surface composition was $Al_{73\pm2}Pd_{19\pm2}Mn_{7\pm1}$, very close to the composition of the bulk. Furthermore, XPS measurements (Fig. 1) showed that the width of the Mn $2p_{3/2}$ peak narrowed considerably, consistent with the previous measurements mentioned above. All of these results suggest that the surface layer of the Al-Pd-Mn alloy has regrown to a bulk terminated structure.

In order to confirm that the rectangular pattern is indeed characteristic of an ordered FCI surface, a LEED pattern was calculated and is shown in Figure 3b [18]. To calculate the pattern we employed the bulk x-ray structure factors measured by Boudard et al. for Al-Pd-Mn [19] , and used these to assign a relative intensity to rods of scattering parallel to the surface normal. We point out, however, that we do not expect the relative intensities of the calculated

LEED spots to find very good agreement with experiment since this comparison has been made at a single LEED energy of 60 eV and, therefore, ignores structure in the surface rods. A proper comparison with experiment requires an energy-averaged LEED pattern. Nevertheless, the qualitative agreement between Figures 3a and 3b is quite gratifying.

For intermediate temperatures (between 700K and 900K), the LEED often exhibited a mixture of both the FCI rectangular and rhombic patterns. In order to more carefully study the transition between the two, we monitored the intensities and widths of diffraction spots of the rhombic and rectangular patterns as a function of temperature while heating the sample at a rate of 0.1K/sec. The results, shown in Figure 5, indicate that there was a rather abrupt transition from the rhombic to rectangular pattern at around 800K. This transition was irreversible based upon the observation that the data of Figure 5 are unchanged (except for variations ascribable to Debye -Waller effects) when the data were acquired at T≤120K after each annealing step, or were acquired at the annealing temperature directly. The width of the diffraction spots are at the resolution limit of the LEED apparatus, and correspond to an effective domain size (Figure 5) greater than 150 Angstroms.

Our study indicates the existence of two distinct stages in the regrowth of the twofold surface of icosahedral Al-Pd-Mn that are correlated with the sample composition as well as the lineshape of the Mn $2p_{3/2}$ peak measured by XPS. In the first stage, upon annealing the damaged surface between 600K and 700K, a nanocrystalline (or nanoquasicrystalline) phase appeared. The rhombic LEED pattern associated with this phase, while very different from the expected FCI pattern, was orientationally coherent with the underlying bulk quasicrystal as well as the FCI LEED pattern that appeared at higher temperatures. The pattern itself consists of diffuse spots, precluding a definitive identification of this phase as quasicrystalline as opposed to, say, a rational approximant of the icosahedral phase[20].

At annealing temperatures above 800K, a bulk-terminated FCI twofold surface was obtained, with evidence of faceting especially at the periphery of the sample. The composition

of the surface, within statistical error, was the same as the bulk. Furthermore, the width of the Mn $2p_{3/2}$ XPS peak returned to the anomalously narrow value reported in previous XPS measurements of icosahedral Al-Pd-Mn. This point is significant since it is consistent with the prior suggestion that the lineshape of the Mn $2p_{3/2}$ peak may be used as a fingerprint of the FCI phase within the Al-Pd-Mn family. Taken together, these results show that after a careful annealing cycle, high quality bulk-terminated twofold surfaces of icosahedral Al-Pd-Mn may be obtained. Further investigations of this surface by STM are planned to address directly the discrepancies observed in previous STM measurements of this material.

We are indebted to M. deBoissieu for providing the bulk x-ray structure factor data for our analysis. This work was supported by the Ames Laboratory, which is operated for the U.S. Department of Energy by Iowa State University under Contract No. W-7405-Eng-82.

REFERENCES

1. A.R. Kortan, R.S. Becker, F.A. Thiel and H.S. Chen, Phys. Rev. Lett **64**, 200 (1990).

2. T.M. Schaub, D.E. Burgler, H.-J. Gutherodt and J.-B. Suck, Phys. Rev. Lett. **73**. 1255 (1994).

3. Ph. Ebert, M. Feuerbacher, N. Tamura, M. Wollgarten and K. Urban, Phys. Rev. Lett., in press.

4. E.G. McRae, R.A. Malic, T.H. Lalonde, F.A. Thiel, H.S. Chen and A.R. Kortan, Phys. Rev. Lett. **65**, 883 (1990).

5. T.M. Schaub, D.E. Burgler, H.-J. Guntherodt and J.-B. Suck, Z. Phys. B**96**, 93 (1994).

6. S.-L. Chang, W.B. Chin, C.-M. Zhang, C.J. Jenks and P.A. Thiel, Surf. Sci. **337**, 135 (1995).

7. M. Gierer, M.A. Van Hove, A.I. Goldman, Z. Shen, S.-L. Chang, C.J. Jenks, C.-M. Zhang and P. A. Thiel, Phys. Rev. Lett., in press.

8. S.-L. Chang, W.B. Chin, C.-M. Zhang, C.J. Jenks and P.A. Thiel, Surf. Sci. **337**, 135 (1995).

9. C.J. Jenks, S.-L. Chang, J.W. Anderegg, P.A. Thiel and D.W. Lynch, Phys. Rev. B**54**, 6301 (1996).

10. S.-S. Kang and J.M. Dubois, J. Mater. Res. **10**, 1071 (1995).

11. J. M. Dubois, S.-S. Kang and Y. Massiani, J. Non-Cryst. Solids **153-154**, 443 (1993).

12. S.-L. Chang, J.W. Anderegg and P.A. Thiel, J. Non-Cryst. Solids **195**, 95 (1996).

13. S.-S. Kang, J.M. Dubois and J. von Stebut, J. Mater. Res. **8**, 2471 (1993).

14. J.M. Dubois, S.-S. Kang and A. Perrot, Mater. Sci Engr. **A179/A180**, 122 (1994).

15. C. Janot and M. deBoissieu, Phys. Rev. Lett. **72**, 1674 (1994).

16. D.W. Delaney, T.E. Bloomer and T.A. Lograsso in *New Horizons in Quasicrystals: Research and Applications*, in press.

17. C.J. Jenks, D.W. Delaney, T.E. Bloomer, S.-L. Chang, T.A. Lograsso, Z. Shen, C.-M. Zhang and P.A. Thiel, Appl. Surf. Sci., in press.

18. An interesting observation here is that the LEED pattern from the twofold surface differs considerably from the higher energy transmission electron microscopy (TEM) patterns taken along the twofold axis. The differences arise from both the lower energy (and hence larger curvature of the Ewald sphere) for the LEED measurements as well as the fact that 2D scattering is characterized by rods rather than points of intensity.

19. M. Boudard et al., J. Phys. Condens. Matter **4**, 10149 (1992).

20. A.I. Goldman and K.F. Kelton, Rev. Mod. Phys. **65**, 213 (1993).

FIGURE CAPTIONS

1. XPS profiles of the Mn $2p_{3/2}$ peak for samples that were a) sputtered and then annealed at b) 600K and c) 900K.

2. LEED pattern of the "rhombic" phase taken at an electron energy of 110 eV. The axes denoted in the figure correspond to the two-, three-, and fivefold directions in the twofold plane for an icosahedral quasicrystal.

3. a) LEED pattern of the "rectangular" phase taken at an electron energy of 70 eV; b) the calculated LEED pattern for an FCI surface as described in the text.

4. LEED pattern taken at the periphery of the sample showing evidence of faceting. Arrows denote the (0,0) beams for twofold surface as well as the three- and fivefold facet surfaces.

5. Temperature dependence of the LEED intensities and domain size for the "rhombic" (solid circles) and "rectangular" (open circles) patterns. The lines serve as a guide to the eye. A distinct transition from the rhombic to rectangular pattern is observed at approximately 800K.

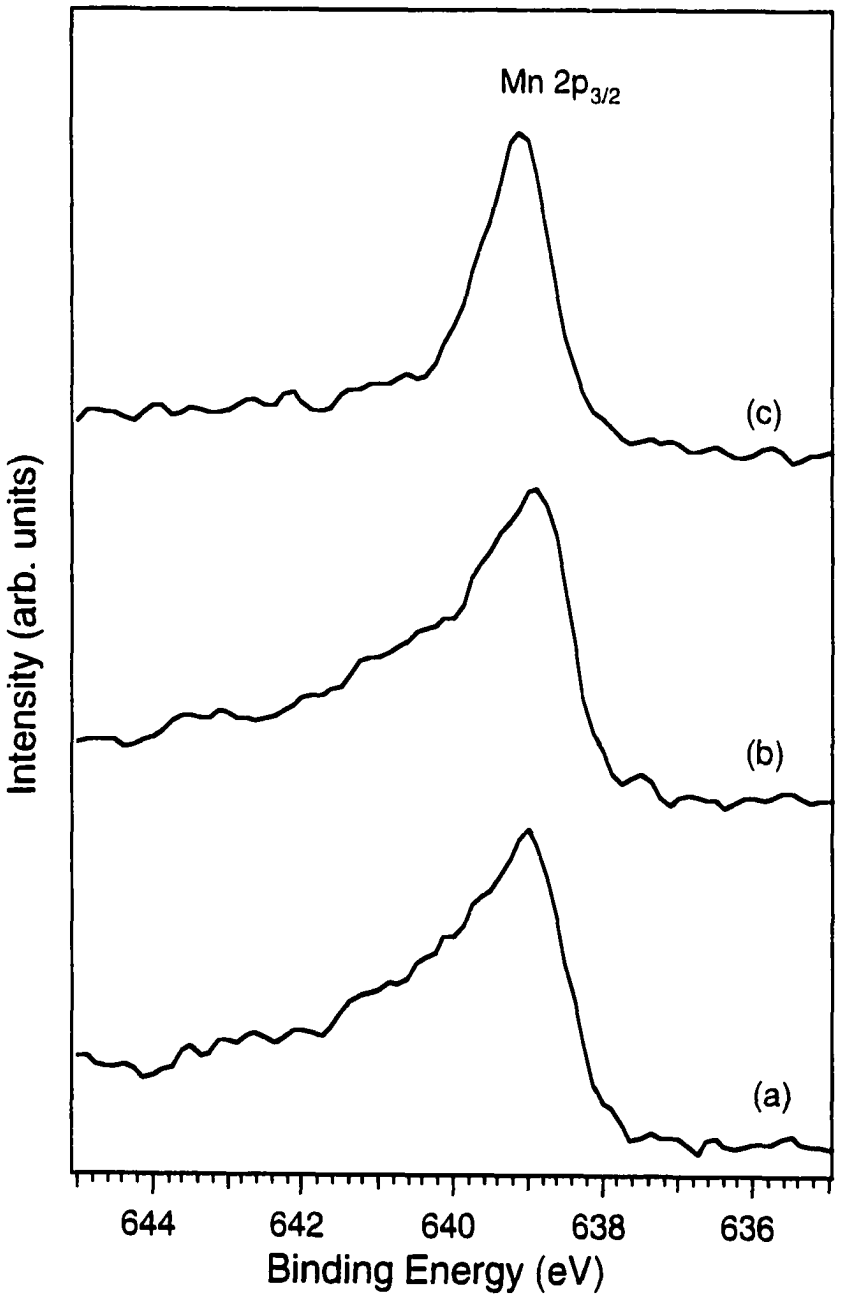
Mn 2p3/2
(c)
(b)
(a)
Intensity (arb. units)
644
642
640
638
636
Binding Energy (eV)

Fig. 1

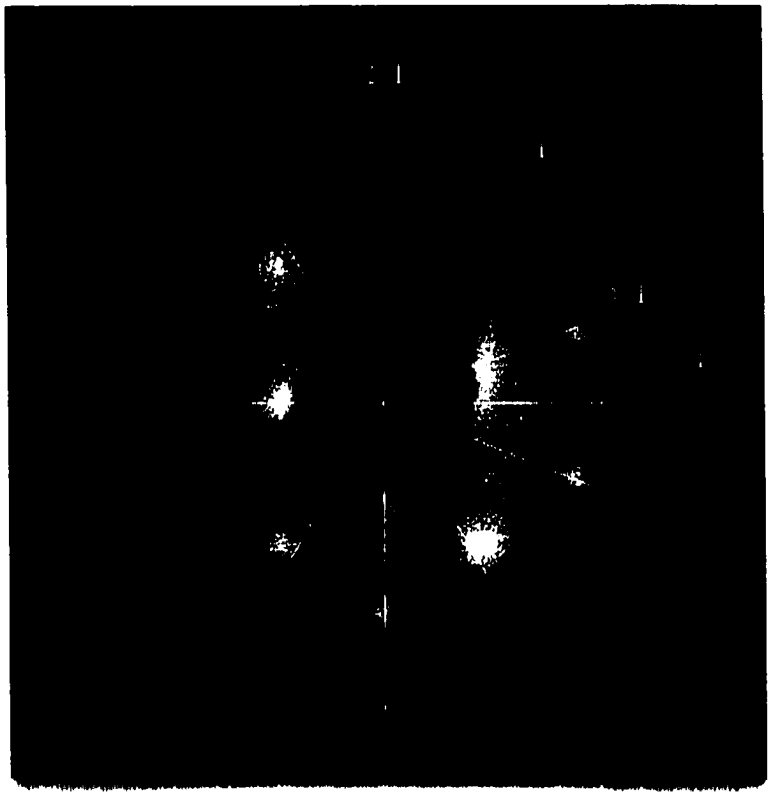

Fig. 2

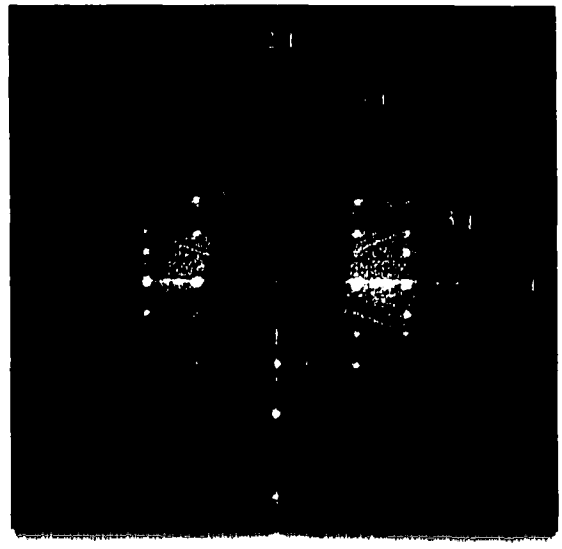

(a)

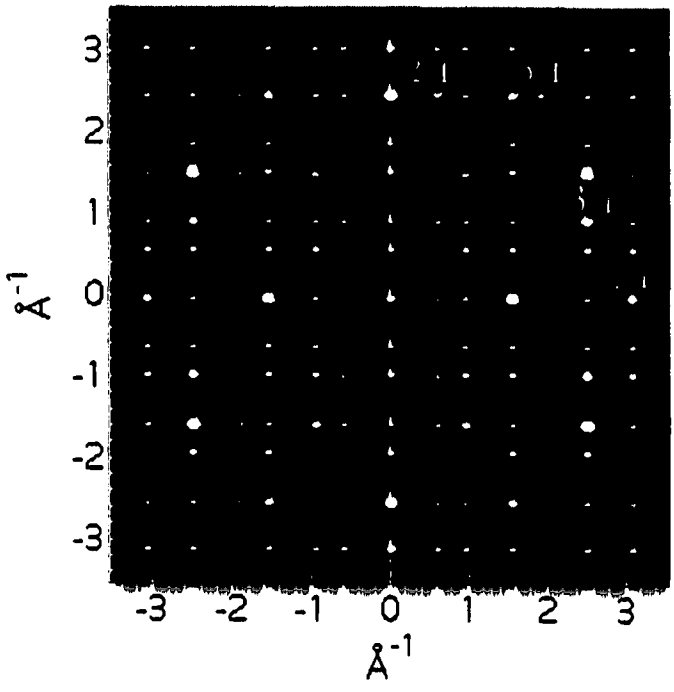

(b)

Fig. 3

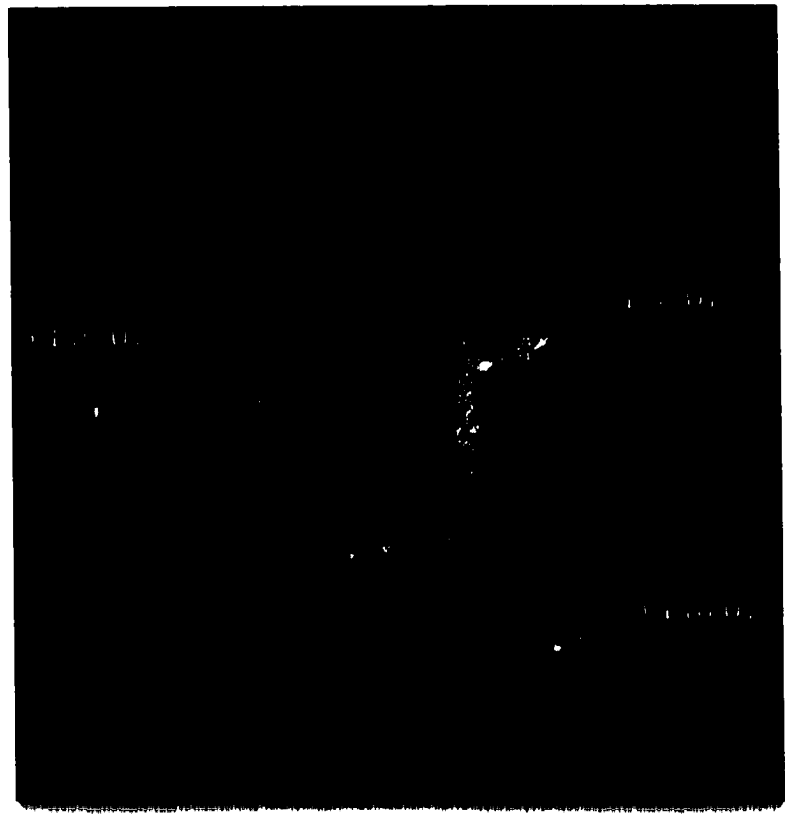

Fig. 4

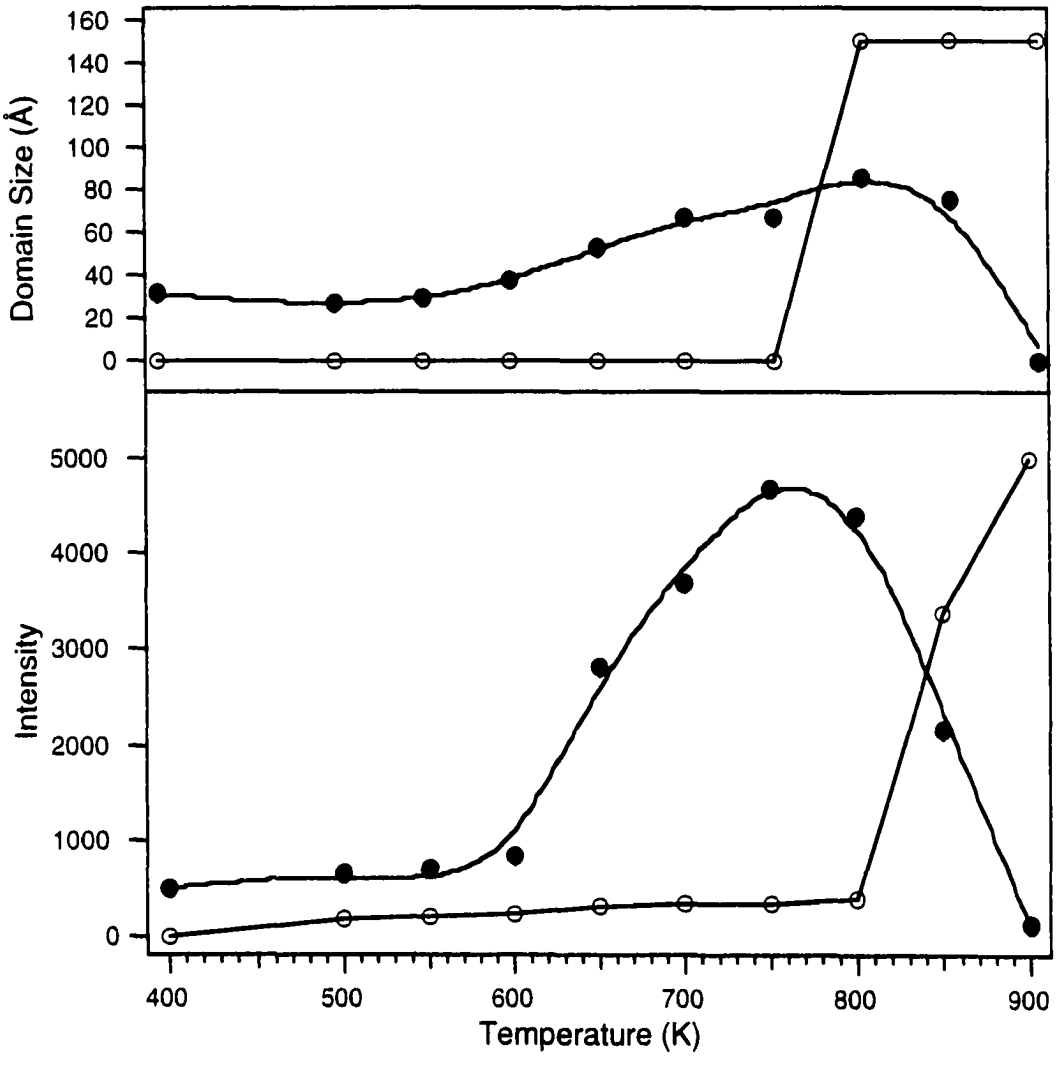
Domain Size (Å)
160
140
120
100
80
60
40
20
0
Intensity
5000
4000
3000
2000
1000
0
400
500
600
700
800
900
Temperature (K)

Fig. 5

THE 5-FOLD SURFACE OF QUASICRYSTALLINE ALCUFE: PREPARATION AND CHARACTERIZATION WITH LEED AND AES

A paper published in Surface Science Letters

Z. Shen, P. J. Pinhero, T. A. Lograsso,
D. W. Delaney, C. J. Jenks, and P. A. Thiel

SSL 97041L

Keywords: Low energy electron diffraction (LEED);
Aluminum; Alloys; Metallic surfaces.

Abstract. We report the first surface characterization of a large, single-grain sample of quasicrystalline AlCuFe. The sample is oriented with its surface perpendicular to a five-fold axis, and has bulk composition 63.4-24.0-12.6 atom %. Following our method of preparation, the surface yields an exceptionally sharp and rich five-fold pattern in low-energy electron diffraction. The spot spacings and symmetries are consistent with expectations for this surface, based upon the unreconstructed structure.

One of the impediments to studies of quasicrystals has been, and continues to be, the scarcity of good, large samples. This problem is particularly acute in surface science, where the demands on sample size often exceed those placed by bulk-probing measurements. The surface area must usually be no less than 2 mm x 2 mm to accommodate focussed electron and ion beams. Large single-grain [1] samples of one particular quasicrystal, icosahedral (or ψ–phase) AlCuFe, have been completely unavailable until a recent breakthrough by Lograsso and Delaney.[2] We have taken advantage of their recent progress to characterize this material using two of the conventional probes of surface science.

It is now generally accepted that quasicrystals, discovered in 1983 by Shechtman and

co-workers,[3] constitute a new class of solids, distinguished by being well-ordered but aperiodic.[4,5] Most of the hundred-odd known quasicrystals are aluminum-rich binary and ternary intermetallics. They are materials of great interest because, in addition to their intriguing physical nature, they show potentially-useful properties. These properties include certain mechanical and tribological characteristics, catalytic activity, low thermal and electrical conductivity, and high hydrogen storage capacity.[6] The mechanical and tribological properties have engendered particular interest in using quasicrystals as coatings. For coating applications, the alloy receiving most attention at present is icosahedral AlCuFe, because it is (among other things) an equilibrium phase, and is comprised of inexpensive, non-toxic metals. It is the relationship of surface phenomena to key properties which drives our interest in this material.

However, surface studies of single grains have been restricted until now to other aluminum-based alloys, notably icosahedral AlPdMn[7-24] and decagonal AlCuCo,[25-28] where sufficiently-large and perfect samples *have* been available--although still rare. Moving away from the single-grain domain, it should be noted that one surface study of a multi-grain sample of icosahedral AlCuFe has in fact been reported, focussing on the material's oxidation resistance.[29] While they can be very enlightening and useful, studies of such samples (which are analogous to polycrystalline samples) cannot exploit the surface-sensitive, diffraction-based techniques, and cannot explore the variation of surface properties with quasicrystallographic surface orientation.

In this paper, we first report some details of our preparation and characterization of the AlCuFe single grain samples. We then present data from Auger electron spectroscopy (AES) which pertain to surface composition, and data from low-energy electron diffraction (LEED) which pertain to surface structure. Our work opens the door to other surface studies of this commercially-relevant material in single-grain form.

Our approach to preparing, screening, and handling icosahedral AlCuFe samples for/in

ultrahigh vacuum (UHV) surface studies is very similar to that described previously for icosahedral AlPdMn.[16] The main issues of concern are the single-grain nature, porosity, and phase purity of the sample, plus the quality of the surface diffraction pattern and surface composition. The first three factors must be examined and controlled outside of the experimental UHV chamber. The last two can be examined and optimized in situ.

The phase equilibrium of icosahedral AlCuFe is such that conventional crystal growth techniques like the Bridgman or Czochralski methods are not successful in preparing large grains. The ψ phase of the AlCuFe alloy does not form directly from the liquid but is the product of a peritectic solidification reaction at » 1130 K between two high temperature crystalline phases (β and λ) and liquid, L: $L + \beta\,(FeCuAl) + \lambda(Al_{13}Fe_4) \rightarrow \psi$.[30,31] The ψ phase is centered at a composition of approximately $Al_{63}Cu_{25}Fe_{12}$ and is thermodynamically stable from its melting point, around 1135 K, down to approximately 875 K. The ψ phase shows a limited range of solubility of several atomic % Cu and Fe between 975 and 1075 K.[30] The solubility range must necessarily decrease with increasing temperature from 1075 K up to its melting point, where a singular composition is required for the four phase equilibrium. Below 875 K, the ψ phase decomposes to crystalline components. This lower temperature decomposition may be avoided at ordinary cooling rates and the ψ phase easily retained down to room temperature due to sluggish kinetics of transformation.[30]

The single grains studied in the present paper were grown by a cyclic heat treatment method described in detail elsewhere.[2] As a result of this treatment, several grains exhibiting five-fold faceting and up to 0.3 cm^3 in size were harvested from a single ingot. Chemical analysis of two spots on one of the grains, and from two points in the boule adjacent to where the grains were harvested, by inductively-coupled plasma atomic-emission spectroscopy (ICP-AES), indicated a slight shift from the starting composition to $Al_{63.4\pm0.4}Cu_{24.0\pm0.9}Fe_{12.6\pm0.5}$. (The uncertainties encompass a 95% confidence limit.)

Optical examination of the grains indicated the existence of a minor quantity (on the order of 5-10 %) of a second phase and porosity in the as-grown state. The second phase was identified as β–AlCuFe (a cubic CsCl phase) by energy dispersive x-ray analysis.

Post-growth solution annealing at a lower temperature than crystal growth (1075 K) for four hours, followed by water quenching, completely dissolved the second phase into the icosahedral matrix, yielding a single phase quasicrystal grain. The single phase nature of one of these grains was verified both by scanning electron microscopy and scanning Auger microscopy to within 0.5 at% by volume. This post-growth annealing apparently circumvents the low solubility range at growth temperatures, and hence is successful in removing the secondary phase.

Unfortunately, the solution annealing treatment had no effect on the porosity in the single grain. On one sample from the ingot, the pores constituted about 2.5% of the total surface area, as determined with scanning electron microscopy. The pores were typically circular. The size distribution appeared to be qualitatively bimodal, with one set averaging 86μm in diameter and a more populous set in the range of 5-10μ diameters. Pores as large as 300μm were occasionally seen but were highly asymmetric (300μm being the largest linear dimension), suggesting a clumping of the individual ~80μm features. We expect pores of this size to have no effect whatsoever on the LEED pattern, although such porosity may be an obstacle to some other types of surface experiments (e.g. temperature-programmed desorption).

Our subsequent experiments were performed on two samples, each originating from a different grain. One, used for the AES and LEED experiments, was a nearly-rectangular slice, approximately 6 x 4 mm in surface area, and 1.6 mm thick. The other was used to check phase purity and porosity (described above). This second sample was a pentagonal wafer, 2.2 mm thick and 6.1 mm from edge to vertex. Both samples were oriented and polished to within 0.2° of a five-fold orientation, based on Laue x-ray diffraction.

For the LEED and AES experiments, the sample was mounted and the temperature measured in a fashion similar to that for icosahedral AlPdMn.[16] The UHV chamber in which the LEED and AES experiments were performed had a consistent base pressure of 3 to 4 x 10^{-11} Torr. The sample was treated initially to remove residual impurities (carbon and oxygen) with cycles of ion bombardment at room temperature (15 minutes, 1.0 keV Ar^+, 15 μA current from the sample to ground with no bias voltage) and annealing (15 minutes). Annealing began at 400 K, and went up in 50 K increments whenever annealing at a given temperature no longer revealed significant surface segregation of carbon or oxygen. The maximum temperature to which the sample was heated in this fashion was 850 K.

It is germane to explain why we chose 850 K as an upper limit for thermal treatment of this sample in UHV. Several studies of metastable bulk ψ-phase samples have shown that, at 800 to 1025 K, they transform to a crystalline phase, and then, at still higher temperature, back to the ψ–phase.[32-36] Clearly, the need to avoid transforming the icosahedral bulk into a crystalline phase sets an upper bound on the temperature which can be used. Some support for our choice is provided by the fact that the sequence of LEED patterns described below was generated many times over, implying that the bulk structure did not transform irreversibly during the course of many bombardment-annealing cycles. However, the exact conditions under which samples transform in these experiments is an issue of ongoing investigation in our group.

The surface composition was monitored with AES (3 keV, 1.8 μA current from sample to ground without bias). A spectrum of the clean surface is shown in Fig. 1. For analyzing trends in composition, we employed the Al, Cu, and Fe transitions at 1396, 920, and 703 eV, respectively. This approach showed that sputtering at room temperature with Ar^+ served to deplete the Al and enrich the Fe. Preferential sputtering of Al has been reported previously for poly-grain AlCuFe by Rouxel et al.,[29] and for single-grain AlPdMn by other groups.[10,13,17] Prolonged annealing (30-150 minutes at temperature) served to reverse the

changes induced by sputtering. A plateau in composition was reached upon annealing at 700-800 K. By analogy to AlPdMn, we expect that annealing at higher temperature would result, eventually, in compositional changes due to preferential evaporation, although higher temperatures were avoided for the reasons presented above.[16]

Ion bombardment with Ar^+ and annealing in UHV yielded two striking LEED patterns. One was obtained reproducibly upon annealing at temperatures between 500 and 750 K, for periods of 30 to 150 minutes; under most conditions, it had a superficial ten-fold symmetry, and we refer to this as the pseudo-ten-fold pattern. This pattern, shown in Fig. 2a, actually consists of five rotational domains of two-fold symmetry.[37] The interpretation of the pseudo-ten-fold pattern, and details of its transition to five-fold symmetry, are given elsewhere.[37]

In this paper, we concentrate mainly on the second LEED pattern, which was much sharper and denser. Photographs of the second pattern, taken at 6 different incident electron energies, are shown in Fig. 2b-g. This pattern was obtained after annealing at temperatures between 750 and 850 K, for periods of 30 to 120 minutes. The LEED patterns were measured with standard, front-view Varian™ optics (nominal instrumental limit 100-300 Å) , and with beam currents of 3.1 μA or less. The photographs of Fig. 2 show that the patterns were exceptionally dense. Furthermore, the spots of the five-fold pattern were very sharp, with widths corresponding to a real-space dimension of ca. 180 Å. (We have observed a similar sharpness also in a previous study of a different quasicrystalline surface.[24]) These values of the spot widths are (almost certainly) limited by the LEED optics; hence, this system makes an interesting candidate for further investigation with a higher-quality instrument.

The diffraction patterns of Fig. 2b-g displayed true five-fold symmetry. Visual inspection showed that the major spots consisted of sets of ten, all equidistant from the specular beam. At some energies these ten could appear about equally bright, as in Fig. 2b, but at other energies this symmetry was broken, as in Fig. 2c. These visual observations were

corroborated quantitatively by measurements of the LEED spot intensities vs. incident beam energies, the so-called I(E) curves, at normal incidence. The I(E) curves revealed quantitatively that each set of ten spots consisted of two sets of five symmetry-equivalent beams, the same as for the LEED pattern of the five-fold surface of icosahedral AlPdMn.[13,23] This symmetry is illustrated in Fig. 3.

The five-fold pattern probably represents the unreconstructed five-fold surface of this icosahedral material.[38] Both the symmetry and spacing of the diffraction features of Fig. 3 support this assignment. Schaub et al. have shown why the symmetry can be five-fold (rather than ten-fold) for a surface of an icosahedral material in the LEED experiment.[11] They have also analyzed the expected relative spacings of the major spots.[10] Their analysis shows that the radii of consecutive rings of major spots, normalized to the smallest such radius (as defined in Fig. 3) should equal the golden mean, τ (τ = 1.618), raised to integral powers:

$$\frac{r_j}{r_0} = \tau^j$$

The extent to which this relation is obeyed is shown by comparing the bottom two rows of Table 1. The agreement between measured and predicted values is excellent. In addition to the statistical uncertainties given in the third and fourth rows, there may be a systematic deviation from the ideal values if the sample is not exactly at the focal point of the LEED optics, which would result in some distortion of the pattern. One would expect that such an inaccuracy should affect ratios of distances less than absolute values of distances determined from LEED; hence, we do not attempt to extract absolute values from the LEED data, other than to note that the average value of r_0 listed in Table 1 is about 10% larger than one would expect from the bulk structure model.[39]

Finally, we note that the ion-bombardment and annealing procedure described here for

AlCuFe may well result in a different atomic-scale morphology than would be obtained by cleavage. [20] Indeed, STM studies of cleaved AlPdMn reveal a self-similar cluster-like morphology [20] whereas STM studies of a sputter-annealed surface reveal (under some conditions) a much smoother morphology, albeit with elements of pentagonal symmetry.[7,8,10] The possibility of obtaining two types of (stable) surface morphologies requires further clarification and comparison, in this and other systems.

In summary, we have described a method by which single-grain samples of icosahedral AlCuFe can be prepared, characterized, and used in UHV experiments. Precautions must be taken to ensure the quality of the sample, in particular its freedom from secondary phases. Porosity is also a consideration. For a surface oriented parallel to a five-fold plane, an excellent five-fold LEED pattern can be obtained following our procedures. The symmetry and spacings of the diffraction features indicate that this represents a quasicrystalline surface.

Acknowledgments. We are indebted to A. I. Goldman for many useful discussions. This work was supported by the Ames Laboratory, which is operated for the U.S. Department of Energy by Iowa State University under Contract No. W-7405-Eng-82.

References.

[1] We use the term "grain" to mean a sample which shares a coherent orientation, i.e. the five-fold, two-fold and three-fold axes of all parts of the grain are common. A "single grain" in this sense is the quasicrystalline counterpart of a "single crystal".

[2] T.A. Lograsso and D.W. Delaney, J. Mat. Res. 11 (1996) 2125.

[3] D. Shechtman, I. Blech, D. Gratias and J.W. Cahn, Phys. Rev. Lett. 53 (1984) 1951.

[4] C. Janot, Quasicrystals: A Primer (Clarendon Press, Oxford, 1992).

[5] A.I. Goldman and K.F. Kelton, Reviews of Modern Physics 65 (1993) 213-230.

[6] J.M. Dubois, in: Proceedings of the Conference "New Horizons in Quasicrystals: Research and Applications"; A.I. Goldman, D.J. Sordelet, P.A. Thiel and J.M. Dubois, Eds.; (World Scientific, Singapore, 1997), pp. 208-215.

[7] T.M. Schaub, D.E. Bürgler, H.-J. Güntherodt and J.B. Suck, Phys. Rev. Lett. 73 (1994) 1255-1258.

[8] T.M. Schaub, D.E. Bürgler, H.-J. Güntherodt and J.-B. Suck, Z. Phys. B 96 (1994) 93-96.

[9] M. Erbudak, H.-U. Nissen, E. Wetli, M. Hochstrasser and S. Ritsch, Phys. Rev. Lett. 72 (1994) 3037.

[10] T.M. Schaub, D.E. Bürgler, H.-J. Güntherodt, J.B. Suck and M. Audier, Appl. Phys. A 61 (1995) 491-501.

[11] T.M. Schaub, D.E. Bürgler, H.-J. Güntherodt, J.B. Suck and M. Audier, in: Proceeding of the 5th International Conference on Quasicrystals, Avignon, France, May 22-26 1995.; C. Janot and R. Mosseri, Eds.; (World Scientific, Singapore, 1995), pp. 132-138.

[12] X. Wu, S.W. Kycia, C.G. Olson, P.J. Benning, A.I. Goldman and D.W. Lynch, Phys. Rev. Lett. 75 (1995) 4540.

[13] S.-L. Chang, W.B. Chin, C.-M. Zhang, C.J. Jenks and P.A. Thiel, Surf. Sci. 337 (1995) 135-146.

[14] S.-L. Chang, J.W. Anderegg and P.A. Thiel, J. Noncryst. Solids 195 (1996) 95-101.

[15] C.J. Jenks, S.-L. Chang, J.W. Anderegg, P.A. Thiel and D.W. Lynch, Phys. Rev. B 54 (1996) 6301.

[16] C.J. Jenks, D. Delaney, T. Bloomer, S.-L. Chang, T. Lograsso and P.A. Thiel, Appl. Surf. Sci. 103 (1996) 485-493.

[17] S. Suzuki, Y. Waseda, N. Tamura and K. Urban, Scripta Materialia 35 (1996) 891-895.

[18] M. Zurkirch, A. Atrei, M. Hochstrasser, M. Erbudak and A.R. Kortan, J. Electron Spectr. and Rel. Phenom. 77 (1996) 233.

[19] Z.M. Stadnik, D. Purdie, M. Garnier, Y. Baer, A.-P. Tsai, A. Inoue, K. Edagawa and S. Takeuchi, Phys. Rev. Lett. 77 (1996) 1777.

[20] P. Ebert, M. Feuerbacher, N. Tamura, M. Wollgarten and K. Urban, Phys. Rev. Lett. 77 (1996) 3827-3830.

[21] J. Chevrier, G. Cappelio, F. Comin and J.P. Palmari, in: Proceedings of the Conference, "New Horizons in Quasicrystals: Research and Applications"; A.I. Goldman, D.J. Sordelet, P.A. Thiel and J.M. Dubois, Eds.; (World Scientific, Singapore, 1997), pp. 144-151.

[22] D. Naumovic, P. Aebi, L. Schlapbach and C. Beeli, in: Proc. Conf. on "New Horizons in Quasicrstals: Research and Applications"; A.I. Goldman, D.J. Sordelet, P.A. Thiel and J.M. Dubois, Eds.; (World Scientific, Singapore, 1997), pp. 86-94.

[23] M. Gierer, M.A. VanxxHove, A.I. Goldman, Z. Shen, S.-L. Chang, C.J. Jenks, C.-M. Zhang and P.A. Thiel, Phys. Rev. Lett. 78 (1997) 467-470.

[24] Z. Shen, C.J. Jenks, J. Anderegg, D.W. Delaney, T.A. Lograsso, P.A. Thiel and A.I. Goldman, Phys. Rev. Lett. 78 (1997) 1050-1053.

[25] E.G. McRae, R.A. Malic, T.H. Lalonde, F.A. Thiel, H.S. Chen and A.R. Kortan, Phys. Rev. Letters 65 (1990) 883.

[26] A.R. Kortan, R.S. Becker, F.A. Thiel and H.S. Chen, Phys. Rev. Letters 64 (1990) 200.

[27] R.S. Becker and A.R. Kortan, in: Quasicrystals: The State of the Art; D.P. DiVincenzo and P. Steinhardt, Eds.; (World Scientific Publishing Co., Singapore, 1991), pp. 111.

[28] A.R. Kortan, R.S. Becker, F.A. Thiel and H.S. Chen, in: Physics and Chemistry of Finite Systems: From Clusters to Crystals; P. Jena, Ed. (Kluwer Academic Publishers, Netherlands, 1992); Vol. 1, pp. 29.

[29] D. Rouxel, M. Gavatz, P. Pigeat, B. Weber and P. Plaindoux, in: Proceedings of the Conference, "New Horizons in Quasicrystals: Research and Applications"; A.I. Goldman, D. Sordelet, P.A. Thiel and J.M. Dubois, Eds.; (World Scientific, Singapore, 1997), pp. 173-180.

[30] F.W. Gayle, A.J. Shapiro, F.S. Biancaniello and W.J. Boettinger, Metall. Trans. A 23A (1992) 2409.

[31] D. Gratias, Y. Calvayrac, J. Devaud-Rzepski, F. Faudot, M. Harmelin, A. Quivy and P.A. Bancel, J. Noncryst. Solids 153-4 (1993) 482.

[32] N. Menguy, M. Audier and P. Guyot, Phil. Mag. Lett. 65 (1992) 7-14.

[33] Z. Zhang, N.C. Li and K. Urban, J. Mater. Res. 6 (1991) 366.

[34] P.A. Bancel, Phil. Mag. Lett. 67 (1993) 43.

[35] A. Waseda, K. Araki, K. Kimura and H. Ino, J. Noncryst. Solids 153-154 (1993) 635.

[36] M. Quiquandon, A. Quivy, J. Devaud, F. Faudot, S. Lefèbvre, M. Bessière and Y. Calvayrac, J. Phys.: Condens. Matter 8 (1996) 2487.

[37] Z. Shen, M.J. Kramer, C.J. Jenks, A.I. Goldman, T. Lograsso, D. Delaney, M. Heinzig, W. Raberg and P.A. Thiel, Phys. Rev. B (1997) submitted.

[38] Comment, While we posit that the surface is unreconstructed, relaxation seems likely. (See Ref. [23]).

[39] M. Cornier-Quiquandon, A. Quivy, S. Lefèbvre, E. Elkaim, G. Heger, A. Katz and D. Gratias, Phys. Rev. B 44 (1991) 2071.

Figure Captions.

Table 1. Ratios of distances to major LEED spots, from the (00000) position, as defined in Fig. 3. The electron beam was at normal incidence. Statistical uncertainties given in the third row encompass a confidence limit of 67%. All accessible spots at a given radius were used in calculating the r_j's, not just the spot indexed in the second row.

Figure 1. AES spectrum of clean ψ-AlCuFe, following ion bombardment (30 min) and annealing at 850 K (60 min).

Figure 2. LEED patterns at normal incidence. (a) Pseudo-ten-fold pattern at 155 eV, produced by annealing at 500 K for 30 minutes after room-temperature sputtering with Ar^+. (b)-(g) Five-fold pattern, produced by annealing at 850 K for 60 minutes after room-temperature sputtering. The incident electron energies are (a) 155 eV, (b) 56 eV, (c) 74 eV, (d) 103 eV, (e) 120 eV, (f) 150 eV, and (g) 190 eV.

Figure 3. Schematic depiction of the five-fold diffraction pattern, and the diffraction spot distances used in Table 1. At any given radius, there are (in principal) ten major spots, which comprise two symmetry-inequivalent sets of five. (In the actual experiment some spots were always blocked out, however, by the sample manipulator.) At any given radius, the two sets are distinguished in the figure by having open centers or not. Pentagonal stars are drawn simply to guide the eye, and to reflect the star shapes evident in the LEED patterns at some energies (e.g. in Figs. 2d-g).

Table 1

	j=0	j=1	j=2	j=3	j=4
Index of a representative spot on the ring	(10000)	(00-1-10)	(10-1-10)	(10-2-20)	(20-3-30)
Energy range in which measured	50-90 eV	70-150 eV	50-190 eV	140-190 eV	180-200 eV
Number of measurements	33	38	86	39	20
r_j (Å^{-1})	0.684 $\pm$ 0.026 (0.6291=bulk value) [39]	1.090 $\pm$ 0.037	1.781 $\pm$ 0.063	2.864 $\pm$ 0.047	4.698 $\pm$ 0.098
experimental r_j/r_0	1 (trivially)	(1.594 $\pm$ 0.115)[1]	(1.614 $\pm$ 0.059)[2]	(1.612 $\pm$ 0.029)[3]	(1.619 $\pm$ 0.024)[4]
ideal ratio, r_j/r_0	1	$1.618 = \tau$	$1.618^2 = \tau^2$	$1.618^3 = \tau^3$	$1.618^4 = \tau^4$

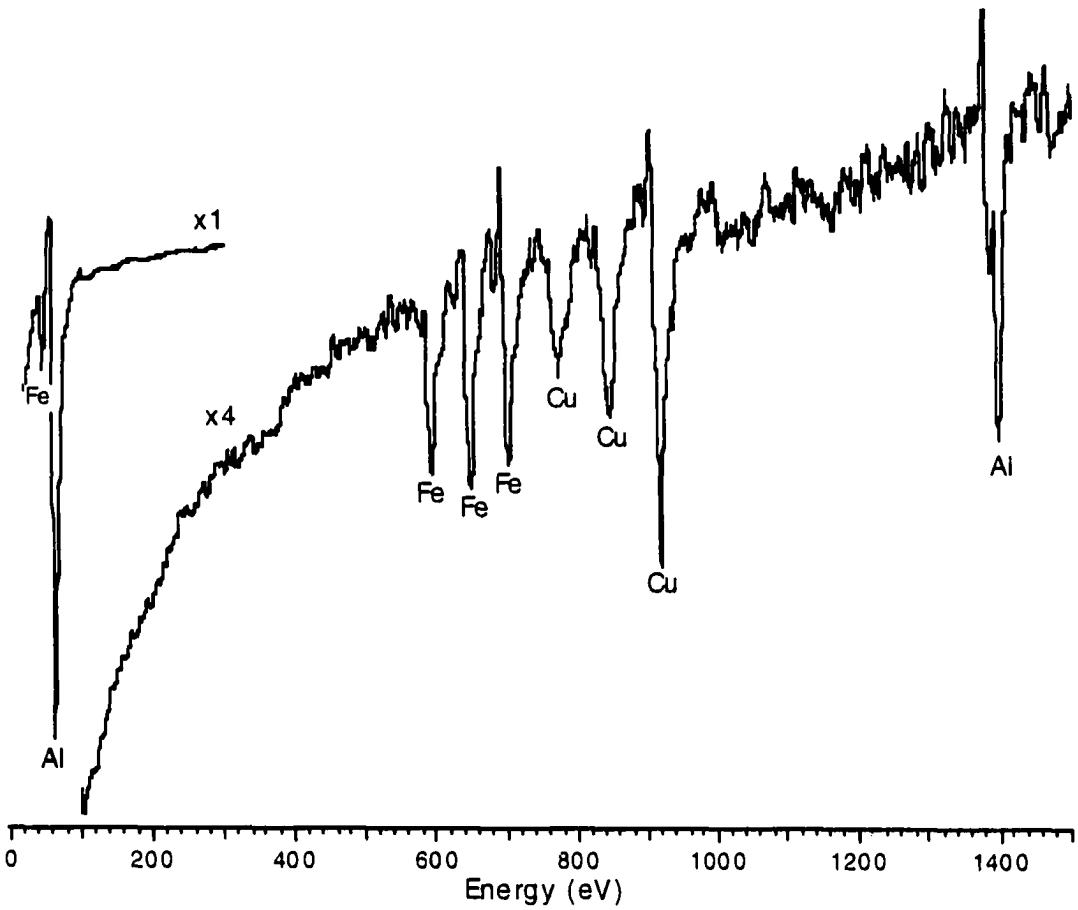
x1
x4
Fe
Al
Fe
Fe
Fe
Cu
Cu
Cu
Al
0
200
400
600
800
1000
1200
1400
Energy (eV)

Fig. 1

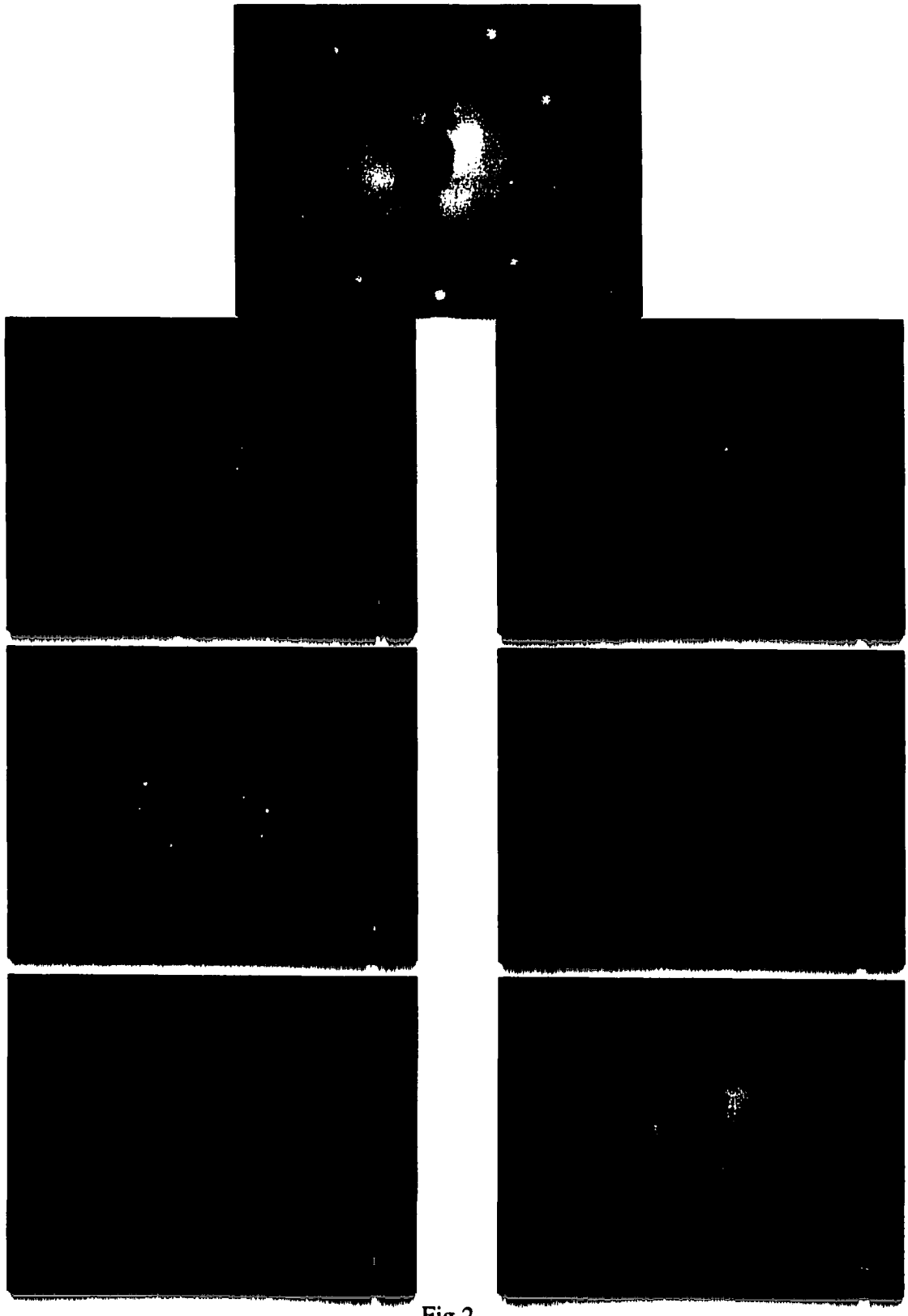

Fig.2

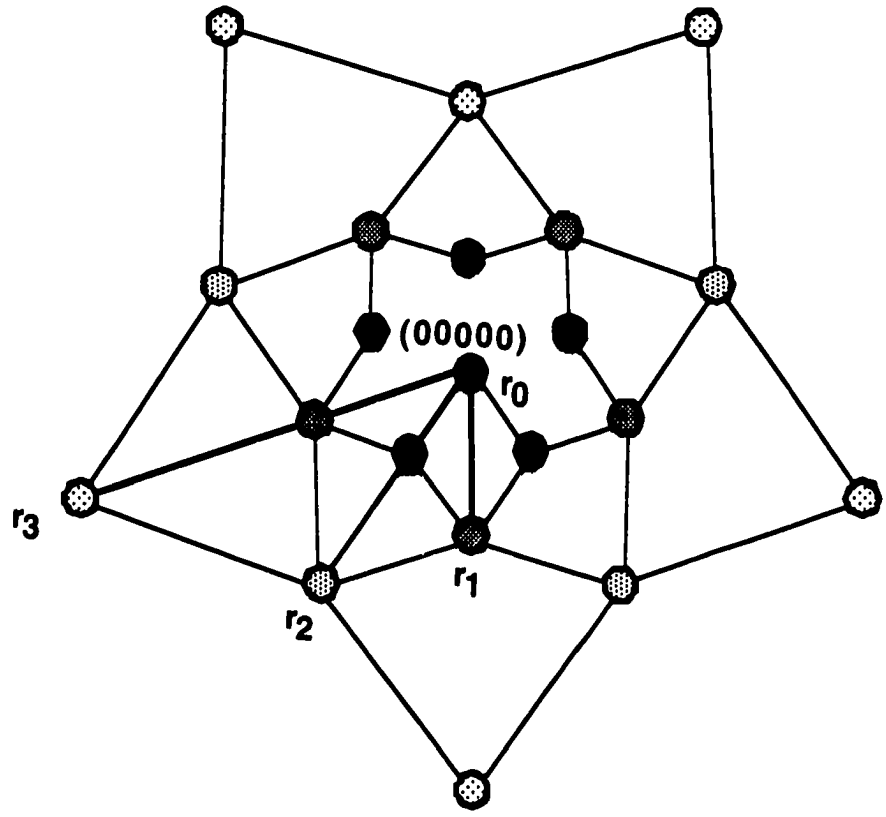

Fig. 3

CRYSTALLINE SURFACE STRUCTURES INDUCED BY ION SPUTTERING OF Al-RICH ICOSAHEDRAL QUASICRYSTALS

A paper submitted to Physical Review B

Z. Shen, M. J. Kramer, C. J. Jenks, A. I. Goldman, T. Lograsso, D. Delaney, M. Heinzig, W. Raberg, and P. A. Thiel*

PACS numbers: 61.44 Br, 68.35 Bs, 61.14 Hg, 81.10.Aj

Abstract. Low-energy electron diffraction patterns, produced from quasicrystal surfaces by ion sputtering and annealing to temperatures below ~700 K, can be assigned to various terminations of the cubic, CsCl structure. The assignments are based upon ratios of spot spacings, estimates of surface lattice constants, bulk phase diagrams vs. surface compositions, and comparisons with previous work. The CsCl overlayers are deeper than about 5 atomic layers, because they obscure the diffraction spots from the underlying quasicrystalline substrate. These patterns transform irreversibly to quasicrystalline(-like) patterns upon annealing to higher temperatures, indicating that the cubic overlayers are metastable. Based upon the data for three chemically-identical, but symmetrically-inequivalent surfaces, a model is developed for the relation between the cubic overlayers and the quasicrystalline substrate. The model is based upon the related symmetries of cubic close-packed and icosahedral-packed materials. The model explains not only the symmetries of the cubic surface terminations, but also the number and orientation of domains. These results may be general among Al-rich, icosahedral materials.

*Corresponding author: Fax 515-294-4709 email thiel@ameslab.gov

1. Introduction.

Quasicrystals, discovered in 1982 by Shechtman,[1,2] are typically binary and ternary metallic alloys, often containing 60 to 70 atomic percent aluminum. They present unique structural features,[3-6] coupled with unusual combinations of physical properties.[7,8] Some of the interesting properties of quasicrystals, such as low friction and 'non-stick' character, involve surface phenomena. This motivates fundamental studies of structure, composition, and chemical reactivity of their surfaces. In many cases, one needs to separate the influence of the oxide that is always present in air, from the influence of the quasicrystalline substrate. This requires comparison of the properties of a clean surface with those of an oxidized surface, if possible.

The preparation and maintenance of a clean (non-oxidized) surface requires ultrahigh vacuum (UHV), because these Al-rich alloys oxidize readily in air. Within UHV, a convenient route to surface preparation is ion sputtering, followed by annealing well above room temperature. Convenience is provided because a new surface can be generated repetitively on a single sample *in situ*. This approach is traditional for preparing metal samples in UHV.[9]

This method, however, can be chemically and physically disruptive. The chemical disruption is perhaps most critical for quasicrystals, since the compositional range of phase stability (in the bulk) spans only a few atomic per cent. Indeed, some workers have suggested[10] that the evolution of the surface structure depends critically upon the local stoichiometry. Several studies, for example, have motivated a comparison, via STM, of sputtered and annealed surfaces with those prepared by in-situ cleavage. Sputtering followed by annealing generally leads to terraced surfaces, which reveal quasiperiodic ordering of structures within and between the terraces. Those surfaces, which result from in-situ cleaving, reveal rough terminations, on the order of cluster sizes proposed by recent structural models for the icosahedral phase.[11-13] With all of this in mind, it is clear that a deeper understanding of

how chemical perturbations can force the surface out of the region of quasicrystalline stability is important for determining the true nature of the surface of quasicrystals.

The chemical changes at the surface can occur in UHV via two routes: (1) preferential sputtering of a particular metal, and (2) preferential evaporation of a particular metal upon annealing. Simple momentum-transfer arguments lead to the expectation that the lightest element will be sputtered preferentially. This paper concerns the chemical perturbation and accompanying surface structures induced by the first of the two treatments, sputtering.

Schaub et al.[14] were the first to report that Ar^+ sputtering of an Al-rich quasicrystal, icosahedral (i-) Al-Pd-Mn, leads to preferential loss of Al, the lightest element. This observation has since been confirmed in other laboratories.[15-18] Similar observations--Al depletion upon Ar^+ sputtering--have been reported also on two other Al-rich alloys, i-Al-Cu-Fe[19, 20] and decagonal Al-Ni-Co.[21]

In the bulk phase diagrams, the Al-based icosahedral alloys generally have a CsCl-type structure on the Al-poor side. Rouxel et al. pointed out that sputtering in UHV moves the surface composition toward the region of a CsCl phase in the Al-Cu-Fe phase diagram.[19] Zurkirch et al. observed a cubic phase induced by Ar^+ sputtering on decagonal Al-Ni-Co.[21] In a similar vein, Naumovic reported that Al depletion induced by high-temperature annealing could produce a CsCl-type structure on the five-fold surface of i-Al-Pd-Mn.[22]

These findings are all qualitatively similar to results generated within scientific communities outside of surface science. In electron microscopy, where Ar^+ treatments are used frequently to modify samples, such treatments have been reported to transform the icosahedral phase to the CsCl-type in the Al-Cu-Fe system.[23-26] In the crystal growth community, it is known that crystals with CsCl structure often coexist with the icosahedral phase.[27-29] Dong et al.[27, 30] pointed out that it is possible to use twinning operations on the CsCl-type unit cell to describe the structure of a decagonal quasicrystal and its approximants.

In the present work, we expand upon these results with a systematic study of the crystalline overlayers produced by sputtering (followed by annealing) on four different quasicrystalline surfaces in UHV. These are all surfaces of icosahedral materials. This database allows comparisons between different high-symmetry surfaces within a single alloy, and between different alloy surfaces having the same symmetry. The three high-symmetry surfaces within a single alloy are the five-fold, three-fold, and two-fold surfaces of i-Al-Pd-Mn. The two different alloys of the same symmetry are the five-fold surfaces of i-Al-Pd-Mn and i-Al-Cu-Fe. The comparisons show that the crystalline overlayers, and their orientational relationship to the substrate, can be understood within a common general framework. This framework may prove useful for predicting and understanding the results of ion sputtering as a surface treatment on the icosahedral, Al-rich quasicrystals.

Finally, a full understanding of the properties of quasicrystals requires comparisons with the properties of crystalline samples of similar chemical composition. For purposes of surface studies in UHV, it would be especially attractive to prepare a quasicrystalline surface and a crystalline surface, from a single sample, and then to perform comparisons in situ. The information presented here provides the desired ability to switch between these types of surfaces, using a single bulk sample.

2. Experimental description.

The nominal compositions (i.e. the initial liquid composition used in growth) of the samples are $Al_{72}Pd_{19.5}Mn_{8.5}$ for all the Al-Pd-Mn samples, and $Al_{63}Cu_{25}Fe_{12}$ for the Al-Cu-Fe sample. Details of sample preparation and characterization, both inside and outside of UHV, are given elsewhere.[31]

The low-energy electron diffraction (LEED) and Auger electron spectroscopy (AES) experiments are performed in a UHV chamber.[15] In these experiments its base pressure is 3 to 4×10^{-11} Torr. Surface preparation in UHV involves sputtering at room temperature and annealing. The sample is sputtered for 15 minutes each time at normal incidence, 1keV, and

12-18 μA sample current without bias. For a sample that has been newly mounted in UHV, annealing begins at 400 K, and goes up in 50 K increments whenever annealing at a given temperature no longer reveals significant surface segregation of carbon and oxygen. The upper limits of annealing temperature are chosen to avoid phase transformations.[20] Annealing periods are typically 15-30 minutes during cleaning, and 1-4 hours before LEED experiments. Most of the LEED experiments are done with low-resolution optics (nominal instrumental limit 100-300 Å), but some experiments are done in a separate chamber with Omicron high-resolution optics, called SPA-LEED (nominal limit 1000 Å).

Surface compositions are monitored with electron-stimulated AES. For analyzing trends in composition, we use the Al KLL (1396 eV), Pd MNN (330 eV), Mn LMM (589 eV), Cu LMM (920 eV), and Fe LMM (703 eV) Auger lines. Published sensitivity factors[32] are used to calculate surface compositions. This, plus the fact that compositions are actually depth-weighted averages over regions which probably contain concentration gradients in most of these experiments (the top 100 Å), means that surface compositions should be taken as qualitative, rather than quantitative, values.

Some selected area electron diffraction (SADP) experiments are done in a transmission electron microscope (TEM), a Philips CM30 operated at 300 keV. The experiments were performed on a small fragment (0.1 g) of a larger ingot of i-$Al_{65}Cu_{23}Fe_{12}$. The piece was ground in ethanol, and a droplet of the suspension was dried in air onto a continuous carbon film supported by a 300 mesh Cu grid. Care was taken so the particles were not in contact with the Cu mesh. The grid was then placed between Pt spacers in a Gatan double tilt TEM stage with resistive heating, and with a Pt/Pt-Rh thermocouple to monitor the temperature. Exact temperature is uncertain due to poor thermal contact, and in the heating experiments a temperature lag of 100 K is not unusual. A thin area of a single grain was obtained for SADP and the grain was tilted to a five-fold zone axis. Heating was performed incrementally, with SADPs taken approximately every 50 K for temperatures up to 1070 K.

3. Results.

Surface compositions after Ar^+ sputtering and annealing at different temperatures are shown in Table 1. It can be seen that the surfaces are all Al-deficient, relative to the nominal bulk composition, after sputtering at room temperature. The Al-Pd-Mn surfaces are all Pd-rich, and the Al-Cu-Fe surface is Fe-rich (relative to the bulk). Heating to 800-900 K in all cases restores the surface to a composition close to that of the bulk.

Ar^+ sputtering and annealing in UHV yields two different types of LEED patterns for all four samples (Fig. 1). The first is obtained upon annealing at relatively low temperature: 600-800 K for the Al-Pd-Mn twofold surface (Fig. 1a), 300–650 K for the Al-Pd-Mn threefold surface (Fig. 1b), 600-750 K for the Al-Pd-Mn fivefold surface (Fig. 1c), and 500-750 K for the Al-Cu-Fe fivefold surface (Fig. 1d). The second is obtained after annealing at higher temperature: 800-900 K for the Al-Pd-Mn twofold surface (Fig. 1e), 650–800 K for the Al-Pd-Mn threefold surface (Fig. 1f), 700-800 K for the Al-Pd-Mn fivefold surface (Fig. 1g), and 750-850 K for the Al-Cu-Fe fivefold surface (Fig. 1h).

Assignment of the high-temperature patterns. The high temperature LEED patterns have very sharp LEED spots, as can be seen in the right-hand column of Fig. 1. The widths of the spots correspond to a real-space dimension greater than 150 Å in width, and are limited by the LEED optics. A further SPA-LEED study on the Al-Pd-Mn fivefold surface shows that the average domain size is about 900 Å (again, close to the resolution limit of the SPA-LEED instrument). The existence of large terraces, with average lengths in the range of hundreds of Å, is also supported by atomic force microscopy on the Al-Pd-Mn threefold[33] and twofold[34] surfaces. The symmetries and spot spacings in the high-temperature LEED patterns correspond well to those expected for unreconstructed quasicrystalline surfaces.[35] Thus, the data are consistent with unreconstructed quasicrystalline surfaces, or, perhaps, with high-order approximants, such as suggested by Dubois.[8]

Turning now to the LEED patterns obtained after the low-temperature anneal, we note that the diffraction spots are quite broad (see Figure 1), and the patterns do not correspond to those expected for bulk terminated icosahedral quasicrystalline surfaces. However, the symmetries of the LEED patterns have an apparent relationship to the underlying bulk structure: twofold LEED pattern for the twofold termination, threefold LEED pattern for threefold termination, and tenfold LEED patterns for fivefold terminations. The nature of the low temperature patterns is discussed later in this paper.

Transitions between low- and high-temperature structures. In order to study the evolution of the low and high temperature LEED patterns, we monitored the intensities and widths of diffraction spots of the both patterns as a function of temperature while heating the sample at a rate of 0.1 K/sec. The results, shown in Fig. 2, indicate that there is a rather abrupt transition from the low temperature to high temperature phase. The transition temperature is around 800 K for the two-fold Al-Pd-Mn surface, 750 K for threefold surface of Al-Pd-Mn, 800 K for the fivefold Al-Pd-Mn surface, and 800 K for fivefold surface of Al-Cu-Fe. These transitions are irreversible based upon the observation that the data of Fig. 2 remain unchanged (expect for variations ascribable to Debye-Waller effects) when the data are acquired at T= 120 K after each annealing step, or are acquired at the annealing temperature directly. The data of Fig. 2 were acquired under the former conditions.

Degeneracies in the low-temperature patterns. By examining LEED patterns at different places on the samples, we found that the low temperature LEED patterns actually consist of multiple rotational domains for fivefold and twofold surfaces: five domains for fivefold surfaces, and two domains for the twofold surface. The degeneracy of the multiple domains is broken in certain spots of the sample, mainly near the edges. This is observed most clearly for the Al-Cu-Fe fivefold surface (Fig. 3). The apparent tenfold pattern (Fig. 3a) actually consists of five rotational domains (Fig. 3b) which are separated by 72^{o} from each

other. The pattern has been called previously[20, 36] the *pseudo*-tenfold pattern. The interpretation is the same for the low temperature LEED pattern of fivefold Al-Pd-Mn.

As a check, we measured the intensity-voltage (IV) curves of LEED spots in the tenfold patterns, both of Al-Cu-Fe (Fig. 3a) and Al-Pd-Mn. For spots that were equidistant from the specular beam, the intensity-voltage curves were equivalent. This is expected for overlapping domains.

For the Al-Pd-Mn twofold surface, the two domains can be described as symmetric about the two icosahedral twofold axes in the twofold plane (Fig. 4). It is interesting that there is an angle of about 34° between the single domain edge and one of the two twofold axes (Fig. 4b). We offer an explanation of this angle later in the paper.

Things are more complicated for the threefold surface. There are actually two sets of LEED patterns in Fig. 1c. The first is obtained just after sputtering at room temperature, with no annealing (Fig. 5a). The diffraction spots are relatively sharp and the pattern has apparent threefold symmetry. This pattern also contains multiple (three) domains (Fig. 5b). These three domains are separated by 120°. Interestingly, the orientations of the single domains deviate slightly (by a few degrees) from the average surface orientation. Thus, they are actually facets on the surface, which is why some of the diffraction spots appear to be split in Fig. 1c. The intensity of this low-temperature pattern--which we call the facetted pattern--decreases as annealing temperature increases (Fig. 2b, solid triangles).

The second low-temperature pattern appears after annealing between 550 K and 700 K (solid circles, Fig. 2b), and before the facetted pattern disappears. The diffraction spots are slightly broader than the first pattern. This pattern has threefold symmetry too, but is distinguished by the streaks shown in Fig. 1c. All attempts to find areas of broken degeneracy at different locations on the crystal failed. However, the distinctive streaks in this pattern suggest that a domain structure is present, although its exact nature is not known at this time.

Assignment of the low-temperature patterns. Surprisingly, the single domain LEED patterns for the twofold and fivefold surfaces are very similar. They share the same geometry and spacing. We concentrate on the Al-Cu-Fe fivefold surface first in the following discussion.

The single domain LEED pattern (Fig. 3b) is periodic, which indicates that the corresponding surface structure is crystalline. The ratio between the two edges of the rectangle is 1.41±0.02. This suggests that the surface structure is probably cubic with (110) orientation, for which the theoretical edge ratio = $\sqrt{2}$ = 1.414.

The cubic CsCl-structure in the Al-Cu-Fe system is called the β-phase. Its general stoichiometry is denoted $Al(Cu_{1-x}Fe_x)$, and it is stable in the bulk for Fe concentrations in the range 10–50 % and Cu concentration in the range 0-40%.[37]

One check on the identification of the CsCl structure is provided by estimating the absolute lattice constant *within the surface plane* from the LEED patterns. The uncertainty in such a measurement is large, mainly because of uncertainty about whether the sample is close to the focal point of the optics. We attempted to compensate for this uncertainty by scaling the LEED value to that determined for the quasicrystalline surface, and assuming that the quasicrystalline surface has the same quasi-lattice constant as the quasicrystalline bulk. The result for the pseudo-tenfold pattern is 2.95 ± 0.05 Å. The bulk lattice constant of β-AlFe (i.e. x=1 in β–$Al(Cu_{1-x}Fe_x)$) is 2.902 to 2.908 Å.[38] However, our β-phase probably contains significant Cu (Table 1d), which might influence the bulk lattice constant. X-ray diffraction data from a hot-isostatically-pressed sample of the β-phase with bulk composition $Al_{50}Cu_{35}Fe_{15}$ indicates a higher bulk lattice constant of 2.9422(4)±0.0004Å. i.e. an expansion of 0.03-0.04 Å relative to the composition with no Cu. This is closer to the value measured from LEED.

The lattice constant *perpendicular* to the surface of the crystalline overlayer can also be determined by a measurement of the step heights in LEED. This relies upon determining the

electron wavelengths at which scattering from successive terraces is in-phase or out-of-phase.[39, 40] The measurement is suggested by the data of Fig. 3b, which show that some diffraction spots are sharp (scattering is in-phase), while others are broad (out-of-phase), at the particular electron energy (= electron wavelength) of 70 eV. This relationship between the different diffraction spots is a consequence of the arrangement of scatterers in successive terraces.[39, 40] A measurement of spot widths vs. electron energy is shown in Fig. 6. The separation between successive maxima or minima corresponds to the average step height. It can be seen that the step height from this measurement is in the range of 2.2 to 2.3 Å. The separation between successive (110)-type planes in the bulk CsCl structure of Al-Cu-Fe should be 2.05 to 2.08 Å, somewhat smaller than the data indicate. The discrepancy may be due to some step bunching, which would increase the average experimental value. (Note that surface relaxations should not play a part in the comparison between expected and measured values, assuming that such relaxations affect all terraces equally.)

Auger compositions (Table 1d) show that Ar^+ sputtering at room temperature serves to deplete the Al and enrich the Fe. As pointed out previously by Rouxel et al.,[19] sputtering moves the surface composition in the direction of the β-phase.

Analysis of LEED intensity-voltage data has been done on the single-domain LEED pattern of the fivefold Al-Cu-Fe surface.[36] The analysis gives preference to a pure unreconstructed β-Al($Cu_{1-x}Fe_x$) (110) surface with a copper-rich composition. The best Pendry R-factor is 0.262, which is considered an acceptable value.

All these results suggest that the low temperature phase is probably β-Al($Cu_{1-x}Fe_x$) with (110) surface orientation. There is an orientational relationship between the β–phase and the underlying quasicrystalline phase.

Similar discussion can be applied to the Al-Pd-Mn quasicrystals. There is a crystalline β-AlPd phase with CsCl structure and a lattice constant of 3.04-3.06Å.[38] The lattice constant after partial substitution of Mn for Pd, β-$Al_{48}Pd_{10}Mn_{42}$, is slightly lower: 3.02Å.[41] The

symmetries of the low temperature single domain LEED patterns of Al-Pd-Mn twofold, threefold, and fivefold surfaces correspond well to expectations for cubic (110), (111), and (110) surfaces, respectively. The lattice constants determined from the LEED patterns are 2.95±0.1Å for the twofold surface, 3.03±0.1Å for the threefold surface (the streaked pattern), and 2.94±0.1Å for the fivefold surface. The ratios of edges of single domain LEED patterns are: 1.42±0.02 for the twofold surface, and 1.42±0.02 for the fivefold surface. Auger compositions (Table 1a-c) of these three surfaces after Ar^+ sputtering are also in the direction of the β-phase.

All these results suggest that a cubic $Al(Pd_{1-x}Mn_x)$ phase forms on the Al-Pd-Mn surfaces after Ar^+ sputtering and mild annealing (to below ~700 K). The surface orientation of this cubic phase is related to the underlying quasicrystalline surface structure. Cubic (110) surfaces are formed on the twofold and fivefold quasicrystal surfaces, and a cubic (111) surface is formed on the threefold quasicrystal surface. After high temperature annealing (above ~700 K), this cubic phase transforms to the quasicrystal.

Note that this discussion does not encompass the facetted pattern on the threefold surface. The average ratio of the edges of the rectangles in Fig. 5b is 1.59, so this is not a 'simple' (110) termination. The nature of this pattern is not known at present.

The present work serves as a revision to a previous report that the low-temperature phase on twofold i-Al-Pd-Mn had icosahedral, or near-icosahedral, symmetry; in that work, the degeneracy of the LEED pattern was not yet identified.[36]

Structural relationship of the low-temperature phases to the quasicrystalline substrate. Obviously, the quasicrystalline substrate exerts a strong influence on the orientation and surface termination of the crystalline overlayer. As a starting point to discuss this relationship, let us take a very simple structural model: packing of equal spheres. In the cubic close-packing (ccp) of equal spheres (Fig. 7a), each sphere is surrounded by 12 nearest neighbors, and there are 4 threefold axes, 6 twofold axes, and 4 fourfold axes in

the cubic structure. In the icosahedral packing (ip) of equal spheres (Fig. 7b), each sphere also has 12 nearest neighbors, and there are 15 twofold axes, 10 threefold axes, and 6 fivefold axes.

The difference between these two dense packings is mainly in the middle layer: in icosahedral packing the layer is buckled instead of planar as in ccp, and it is rotated by 30° compared to ccp (Fig. 7 top). So if one starts from a ccp cluster, then rotates the middle 6 spheres by 30°, displaces three of them up by about 20% and the other three down by about 20% of the inter-sphere distance, one gets icosahedral packing. The total displacement of the spheres is about 50% of the inter-sphere distance for the middle six spheres and about 4% for the top and bottom six spheres.

Based upon this transformation, there is a close relationship between the symmetry axes of these two types of packing. This can be shown more clearly in stereographic projections. Since the threefold axis is common in the ccp and ip symmetries, that is the starting point. Figure 8 is a comparison of the ccp (111) projection and the ip threefold projection. The three [110]-type axes of ccp that are perpendicular to the [111] axis, are lined up with the three twofold axes of ip. The other three [110]-type axes of ccp which are 35.26° away from the [111] axis are almost parallel to three fivefold axes of ip (2.1° off).

The experimental data for the twofold Al-Pd-Mn surface show that the two domains of the cubic phase are symmetric about the two icosahedral twofold axes in the twofold plane (Fig. 4). This can be explained by the twofold stereographic projection of the icosahedral surface (Fig. 9a), where there are two twofold axes and two threefold axes in the plane which are perpendicular to the surface normal. According to our model, there are two possible domains of the cubic phase that can grow on the quasicrystal twofold surface: the [111] directions of these two domains are parallel to the two threefold axes which are perpendicular to the surface normal. From Fig. 9a, it is easy to see that these two domains are symmetric about the two icosahedral twofold axes in the plane.

The angle of 34° between the edge of the cubic, single-domain LEED pattern and one of the twofold axes in the quasicrystal LEED pattern (Fig. 4b) can also be explained. The angle between the ip threefold and twofold axes (labeled 3f and 2f, respectively, in the twofold projection of Fig. 9a) is 20.9°. The angle between a threefold axis and a [001]-type axis in the ccp twofold projection (not shown) is 54.7°. The [001] axis is parallel to the edge of the rectangular unit cell indicated in Fig. 4b. This implies that the angle between the ip twofold axis and the ccp [001]-type axis is 54.7°-20.9°=33.8°, in quantitative agreement with experiment.

As a check, let us examine the LEED patterns of the twofold surface in this context. Again, we start from the threefold surface because, according to our model, the ccp (111) surface and ip threefold surfaces should be aligned to each other. So we align the simulated LEED patterns of ccp (111) and ip threefold surfaces to each other (Fig. 10a, b). Then we rotate both the cubic (111) surface and icosahedral threefold surface 90° to one of the three cubic (110) type or icosahedral twofold surfaces (following the dashed arrows in Fig. 8). The simulated LEED patterns after the rotation are shown in Fig. 10c, d. The angle between the cubic [001] direction and one of the icosahedral twofold axes is 33.8°. To get the other domain, one would start from a different threefold axis, and rotate into the same twofold axis.

Similar discussion can be applied to fivefold surfaces. Fig. 9b shows there are five possible growth directions (along five icosahedral threefold axes) for the cubic phase on the fivefold quasicrystal surface, which generates five cubic (110) domains on the surface.

We conclude that there is a close structure relationship between cubic close-packing and icosahedral packing, and that this controls the growth orientation in our experiments. The key relationships between ccp and are: [110] of ccp || twofold of ip, [110] of ccp almost || fivefold of ip, and [111] of ccp || threefold of ip.

Table 2a compares these LEED results with previous electron microscopy and high-energy electron diffraction studies. This comparison is restricted to systems where the cubic structure exhibits a CsCl structure. For the twofold icosahedral axis, the relationship [110] of

CsCl || twofold of ip, is observed. Two additional observations, [112] or [111]||twofold, can be rationalized on the basis that the [112] and [111]-type axes are only 1.44-1.45° away from the remaining twofolds of ip, based on our model. For the fivefold and threefold icosahedral axes, the relationship [110]||fivefold seems robust. The additional observation of [113]||fivefold can be rationalized similarly: the [113]-type axis is within 0.8° of three of the fivefolds of ip, in our model. In comparing the experimental data of Fig. 2, note that our experiments measure only the orientation of the axes that are parallel to the surface normal. Electron microscopy techniques also probe axes that are not parallel to the surface normal, due to the ease of sample rotation and higher penetration depth of the electrons. (Other differences also exist, which complicate the comparison between LEED and electron microscopy techniques.[42]) A general observation from our experiments is that the system selects surface planes that maximize the alignment between high-symmetry axes of substrate and overlayer. This explains, for instance, why the surface of the cubic layer on the twofold surface is not (112) or (111), which would incur a misalignment of 1.44-1.45°, but rather (110).

SADPs of an $Al_{65}Cu_{23}Fe_{12}$ single grain in our laboratory also support one of these relationships (Fig. 11). In the SADP experiment, an icosahedral grain was oriented to a fivefold zone axis (Fig. 11a), and was heated until peritectic decomposition yielded a large grain of the β-phase (Fig. 11b), surrounded by fine grains of the λ–phase. This transformation occurred abruptly between about 1220 and 1240 K (but there is considerable uncertainty in the exact temperature--see Section 2). It can be seen that the (110) reflections of the β-phase show good lattice match with the fivefold axes of the icosahedral phase. Also note that the spatial orientation of one of the (110) reflections corresponds to one of the twofold reflections (arrows in Fig. 11). Energy dispersive spectroscopy showed that the β-phase was lower in Al than the quasicrystal.

An alternative means of transforming a ccp cluster into an ip cluster, while retaining a close relationship among some high-symmetry axes, was described by Mackay.[43] The result is

shown in Fig. 12. In Mackay's transformation, the three-fold axis remains parallel in both ccp and ip structures, but rotates by 37.8°. This is equivalent to rotating the stereographic projection in Fig. 8a clockwise by 37.8°, and it serves the purpose of aligning the other three threefold axes of ccp with three of the threefold axes of ip. Also, the ccp fourfold axes align with some of the ip twofold axes. The ccp [-211]-type axes come within 7.8° of other ip twofold axes. These alignments, shown in Fig. 12a-b, have been observed experimentally in at least three systems,.[44-46] These are shown in Table 2b. (From comparing Tables 2b with 2a, one might generalize that the Mackay transformation seems to apply to systems of the Al-Si-Mn structure-type. In such systems, the cubic phase is not a simple CsCl packing of atoms, but rather a bcc packing of large clusters, with lattice constant of 12-14 Å.)

However, the Mackay transformation is not consistent with our experimental data. First, the 37.8° rotation of the threefold axis should be easily visible by comparing Figs. 1c and 1d, but it is not present. Second, the diffraction pattern of the overlayer on the twofold icosahedral surface should have fourfold symmetry, rather than the observed twofold symmetry (Fig. 4). Finally, the ip fivefold axis would come closest to the [210]-type ccp axis (5.2° off). The (210) surface would have a rectangular unit cell, as observed. Five equivalent threefold axes would surround the fivefold axes, also consistent with the observation of five rectangular domains on the fivefold surfaces. However, the edge lengths of the rectangles would be in the ratio 2.24, far from the observed ratio of 1.4. Hence, the experimental data for all three surfaces are much more consistent with the transformation shown in Fig. 7 and 9.

Note that the above discussion is based on the symmetry relationships between cubic and icosahedral systems, and not on details of atomic arrangements within those systems. In reality, we are dealing with binary or ternary systems, with 2 or 3 different atomic radii, instead of equally-sized spheres. The atomic structure of icosahedral quasicrystals is so complicated that there is no universally-accepted structure model in existence thus far. However, all cubic structures have symmetries similar to ccp, and all icosahedral quasicrystals

have the same symmetry as ip. Hence, the simple model presented in Fig. 7a is not too unrealistic. In fact, its ability to explain our experimental data suggests that it is quite plausible.

4. Discussion.

Overlayers of the cubic, CsCl structure can be produced on surfaces of quasicrystals by ion sputtering and annealing to temperatures below ~700 K. The CsCl overlayers are deeper than about 5 atomic layers, because they obscure the diffraction spots from the underlying quasicrystalline substrate.

The low-temperature phases are metastable. They transform irreversibly to the quasicrystalline(-like) patterns above ~700 K. Presumably, the low-temperature annealing serves to activate surface and near-surface diffusion, allowing localized rearrangement. However, the temperature is too low to allow long-range diffusion to/from the bulk, so the composition of the surface and near-surface region remains off-stoichiometry. At higher temperatures, the surface composition is restored by equilibration with the bulk, leading to the LEED patterns that we assign to a quasicrystal or high-order approximant. A similar phenomenon has been found in the crystalline FeAl system.[47] After sputtering and subsequent annealing to about 670 K, the FeAl (100) surface formed an Al-deficient phase, Fe_3Al. After annealing at or above 870 K, a well-ordered FeAl(100) surface was reestablished. Kottcke et al.[47] postulated that this was driven by sputtering-induced changes in surface composition.

The LEED data indicate that the low-temperature structures which form on two chemically different, but symmetrically equivalent quasicrystal samples--fivefold Al-Cu-Fe and fivefold Al-Pd-Mn--are the same. This indicates that the results may be general among Al-rich, icosahedral materials. Furthermore, a series of patterns is observed on chemically identical, but symmetrically inequivalent surfaces (twofold, threefold, and fivefold Al-Pd-Mn). This series can be understood within a general framework based upon the related symmetries of ccp and ip materials. Our model explains not only the symmetries of the surface terminations of the CsCl overlayers, but also the number and orientations of domains.

The threefold surface presents several exceptions to these generalizations. First, not one but two distinguishable patterns are present in the temperature range below 700 K. The first, the facetted pattern, is not assigned to a real-space model at present. It is different from the other low-temperature patterns in that it is visible immediately after sputtering, without annealing (although this effect is not unprecedented [48, 49]). The second pattern contains distinctive streaks that may arise from domain structure. The detailed nature of the crystalline overlayers on the threefold surface requires further investigation. However, these unresolved issues should not obscure the fundamental observations: The data support the assignment of the streaked pattern as the CsCl phase, and are consistent with the model for the symmetry relationship given in Figs. 8 and 9. Hence, the streaked pattern falls within the framework described above.

Acknowledgments. Michel Van Hove, Tanja Drobek, and Jean Marie Dubois provided valuable comments and suggestions. We also wish to acknowledge that three other groups (led by J. Chevrier, L. Schlapbach, and M. Erbudak) have been working in parallel with us, studying cubic overlayers on quasicrystalline substrates. We especially thank D. Naumovic from one of those groups, for sharing results and ideas. This work was supported by the Director, Office of Energy Research, Office of Basic Energy Sciences, Materials Sciences Division, of the U.S. Department of Energy under Contract No. W-405-Eng-82.

References.

1. D. Shechtman, I. Blech, D. Gratias and J. W. Cahn, *Phys. Rev. Lett.* **53** (1984) 1951.

2. D. Shechtman and I. Blech, *Metall. Trans. A* **16** (1985) 1005.

3. A. I. Goldman and M. Widom, *Ann. Rev. Phys. Chem.* **42** (1991) 685-729.

4. P. W. Stephens and A. I. Goldman, *Scientific American* (April 1991) 24-31.

5. C. Janot, *Quasicrystals: A Primer*, C. J. Humphreys, P. B. Hirsch, N. F. Mott, and R. J. Brook, Series Ed., *Monographs on the Physics and Chemistry of Materials* **48** (Clarendon Press, Oxford, 1992).

6. A. I. Goldman and K. F. Kelton, *Reviews of Modern Physics* **65** (1993) 213-230.

7. J. M. Dubois and P. Weinland, CNRS, Nancy, France, "Coating materials for metal alloys and metals and method," European Patent EP 0356287 A1 and US Patent 5204191 (April 20 1993).

8. J. M. Dubois, in *Introduction to the Physics of Quasicrystals*, J. B. Suck, Ed. (Springer Verlag, Berlin, 1998) in press.

9. R. G. Musket, W. McLean, C. A. Colmenares, D. M. Makowiecki and W. J. Siekhaus, *Appl. Surf. Sci.* **10** (1982) 143.

10. P. Ebert, F. Yue and K. Urban, *Phys. Rev. B* **57** (1998) 2821-2825.

11. C. Janot and M. de Boissieu, *Phys. Rev. Lett.* **72** (1994) 1674-1677.

12. C. Janot, *Phys. Rev. B* **53** (1996) 181-191.

13. C. Janot and J.-M. Dubois, in *Introduction to Quasicrystals*, J. B. Suck, Ed. (Springer Verlag, 1998) in press.

14. T. M. Schaub, D. E. Bürgler, H.-J. Güntherodt, J. B. Suck and M. Audier, *Appl. Phys. A* **61** (1995) 491-501.

15. S.-L. Chang, W. B. Chin, C.-M. Zhang, C. J. Jenks and P. A. Thiel, *Surf. Sci.* **337** (1995) 135-146.

16. S.-L. Chang, J. W. Anderegg and P. A. Thiel, *J. Noncryst. Solids* **195** (1996) 95-101.

17. S. Suzuki, Y. Waseda, N. Tamura and K. Urban, *Scripta Materialia* **35** (1996) 891-895.

18. D. Naumovic, P. Aebi, L. Schlapbach, C. Beeli, T. A. Lograso and D. W. Delaney, in *Proceedings of the Sixth International Conference on Quasicrystals (ICQ6)*, T. Fujiwara, and S. Takeuchi, Ed. (World Scientific, Singapore, 1998) 749-756.

19. D. Rouxel, M. Gavatz, P. Pigeat, B. Weber and P. Plaindoux, in *Proceedings of the Conference, "New Horizons in Quasicrystals: Research and Applications"*, A. I. Goldman, D. Sordelet, P. A. Thiel, and J. M. Dubois, Ed. (World Scientific, Singapore, 1997) 173-180.

20. Z. Shen, P. J. Pinhero, T. A. Lograsso, D. W. Delaney, C. J. Jenks and P. A. Thiel, *Surf. Sci. Lett.* **385** (1997) L923-L929.

21. M. Zurkirch, M. Erbudak and A. R. Kortan, in *Proceedings of the 6th International Conference on Quasicrystals,* S. Takeuchi, and T. Fujiwara, Ed. (World Scientific, Singapore, 1998) 67-70.

22. D. Naumovic, (1996) unpublished results.

23. Z. Zhang, Y. C. Feng, D. B. Williams and K. H. Kuo, *Phil. Mag. B* **1993** (1993) 237.

24. Z. Wang, X. Yang and R. Wang, *J. Phys.: Condens. Matter* **5** (1993) 7569-7576.

25. R. Wang, X. Yang, H. Takahashi and S. Ohnuki, *J. Phys.: Condens. matter* **7** (1995) 2105-2114.

26. X. Yang, R. Wang and X. Fan, *Philosophical Magazine Letters* **73** (1996) 121-127.

27. C. Dong, J. M. Dubois, S. S. Kang and M. Audier, *Philosophical Magazine B* **65** (1992) 107-126.

28. C. Dong, K. Chattopadhyay and K. H. Kuo, *Scripta Metall.* **21** (1987) 1307-1312.

29. C. Dong, K. H. Kuo and K. Chattopadhyay, *Mat. Sci. Forum* **22-24** (1987) 555-564.

30. C. Dong and J. M. Dubois, *J. Non-Cryst. Solids* **159** (1993) 107-120.

31. C. J. Jenks, P. J. Pinhero, Z. Shen, T. A. Lograsso, D. W. Delaney, T. e. Bloomer, S.-L. Chang, C.-M. Zhang, J. W. Anderegg, A. H. M. Z. Islam, A. I. Goldman and P. A. Thiel, in *Proceedings of the Sixth International Conference on Quasicrystals (ICQ6),* S. Takeuchi, and T. Fujiwara, Ed. (World Scientific, Singapore, 1998) 741-748.

32. L. E. Davis, N. C. MacDonald, P. W. Palmberg, G. E. Riach and R. E. Weber, *Handbook of Auger Electron Spectroscopy*, Series Ed., (Physical Electronics Division, Perkin-Elmer Corporation, Eden Prairie, Minnesota, 1978).

33. W. Raberg, Ph.D., Universität Bonn (1998).

34. J. Chevrier, G. Cappello, F. Comin and J. P. Palmari, in *Proceedings of the Conference, "New Horizons in Quasicrystals: Research and Applications"*, A. I. Goldman, D. J. Sordelet, P. A. Thiel, and J. M. Dubois, Ed. (World Scientific, Singapore, 1997) 144-151.

35. Z. Shen, W. Raberg, M. Heinzig, C. J. Jenks, T. Lograsso, D. Delaney and P. A. Thiel, (1998) in preparation.

36. F. Shi, Z. Shen, D. W. Delaney, A. I. Goldman, C. J. Jenks, M. J. Kramer, T. Lograsso, P. A. Thiel and M. A. Van Hove, *Surface Science* (1998) in press.

37. A. J. Bradley and H. J. Goldschmidt, *J. Inst. Met.* **65** (1939) 389-401.

38. P. Villars and L. D. Calvert, *Pearson's Handbook of Crystallographic Data for Intermetallic Phases*, Series Ed., **1** (ASM International, Materials Park, Ohio, 1991).

39. M. Henzler, *Surface Sci.* **22** (1970) 12.

40. D. K. Flynn, W. Wang, S.-L. Chang, M. C. Tringides and P. A. Thiel, *Langmuir* **4** (1988) 1096.

41. C. J. Jenks, S.-L. Chang, J. W. Anderegg, P. A. Thiel and D. W. Lynch, *Phys. Rev. B* **54** (1996) 6301.

42. In the previous in-situ high energy irradiation studies by R. Wang et al. (Ref. 24-26), the electron transparent region was fully penetrated by the Ar ions. This disrupted the quasicrystal through the full thickness of the analyzed region, not just at the surface, as in this study. Hence, the crystallographic relationships in the previous work are more tenuous since the bulk transformation involves both nucleation and growth of the new phase. In the irradiation experiments, the b phase probably nucleated tens of microns away from the remaining quasicrystalline region, not nanometers away as in this study.

43. A. L. Mackay, *Acta Cryst.* **15** (1962) 916-918.

44. D. C. Koskenmaki, H. S. Chen and K. V. Rao, *Phys. Rev. B* **33** (1986) 5328-5332.

45. M. Audier, P. Sainfort and B. Dubost, *Phil. Mag. B* **54** (1986) L105-L111.

46. X. Zhang and K. F. Kelton, *Phil. Mag. Lett.* **63** (1991) 39-47.

47. M. Kottcke, H. Graupner, D. M. Zehner, L. Hammer and K. Heinz, *Phys. Rev. B* **54** (1996) R5275-R5278.

48. D. Naumovic, (1997) private communication.

49. M. Heinzig, (1998) unpublished results.

Figure Captions.

Figure 1. LEED patterns at normal incidence. (a) pseudo-twofold pattern of Al-Pd-Mn twofold surface obtained by annealing at 600 K for 3.5 hours. E=110 eV; (b) twofold pattern of Al-Pd-Mn twofold surface obtained by annealing at 900 K for 4 hours. E=110 eV; (c) pseudo-threefold pattern of Al-Pd-Mn threefold surface obtained by annealing at 650 for 1 hour; (d) threefold pattern of Al-Pd-Mn threefold surface obtained by annealing at 700 K for 1 hour. E=60 eV; E=60 eV; (e) pseudo-tenfold pattern of Al-Pd-Mn fivefold surface obtained by annealing at 650 K for 0.5 hour. E=50 eV; (f) fivefold pattern of Al-Pd-Mn fivefold surface obtained by annealing at 800 K for 2 hours. E=50 eV; (g) pseudo-tenfold pattern of Al-Cu-Fe fivefold surface obtained by annealing at 500 K for 0.5 hour. E=150 eV; (h) fivefold pattern of Al-Cu-Fe fivefold surface obtained by annealing at 850 K for 1 hour. E=150 eV.

Figure 2. Temperature dependence of the LEED intensities and domain size for the low temperature patterns (solid circles) and high temperature patterns (open circles). (a) Al-Pd-Mn twofold surface; (b) Al-Pd-Mn threefold surface (solid triangles are the first crystalline phase after sputtering); (c) Al-Pd-Mn fivefold surface; (d) Al-Cu-Fe fivefold surface. These intensities were all measured at 120 K, after heating to the temperature indicated.

Figure 3. (a) Pseudo-tenfold LEED pattern of Al-Cu-Fe obtained after annealing at 500 K for 0.5 hour. E=70 eV; (b) Single domain LEED pattern obtained by annealing at 550 K for 2 hours.

Figure 4. LEED patterns and schematic drawing of Al-Pd-Mn twofold surface after sputtering and annealing at 750 K for 5 hours, E=60 eV. Both cubic and quasicrystal patterns are present. (a) two domains of cubic phase; (b) one domain of cubic phase.

Figure 5. (a) LEED pattern of Al-Pd-Mn threefold surface just after sputtering; (b) with schematic drawing of three domains (or facets), E=45 eV.

Figure 6.Widths of two symmetry-equivalent LEED spots, as a function of electron wavelength. Minima correspond to out-of-phase scattering, and maxima correspond to in-phase scattering.

Figure 7. Structure models of (a) cubic close packed (ccp) cluster; (b) icosahedral packed (ip) cluster. Top row is side view, and bottom row is top view

Figure 8. Stereographic projection of (a) cubic [1 1 1] zone axis; (b) icosahedral threefold zone axis. The azimuthal relationship between the two projections is that proposed in this paper. The high-symmetry axes which are parallel, or nearly so, in the two structures are labeled.

Figure 9. Stereographic projection of icosahedral (a) twofold surface; (b) fivefold surface.

Figure 10. Simulated LEED patterns of (a) cubic (1 1 1) surface; (b) icosahedral threefold surface; (c) cubic (1 1 0) surface; (d) icosahedral twofold surface.

Figure 11. SADP patterns of an i-Al-Cu-Fe single grain (a) at room temperature, and (b) after heating to 970 K. The arrow in (a) denotes a (1 1 0)-type reflections, and in (b) it denotes one of the icosahedral twofold reflections.

Figure 12. Stereographic projection of (a) cubic [1 1 1] zone axis; (b) icosahedral threefold zone axis. The azimuthal relationship between the two projections is that proposed by Mackay. The high-symmetry axes which are parallel, or nearly so, in the two structures are labeled.

Table 1. Auger compositions after sputtering and annealing to different temperatures. ICP-AES compositions are for samples cut from the same boule, and in most cases for a sample immediately adjacent to the one used in the UHV experiments.

1a. Al-Pd-Mn twofold surface (ICP-AES composition: $Al_{71.0}Pd_{19.8}Mn_{9.2}$)

Annealing T (K)	Al%	Pd%	Mn%	LEED pattern
300 K	61±3	33±3	6±1	no pattern
600 K	68±2	27±2	5±2	two domains of cubic (110)
900 K	73±2	19±2	7±1	twofold quasicrystal

1b. Al-Pd-Mn three fold surface (ICP-AES composition: $Al_{71.7}Pd_{21.8}Mn_{6.5}$)

Annealing T (K)	Al%	Pd%	Mn%	LEED pattern
300 K	49±2	45±2	5±1	three facets
600 K	62	36	2	three facets + cubic (111)
800 K	74±1	20±2	6±1	threefold quasicrystal

1c. Al-Pd-Mn fivefold surface (ICP-AES composition: $Al_{71.3}Pd_{19.1}Mn_{9.6}$)

Annealing T (K)	Al%	Pd%	Mn%	LEED pattern
300 K	52±2	43±2	5±1	no pattern
600 K	63±3	33±2	4±2	five domains of cubic (110)
850 K	71±1	23±2	6±1	fivefold quasicrystal

1d. Al-Cu-Fe fivefold surface (ICP-AES composition: $Al_{63.4}Cu_{24.0}Fe_{12.6}$)

Annealing T (K)	Al%	Cu%	Fe%	LEED pattern
300 K	54±2	22±1	24±1	no pattern
600 K	64±1	18±1	18±1	five domains of cubic (110)
800 K	72±1	18±1	10±1	fivefold quasicrystal

Table 2a. Observed relations between symmetry axes in icosahedral and CsCl-type systems. Results from different groups are listed separately.

Icosahedral axis	Parallel CsCl axis-type in Fe-Ti [28, 29]	Parallel CsCl axis-type in Al-Cu-Fe [23]	Parallel CsCl axis-type in Al-Cu-Fe [24-26]	Parallel CsCl axis-type in Al-Pd-Mn and Al-Cu-Fe (present work)
2f	[110] or [112]	[110] or [111]	[111]	[110]
5f	[110]	[110]	[110] or [113]	[110]
3f	[111]	[111]		[111]

Table 2b. Observed relations between symmetry axes in icosahedral and bcc-type systems.

Icosahedral axis	Parallel bcc axis-type in Al-Si-Mn [44]	Parallel bcc axis-type in Al-Cu-Li [45]	Parallel bcc axis-type in Ti-Si-V [46]
2f	[001]	[001]	[001]
5f	~[530]	~ [530]	~ [530]
3f	[111]	[111]	[111]

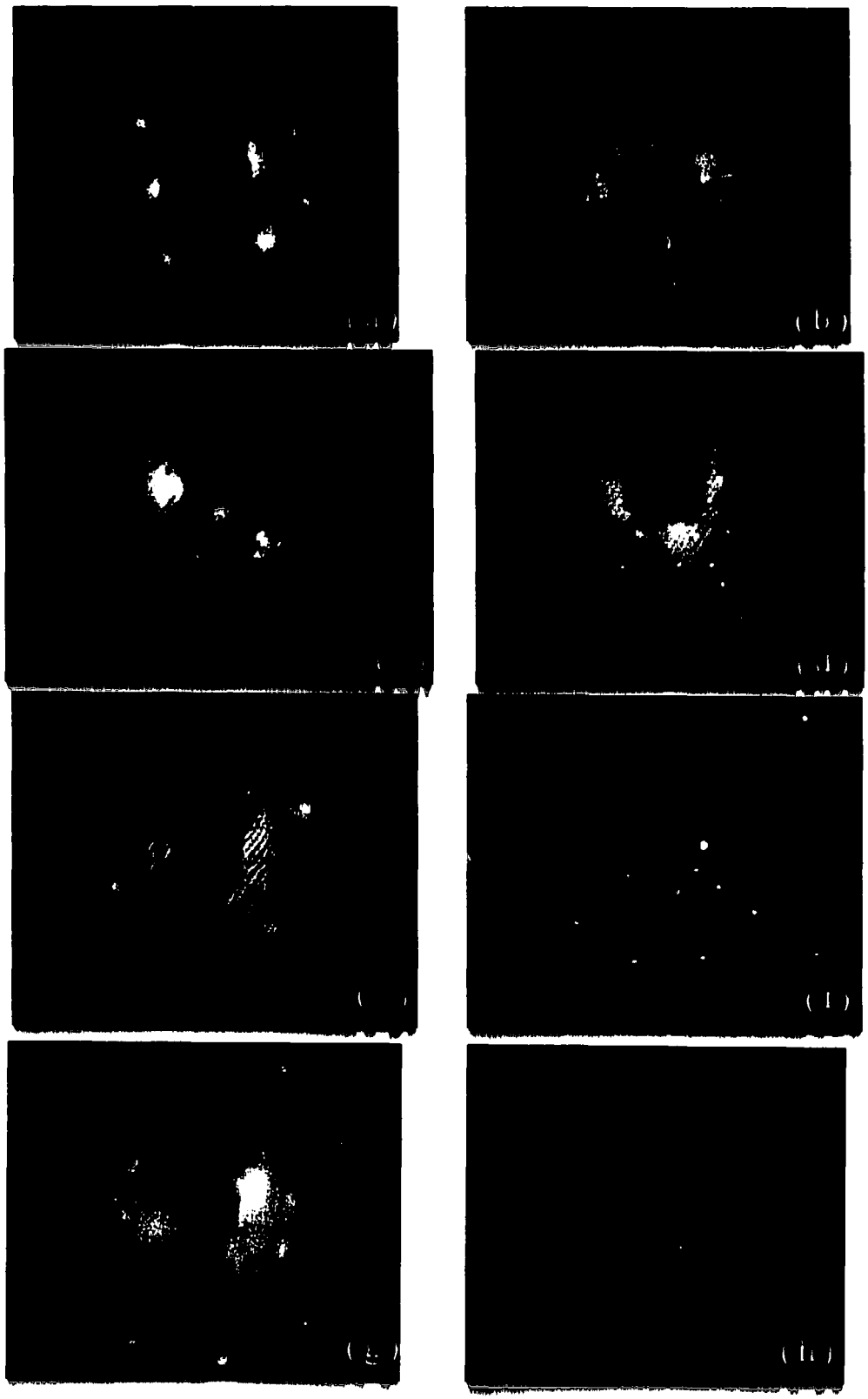

Fig. 1

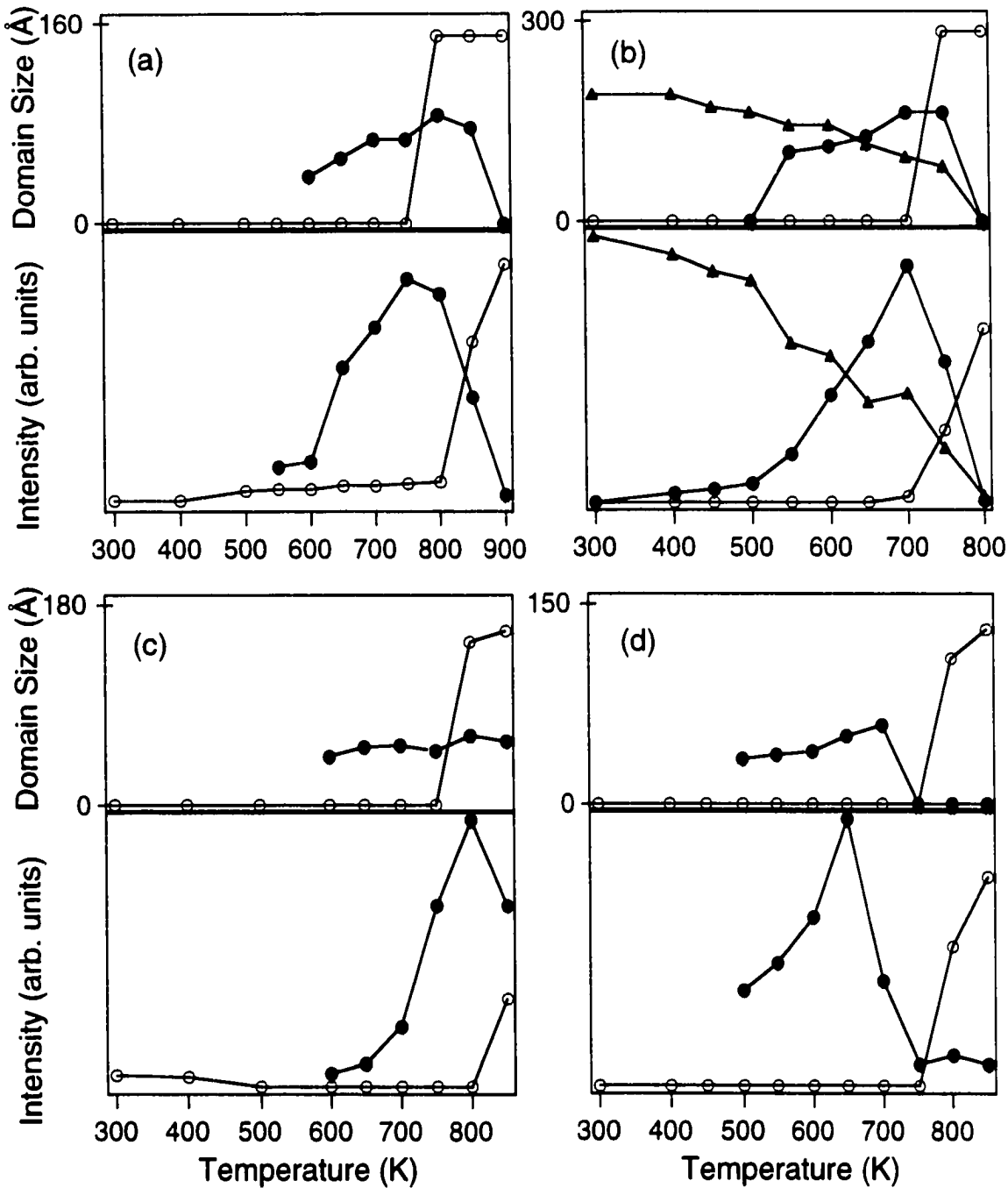
(a)
(b)
(c)
(d)
Domain Size (Å)
Intensity (arb. units)
160
0
300
180
150
300 400 500 600 700 800 900
Temperature (K)

Fig. 2

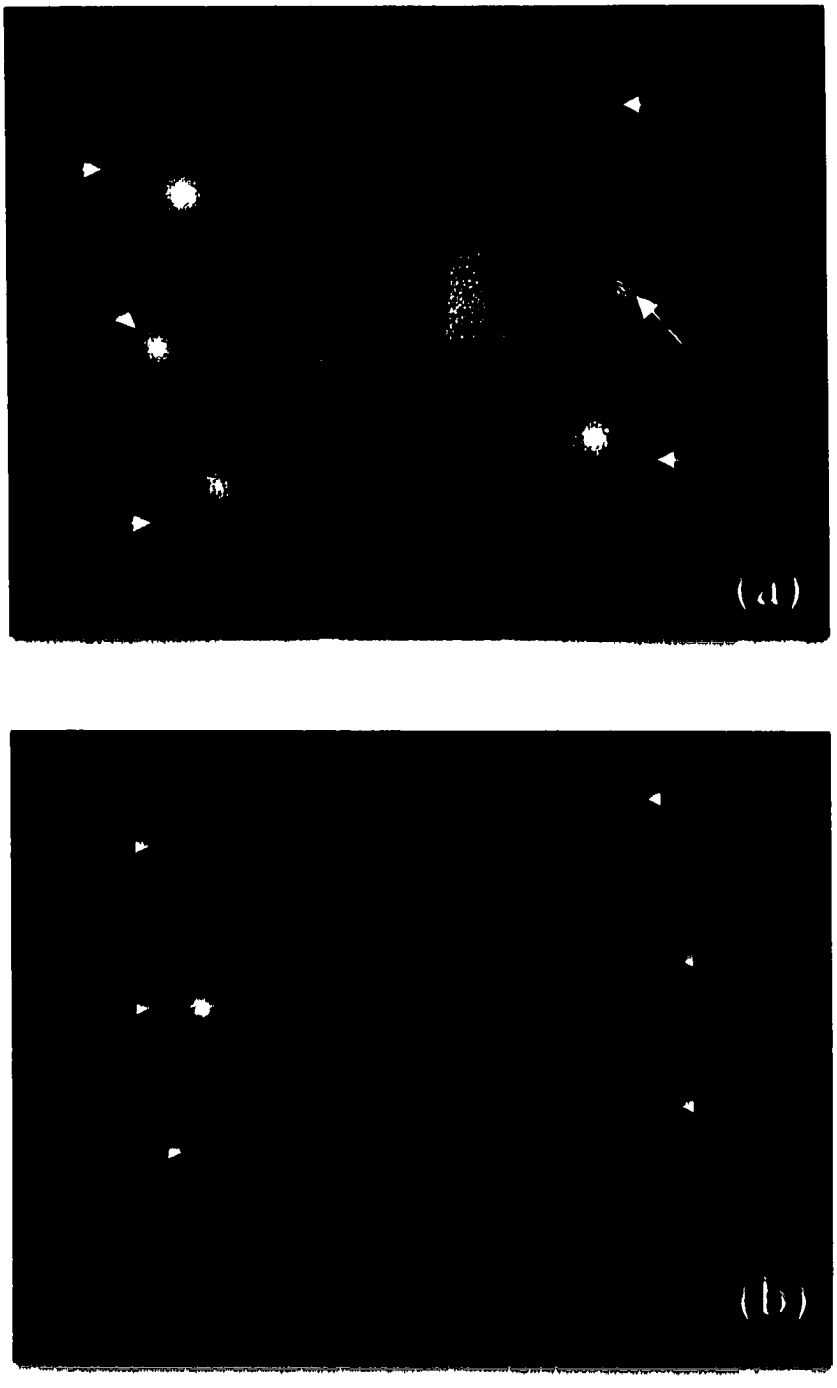

Fig. 3

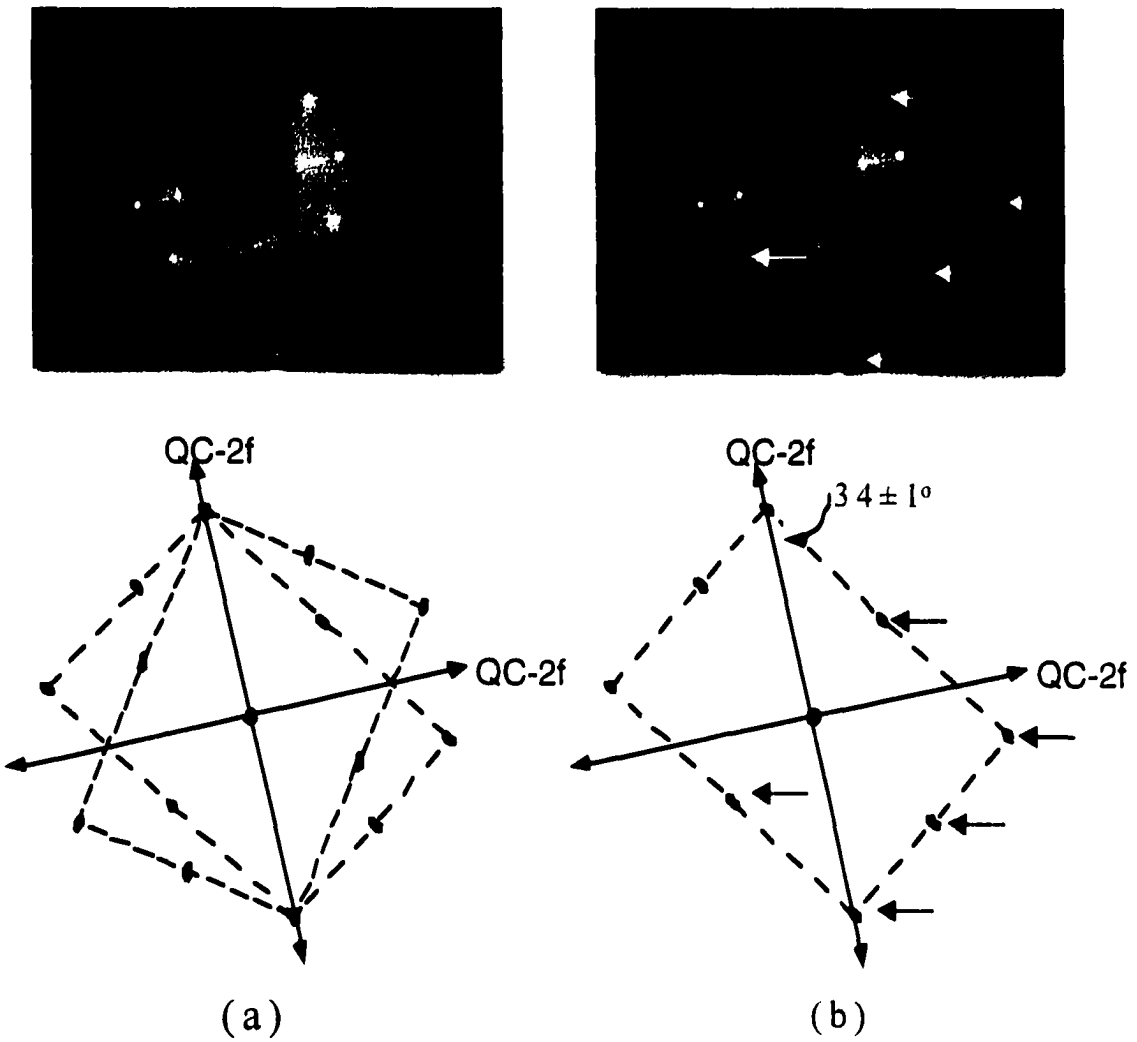

Fig. 4

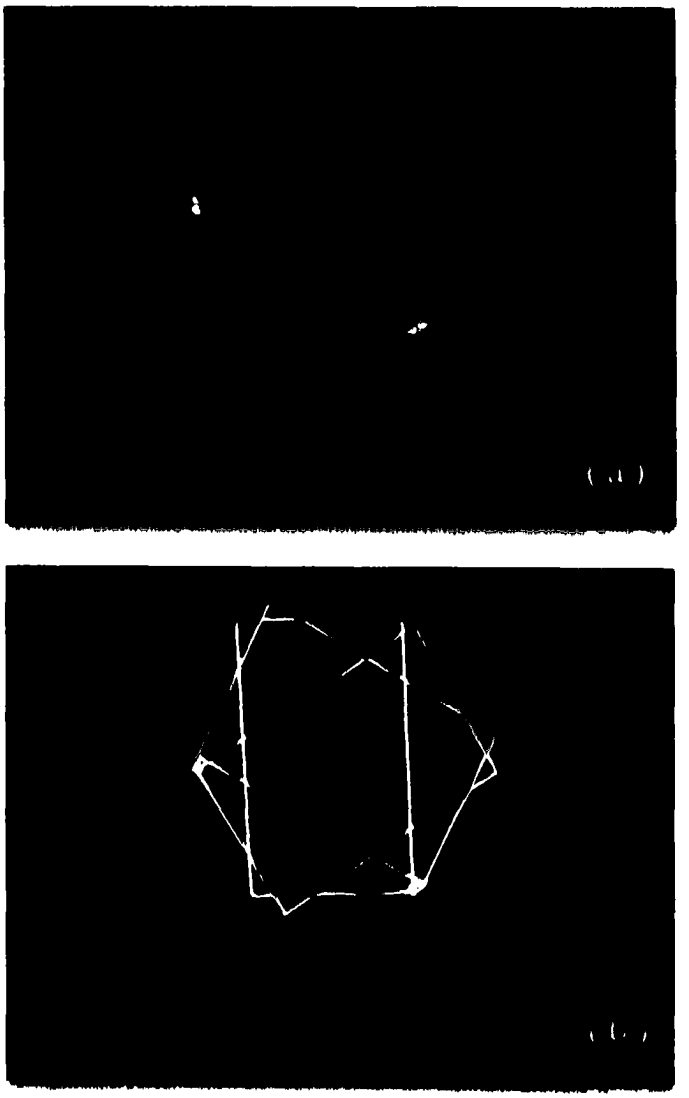

Fig. 5

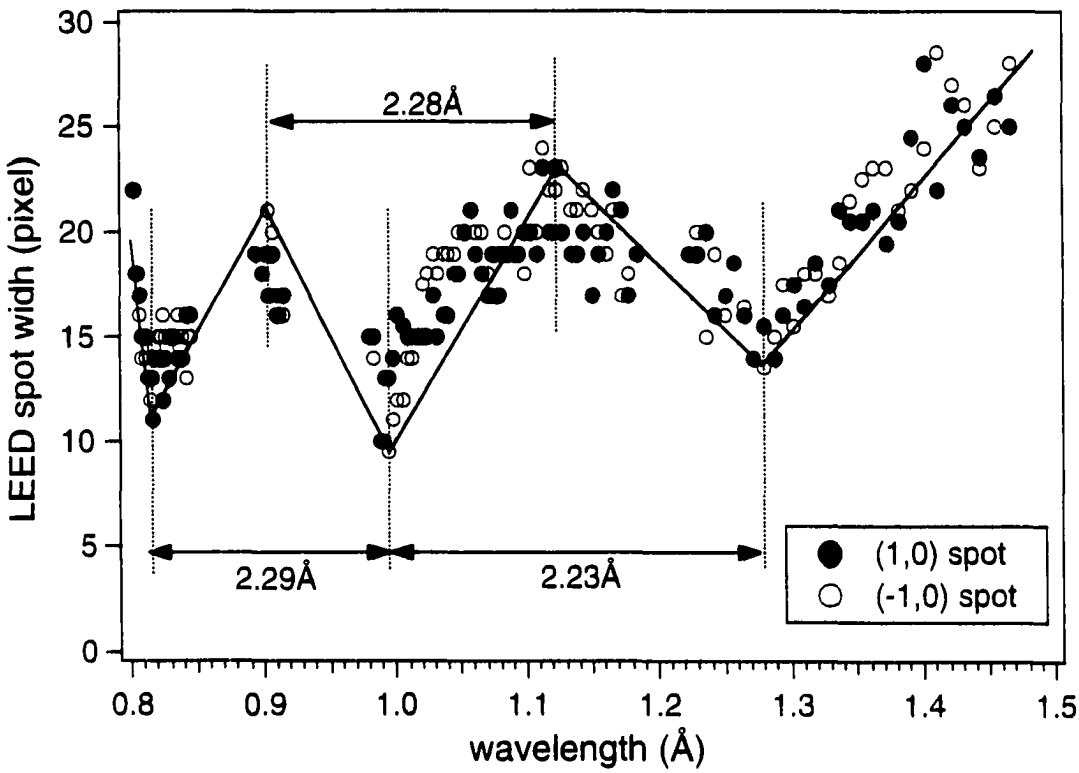
30
25
20
15
10
5
0
LEED spot widh (pixel)
2.28Å
2.29Å
2.23Å
(1,0) spot
(-1,0) spot
0.8
0.9
1.0
1.1
1.2
1.3
1.4
1.5
wavelength (Å)

Fig. 6

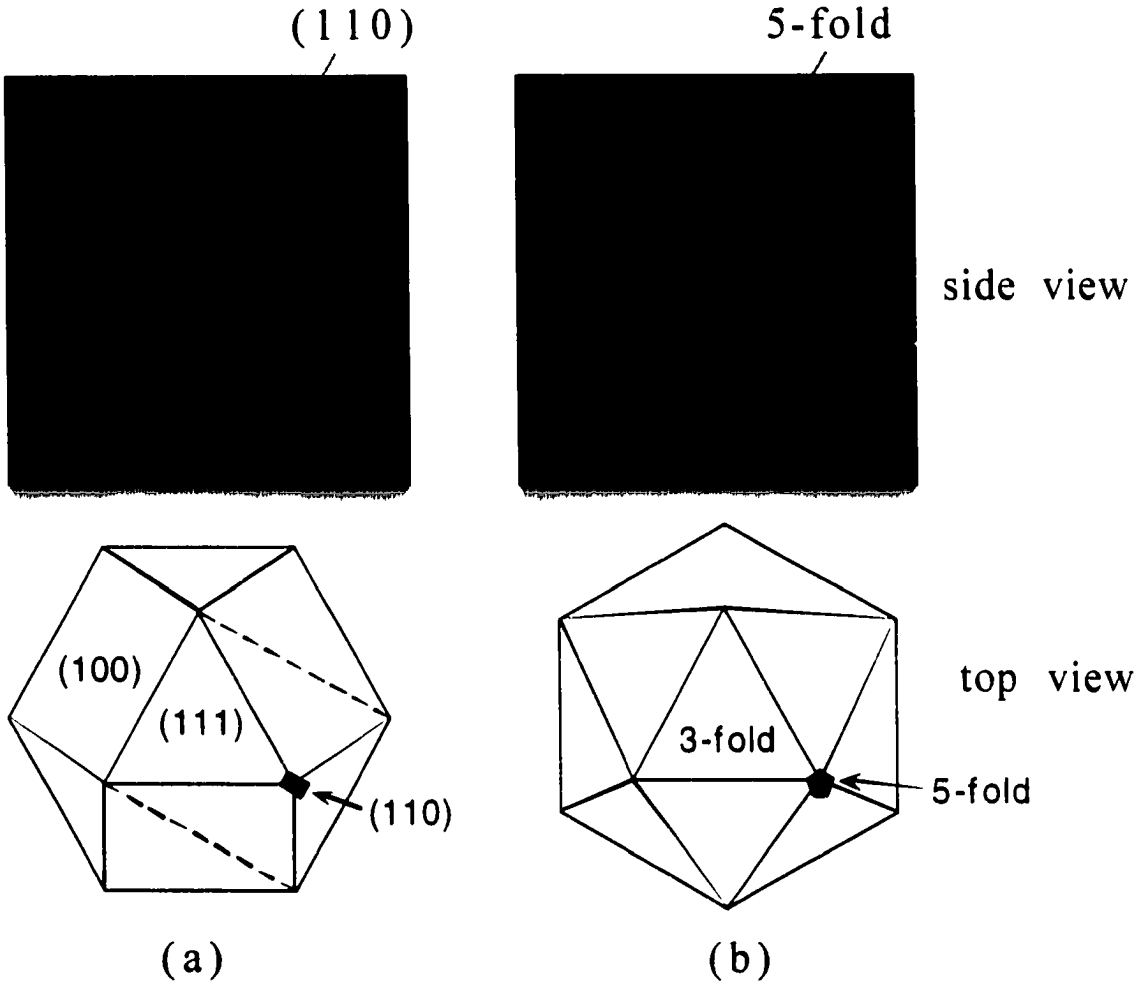

Fig. 7

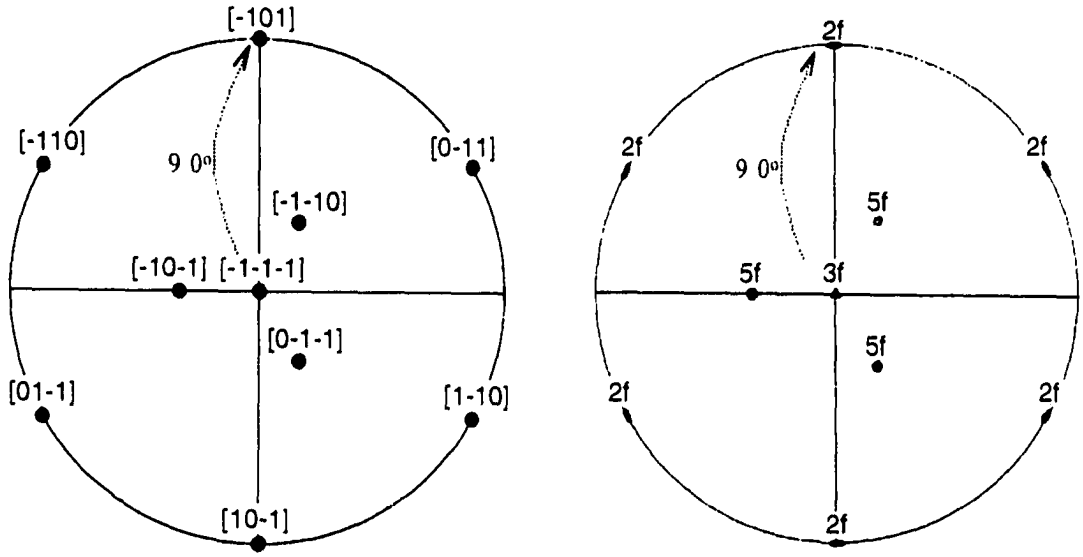
[-101]
[-110]
[0-11]
9 0°
[-1-10]
[-10-1]
[-1-1-1]
[0-1-1]
[01-1]
[1-10]
[10-1]
2f
2f
2f
9 0°
5f
5f
3f
5f
2f
2f
2f

(a) (b)

Fig. 8

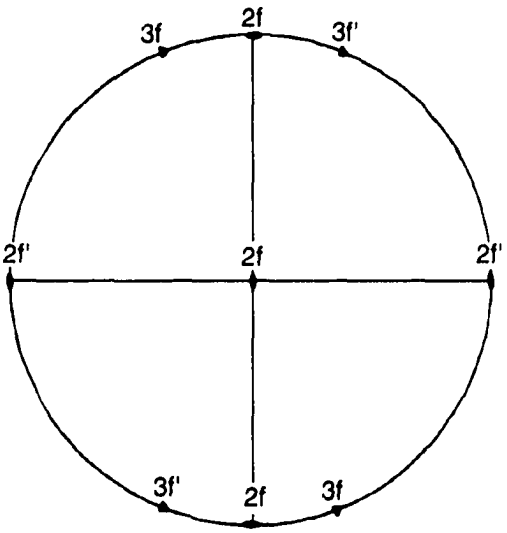

(a)

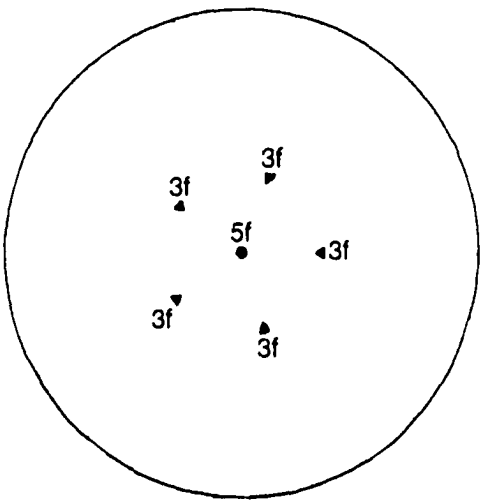

(b)

Fig. 9

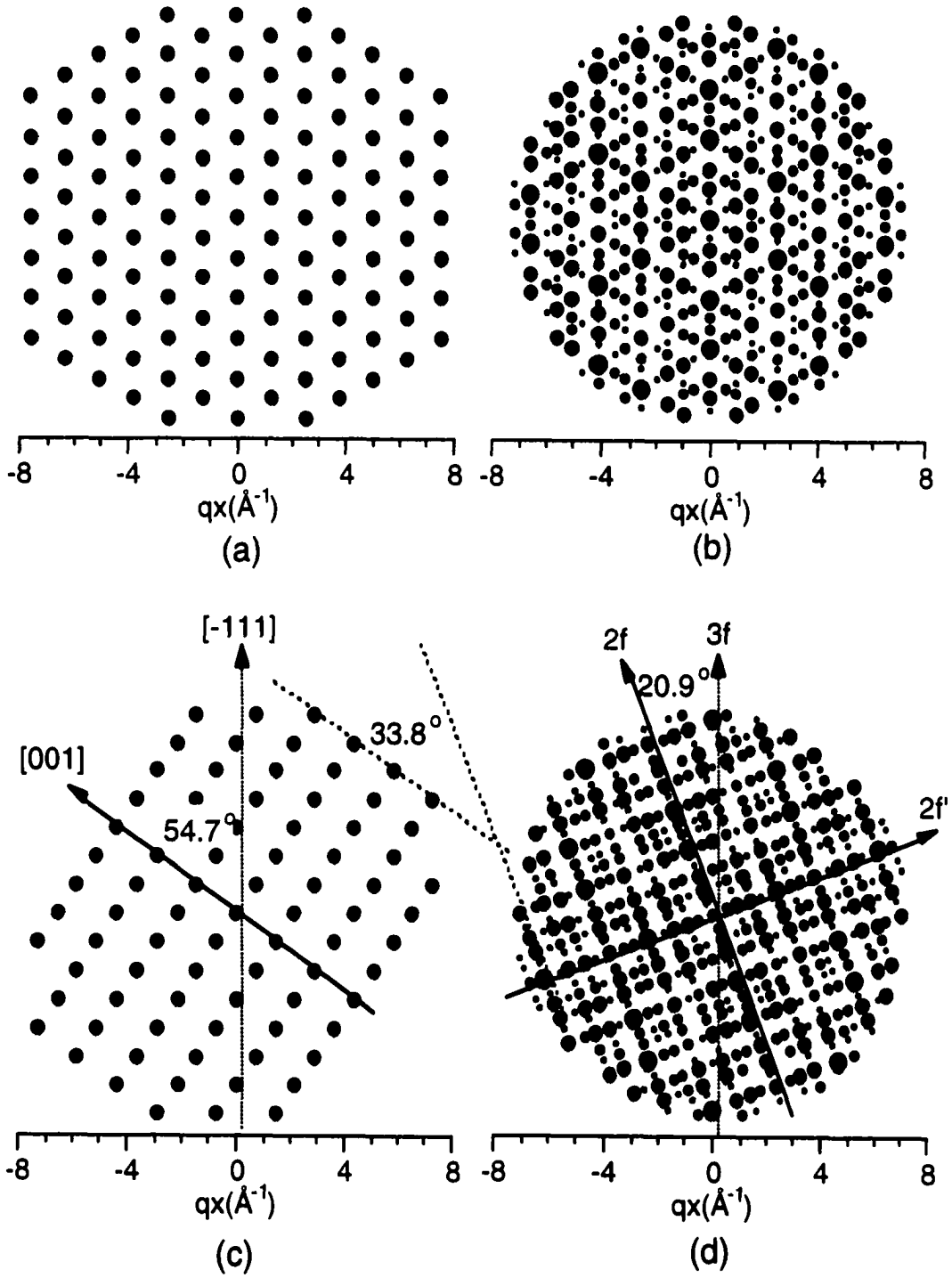

Fig. 10

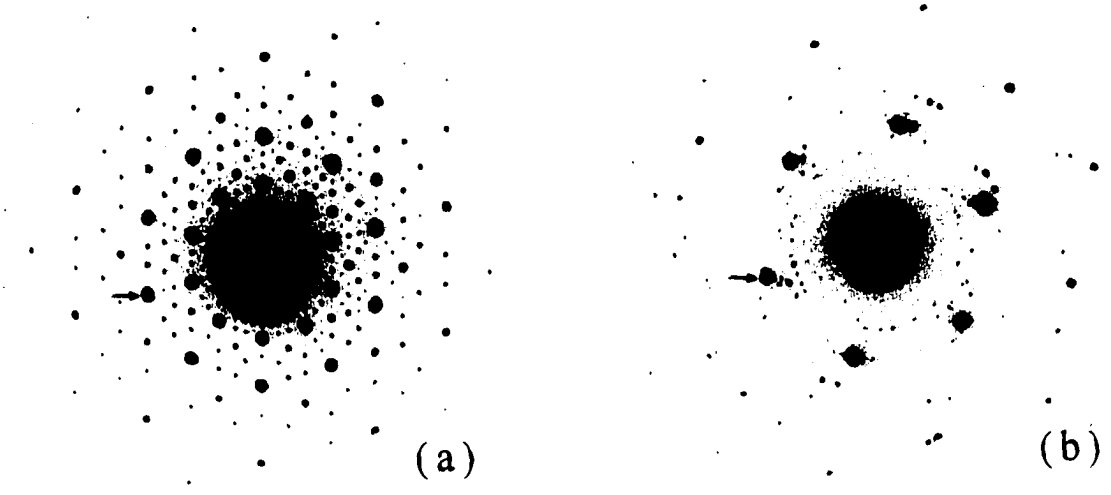

Fig. 11

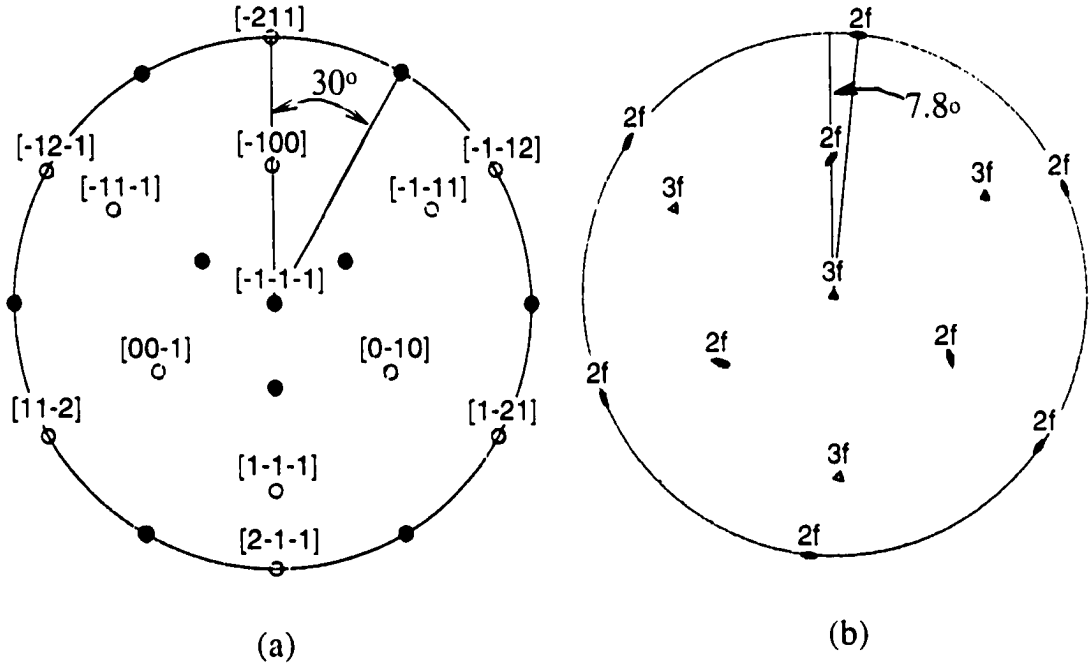

(a) (b)

Fig. 12

A COMPARISON OF THE THREE HIGH-SYMMETRY SURFACES OF Al-Pd-Mn QUASICRYSTALS

A paper to be submitted to Surface Science

Z. Shen, W. Raberg, M. Heinzig, C. J. Jenks, P. J. Pinhero, M. Gierer, M. A. Van Hove, T. Lograsso, D. Delaney, T. Cai, and P. A. Thiel*

Keywords: Low energy electron diffraction (LEED); Aluminum; Alloys; Metallic surfaces.

Abstract. Based upon LEED and XPS data, the three high-symmetry surfaces of icosahedral Al-Pd-Mn are very similar, both structurally and electronically. We do not see evidence of massive reconstruction, although a subtle rearrangement, e.g. to a high-order approximant, cannot be ruled out. If the surface has the structure of the bulk icosahedral phase (with, however, probable surface relaxations), then a set of terminations is postulated which maximizes the density of pseudo-Mackay icosahedra tangent to the surface. The densities of these clusters, plus the high atomic densities and Al-rich compositions, may act in concert to stabilize all three high-symmetry surfaces.

1. Introduction.

Quasicrystals, discovered in 1982 by Shechtman,[1,2] are typically binary and ternary metallic alloys, often containing 60 to 70 atomic percent aluminum. They present unique structural features,[3-6] coupled with unusual combinations of physical properties.[7,8] Some of the interesting properties of quasicrystals, such as low friction and 'non-stick' character,

*Corresponding author: Fax 515-294-4709 email thiel@ameslab.gov

involve surface phenomena. This motivates fundamental studies of structure, composition, and chemical reactivity of their surfaces.

This paper focuses on one particular alloy, Al-Pd-Mn. The bulk alloy is icosahedral and, as such, exhibits three high-symmetry axes: five, three, and two-fold. These axes are perpendicular to the three possible high-symmetry surfaces. The relative stabilities of these three surface types has long been of interest in the quasicrystal community,[9] motivated by the simple observation that small grains of some icosahedral alloys grow with beautiful facets. Triacontahedra and dodecahedra, as well as more complex structures, have been observed, depending on alloy type.[10] (Perfect dodecahedra expose 12 fivefold facets, whereas triacontahedra expose 30 twofold facets, and icosahedra expose 20 threefold facets. All are compatible with icosahedral symmetry; more complex structures can be created from superpositions of these.)

For i-Al-Pd-Mn, grains as well as voids can be grown exposing fivefold faces (dodecahedra)[Beeli, 1992 #1443 and threefold plus fivefold faces (icosadodecahedra)[10,11]. Assuming that thermodynamics predominate in selection of facets, these data suggest that the relative surface stabilities are: 5f _ 3f > 2f.

Hence, it is of interest to compare clean, high-symmetry surfaces of quasicrystals, to determine whether differences in stability can be detected. It is well-known that clean *crystalline* materials can have different surface stabilities depending upon surface symmetry. These different stabilities are often distinguished by the tendency to reconstruct.[12] (Reconstruction is a lateral perturbation from the bulk-terminated atomic positions.) A general rule of thumb is that the least-dense surfaces are most prone to reconstruct.[12]The present comparison is a limited test of the extent to which our understanding of crystalline surfaces can be extrapolated to quasicrystalline surfaces.

2. Experimental Details.

The i-Al-Pd-Mn samples used in these experiments were grown via the Bridgeman technique.[13] The grains were harvested from boules, and oriented to the selected zone axes within 0.25° using Laue X-ray diffraction. The nominal composition (i.e. the initial liquid composition used in growth) of each sample is $Al_{72}Pd_{19.5}Mn_{8.5}$. Prior to experiments, scanning Auger and electron microscopies showed the samples to be single-phase.

The LEED experiments were performed in a well-equipped ultrahigh vacuum (UHV) chamber,[14] with a typical base pressure of 3×10^{-11} Torr. There, the sample was cleaned with cycles of Ar ion bombardment and annealing, to a maximum of 900 K. Elsewhere, we provide details of our surface preparation techniques,[15] and the conditions of the XPS experiments.[16]

3. Experimental Results.

For all three surfaces, the observed LEED patterns can be divided into three categories. We call these cubic, facetted, and quasicrystalline(-like).

The first type of pattern results after sputtering, and usually requires annealing in the range 500-700 K. These patterns (with one exception) can be assigned to crystalline overlayers of the cubic CsCl (B2) structure.[17,18] They are characterized by broad spots, corresponding to real-space domains of size 40-80 Å, and high backgrounds. These patterns are discussed extensively elsewhere.[17]

The second type of LEED pattern, the facetted one, typically appears after annealing in the temperature range 800 to 900 K. It often coexists with the quasicrystalline(-like) pattern, although the two are not distributed uniformly over the surface. This non-uniformity suggests that the facets may form preferentially at chemical or structural defects. The signature of facetting in LEED is the non-convergence of spots toward the center of the LEED optics as beam voltage increases, using normal incidence.[19,20]

Facetting has been reported previously by Chevrier, et al. for fivefold and twofold surfaces that were heated to unspecified temperatures in ultrahigh vacuum; the facets were imaged as depressions, and were attributed to sublimation.[21]Facets have also been observed on the twofold surface by Schaub et al., who found fivefold microfacets after heating close to the melting point, 1100 K.[22-25] In our experiments, no facetting is observed for fivefold surfaces when heated to temperatures of 900 K or below. Facets are observed, however, for twofold[26] and threefold surfaces after annealing at these temperatures. Our data cannot distinguish between facets as depressions or protrusions.

This paper concerns mainly the third type of LEED pattern. Such patterns are obtained by annealing to temperatures in the range 700-900 K, and are shown in the top three frames of Fig. 1. These patterns are characterized by very sharp, dense LEED spots. The widths of the spots correspond to a real-space dimension greater than 150 Å,[17] and the widths are instrument-limited in the low-resolution experiments. A high-resolution LEED study on the fivefold surface shows that the average domain size is about 900 Å (again, close to the resolution limit of the instrument). The data from the high- and low-resolution experiments are compared in Fig. 2, for similar conditions of sample preparation. The existence of large terraces, with average lengths in the range of hundreds of Å, is also supported by data from scanning probe microscopies. Such data are available for the fivefold surface of Al-Pd-Mn,[21] and for the threefold surface of Al-Pd-Mn.[27]

A second type of information to be extracted from the LEED patterns concerns the arrangements of the diffraction spots, and whether this arrangement is consistent with expectations for the bulk-terminated structure. For a crystalline material, it is straightforward to predict the arrangement for a low-index surface, and to compare this prediction with experiment. However, this prediction and comparison is not so trivial for a quasicrystalline material. The approach we use is to project an x-ray diffraction pattern taken along the

appropriate zone axis, onto the conditions of the LEED experiment. To calculate the patterns we employed the bulk x-ray structure factors measured by Boudard et al. for the icosahedral phase of Al-Pd-Mn,[28] and used these to assign a relative intensity to rods of scattering parallel to the surface normal. The predictions based on x-ray data are shown in the bottom panels of Fig. 1.

First, consider the gross symmetries of the patterns. The surface cut perpendicular to the twofold axis displays a LEED pattern (Fig. 1a) with twofold, rectangular symmetry, consistent with the projection from x-ray scattering shown in Fig. 1d. An interesting observation here is that the LEED pattern from the twofold surface differs considerably from the higher energy transmission electron microscopy (TEM) patterns taken along the twofold axis. The differences arise from both the lower energy (and hence larger curvature of the Ewald sphere) for the LEED measurements, and from the fact that 2D scattering is characterized by rods rather than points of intensity. In fact, the LEED pattern measured from the twofold surface is misleadingly similarity to the TEM pattern of the "pseudo-twofold" orientation.[Shen, 1997 #1518] Hence, it is important to project carefully the conditions of one diffraction experiment onto the other.

The symmetries of the LEED patterns of the other two surfaces are also consistent with expectation, as seen by comparing the top and bottom panels of Fig. 1. At the electron energies chosen for Fig. 1, the threefold surface (Fig. 1b) seems nearly sixfold, and the fivefold surface (Fig. 1c) seems tenfold. However, at other energies these symmetries are reduced clearly to threefold and fivefold, respectively. Patterns at other energies are shown in Fig. 3 for the threefold surface, and are shown elsewhere for the fivefold surface, .[14,15,29]. Again, the differences in symmetry between the LEED and x-ray diffraction patterns (threefold vs. sixfold, and fivefold vs. tenfold), are due to differences in the scattering conditions.

Predictions of relative spot intensities also compare well with experiment under the conditions of Fig. 1, which is somewhat surprising, given that LEED intensities are highly

sensitive to multiple scattering whereas x-ray data are not. Presumably, at the energies chosen for Fig. 1, kinematic scattering happens to dominate in LEED, making the comparison appear optimal. At other energies, the relative intensities change dramatically, as one would expect. See, for instance, Fig. 3. A more rigorous comparison between calculated and experimental data might be made if the experimental data could be energy-averaged. This was not feasible in our work, however, because different spots were visible over much different energy ranges.

A final aspect of information contained in the data is the spot spacing, both absolute and relative. The spot spacings are shown in Table 1. The parameter k_j is the magnitude of the component of the scattering vector which is parallel to the surface, in $Å^{-1}$. Each index j denotes a set of intense diffraction spots which are equidistant from the specular beam. First, consider the absolute values of k_j. It can be seen that the measured values are consistently larger than those predicted from bulk data, the deviation being in the range 3 to 8 %. This corresponds to the (quasi)lattice constant of the surface being smaller than that of the bulk by the same percentage. Note that LEED is not a good technique generally for measurement of absolute lattice constants, because systematic errors arise if the sample is not exactly at the focal point of the LEED optics. However, a similar reduction of k, relative to the bulk value, was found in a LEED study of another icosahedral alloy in our laboratory, [30] and also in the LEED and STM work of Schaub, et al.[22-25] The persistence of this trend in various measurements and among various laboratories, indicates that it could be a real effect.

Ratios of distances should be affected less by such a possible error than absolute values. Table 1 also shows such ratios for the major spots. A similar analysis has been implemented by Schaub, et al. for the fivefold surface. [23] The ideal ratios in Table 1 are again taken from the calculations (e.g. Fig. 1d-f). It can be seen that the ideal ratios should equal the golden mean, τ ($\tau = 1.618$), raised to integral powers. For instance, for the threefold and fivefold surfaces,

$$\frac{k_j}{k_0} = \tau^j$$

Table 1 shows that the measured ratios equal the predicted ones, within experimental uncertainty, for all three surfaces.

In short, the LEED patterns observed after annealing in the range 700-900 K are consistent with expectations for the bulk quasicrystal, for all three surfaces. If this assignment is correct, the surface is probably not truly bulk-terminated. Rather, a contraction of the first interlayer spacing has been postulated for the fivefold surface from electron- and x-ray-based structure determinations.[29,31,32] Such a relaxation would, in principle, not be detected in the LEED spot spacings or arrangements, because it would not necessarily change the lateral surface structure.

The data could also be compatible with a high-order approximant. In fact, it has been proposed[8] that the LEED pattern of the fivefold surface is a pentagonal approximant, analogous to the two known to exist in the Al-Cu-Fe system.[33] Spot spacings and intensities in an approximant can be very similar to those in the parent quasicrystal.[6] One would expect a pentagonal approximant to show the greatest deviation from quasicrystallinity in the LEED patterns of the twofold surface, which should contain a fivefold periodic axis.[33] Such a deviation is not apparent (Fig. 1a), but could be very subtle. Hence, our data cannot distinguish between the two possibilities conclusively. In order to acknowledge both possibilities, we call these LEED patterns quasicrystalline(-like).

Data are also available which allow some comparison of the electronic structure of the three high-symmetry surfaces. We have previously reported that the fivefold[16] and twofold[26] quasicrystalline(-like) surfaces display a distinctively narrow and symmetrical line in X-ray photoelectron spectroscopy (XPS) for the Mn $2p_{3/2}$ transition. This result has been reproduced

for the fivefold surface by Chevrier et al.[34]This distinctive lineshape exists for the threefold surface as well, as shown in Fig. 4. There, the Mn $2p_{3/2}$ transition is shown directly after sputtering at room temperature (Fig. 4a), after annealing to conditions known to produce the CsCl (B2) structure[17] (Fig. 4b), and after annealing to conditions known to produce the quasicrystalline(-like) surface (Fig. 4c). The full-width at half-maximum (FWHM) is also given for each curve. The FWHM of the line is large for the sputtered, and CsCl-type surfaces, but decreases sharply for the quasicrystalline(-like) surface. The final FWHM of 1.08 eV falls between those reported previously for the twofold and fivefold quasicrystalline(-like) surfaces: 1.13 and 1.01 eV, respectively.[16,26] (The difference between the values is probably within experimental uncertainty.) This similarity indicates that the narrow, relatively symmetric shape of the line is characteristic of all three high-symmetry surfaces when treated under similar conditions. We have previously attributed this lineshape, on the fivefold surface, to a combination of two final-state effects: lifetime-broadening, combined with core-hole screening, both attributed to a reduction in the density of Mn states near the Fermi edge.[16] Such a reduction in density of Mn states is compatible qualitatively with the pseudogap, which is a signature of the bulk electronic structure.[35-37]

4. Discussion. Based upon the LEED and XPS data, the three quasicrystalline(-like) surfaces are very similar, both structurally and electronically. The conditions required for the formation of these structures—long anneals in the temperature range 700 to 900 K—are also very similar. These similarities are somewhat surprising, given that high-symmetry surfaces of a clean crystalline material often show more variation, particularly in their tendency to undergo massive lateral rearrangement (reconstruction).[12] In many cases, a reconstruction is understood as a rearrangement of the least-dense planes into a semblance of close-packing, and is marked by development of extra LEED spots at positions incompatible with the bulk-terminated structure. We do not see this, indicating that the quasicrystalline surfaces do not

undergo a massive lateral rearrangement. This is also supported by the XPS data. If one surface reconstructed massively (and the others did not), this would probably destroy the pseudogap and be evident as a significantly broader Mn $2p_{3/2}$ line in the XPS. We cannot rule out subtle rearrangements, however, such as reconstruction to a high-order approximant with an electronic structure similar to that of the quasicrystal. Apparently, the energetic differences between these three surfaces, which (presumably) cause the facetted grains and voids, are not large enough to be manifest in these experiments.

If we assume, for the moment, that the quasicrystalline(-like) surfaces are truly quasicrystalline, then the structures of the three high-symmetry surfaces may be, in fact, rather similar. We use the bulk structural model of Boudard, et al.,[28] for i-Al-Pd-Mn, to calculate the densities of the high-symmetry surfaces. We assume, after Janot, that the basic structural unit is the pseudo-Mackay icosahedron, and that this unit is extremely stable.[38-40] Then we postulate that the surface terminations are those which minimize the number of pseudo-Mackay clusters cut by the surface plane. The results are shown in Table 2.

Unlike a crystalline material, a quasicrystal has many possible types of bulk-like terminations. No two are identical in composition or structure. However, the terminations can be divided into groups that are self-similar.[29,31] The compositions and densities shown in each row of Table 2 are calculated for one particular type of termination, averaged over ten individual ones.

It can be seen that there are both differences and similarities between these terminations. Considering first the similarities, all three have two top planes that are separated by less than 1 Å, so the two planes might reasonably be considered a single puckered layer. This idea would be even more valid if all three surfaces exhibited a contraction of the spacing between the first and second layers, relative to the bulk value. Indeed, such a contraction (about 20%) has been measured for the fivefold surface, both using electron- and x-ray diffraction,[29,31,32] and a contraction of 23% has been suggested for the twofold surface on the basis of electron

diffraction.[41] Using this framework, the lateral densities of the two topmost layers combined vary by 21% across the high-symmetry faces. This is significantly less than for crystalline surfaces. For instance, in an fcc material, the density increases by 63% in going from bulk-terminated twofold, (110), to threefold, (111), surfaces. (This does not depend upon whether one considers only the topmost layer, or the two topmost layers combined.) In elemental Al, for instance, the surface density of the topmost plane falls between 0.0866 for the (110), and 0.141 $Å^{-2}$ for the (111). Because lateral density is known to stabilize surfaces, the relatively high density and small variation across the three quasicrystal terminations may contribute to their stability.

Alternatively, it could be that surface stability is controlled by the density of subsurface PMI's which are tangent to the topmost plane. This value also varies relatively little, from 0.0060 to 0.0073, across the high-symmetry surfaces.

A final similarity is in the composition of the topmost plane, which is always rich in Al, varying from 76 to 95 atomic %. The underlying plane is never as Al-rich as the top one, so that the combined composition of the two spans a range of lower values. Even this combined surface composition, however, is always predominantly Al, ranging from 63 to 72 atomic %. As we have pointed out previously,[29,31] an Al-rich composition is consistent with a lower surface energy than a Pd- or Mn-rich composition.

There are also differences between the three types of high-symmetry terminations described in Table 2. For instance, the bulk interplanar spacing between the top two planes in the fivefold surface is almost half that in the twofold surface. The relative densities of the first and second planes reverses upon going from the fivefold to the twofold or threefold. Differences in composition could also be emphasized.

The terminations in Table 2 were selected on the basis of the density of intact, or nearly-intact, PMI's, relative to other classes of termination. The idea that these terminations are real surfaces in fact has some substantiation, at least for the fivefold and twofold surfaces. For the

fivefold surface, a LEED structural analysis selected these types.[29] Recent X-ray scattering[32] and LEIS data[31] are consistent with the LEED result, although both suggest that the surface composition may be deficient in Mn. For the twofold surface, a LEED structural analysis has also selected the types of terminations shown.[41] There are no such data yet for the threefold surface.

A comparison to an approximant phase would, of course, be highly desirable. Such an approximant might be considered a subtle reconstruction of the surface. The approximant must have fivefold symmetry to be compatible with the fivefold symmetry of the LEED patterns, first observed by Schaub[23-25] but substantiated by other groups.[14,29,42] To be compatible with the fivefold symmetry, a pentagonal approximant has been suggested as an alternative candidate for the surface structure,[8] even though there is no pentagonal approximant known (yet) in the bulk Al-Pd-Mn system. The approximants known in Al-Pd-Mn are all decagonal or related in structure, although two pentagonal approximants are known in the related alloy, Al-Cu-Fe.[33] At present no atomic coordinates are available, even for Al-Cu-Fe, so a comparison of an approximant with our data, or with the postulated terminations of the bulk quasicrystal (Table 2), is not possible.

In conclusion, if the surface has the structure of the bulk icosahedral phase (with, however, possible surface relaxations), then we postulate that the surface terminations are those described in Table 2. These are the terminations which maximize the density of intact, or nearly-intact, PMI's tangent to the surface. For all three high-symmetry surfaces, such terminations consist of two planes of atoms separated by less than an Ångstrom. If the top two planes are considered as a single rumpled layer, then the variation of atomic density across the three low-index surfaces is significantly smaller than the variation across the three low-index surfaces of a crystalline material. Furthermore, all surfaces are Al-rich, a composition which should have a low surface energy relative to other possible terminations. These three

factors—similar densities of PMI's, high atomic densities, and Al-rich compositions—may act in concert to stabilize these surfaces.

Acknowledgments. M. Quiquandon and J. M. Dubois provided valuable comments and suggestions. This work was supported by the Director, Office of Energy Research, Office of Basic Energy Sciences, Materials Sciences Division, of the U.S. Department of Energy under Contract No. W-405-Eng-82.

References.

[1] D. Shechtman, I. Blech, D. Gratias and J.W. Cahn, Phys. Rev. Lett. 53 (1984) 1951.

[2] D. Shechtman and I. Blech, Metall. Trans. A 16 (1985) 1005.

[3] A.I. Goldman and M. Widom, Ann. Rev. Phys. Chem. 42 (1991) 685-729.

[4] P.W. Stephens and A.I. Goldman, Scientific American (April 1991) 24-31.

[5] C. Janot, Quasicrystals: A Primer (Clarendon Press, Oxford, 1992).

[6] A.I. Goldman and K.F. Kelton, Reviews of Modern Physics 65 (1993) 213-230.

[7] J.M. Dubois and P. Weinland "Coating materials for metal alloys and metals and method," CNRS, Nancy, France, 1993.

[8] J.M. Dubois, in: Introduction to the Physics of Quasicrystals; J.B. Suck, Ed. (Springer Verlag, Berlin, 1998), pp. in press.

[9] T.-L. Ho, in: Quasicrystals: The State of the Art; D.P. DiVincenzo and P. Steinhardt, Eds.; (World Publishing Co., 1991), pp. 403-428.

[10] C.M.H. Beeli, Ph.D. Dissertation, Technische Hochschule Zürich, 1992.

[11] A.P. Tsai, A. Inoue, Y. Yokoyama and T. Masumoto, Mat. Trans. JIM 31 (1990) 98.

[12] P.A. Thiel and P.J. Estrup, in: CRC Handbook of Surface Imaging and Visualization; A.T. Hubbard, Ed. (CRC Press, Boca Raton, Florida, 1995), pp. 407.

[13] D. Delaney, T.E. Bloomer and T.A. Lograsso, in: New Horizons in Quasicrystals: Research and Applications; A.I. Goldman, D.J. Sordelet, P.A. Thiel and J.M. Dubois, Eds.; (World Scientific, Singapore, 1997), pp. 45-52.

[14] S.-L. Chang, W.B. Chin, C.-M. Zhang, C.J. Jenks and P.A. Thiel, Surf. Sci. 337 (1995) 135-146.

[15] C.J. Jenks, P.J. Pinhero, Z. Shen, T.A. Lograsso, D.W. Delaney, T.e. Bloomer, S.-L. Chang, C.-M. Zhang, J.W. Anderegg, A.H.M.Z. Islam, A.I. Goldman and P.A. Thiel, in: Proceedings of the Sixth International Conference on Quasicrystals (ICQ6); S. Takeuchi and T. Fujiwara, Eds.; (World Scientific, Singapore, 1998), pp. 741-748.

[16] C.J. Jenks, S.-L. Chang, J.W. Anderegg, P.A. Thiel and D.W. Lynch, Phys. Rev. B 54 (1996) 6301.

[17] Z. Shen, M.J. Kramer, C.J. Jenks, A.I. Goldman, T. Lograsso, D. Delaney, M. Heinzig, W. Raberg and P.A. Thiel, Phys. Rev. B (1998) submitted.

[18] D. Naumovic, P. Aebi, L. Schlapbach, C. Beeli, T.A. Lograsso and D.W. Delaney, in: Proceedings of the Sixth International Conference on Quasicrystals (ICQ6); T. Fujiwara and S. Takeuchi, Eds.; (World Scientific, Singapore, 1998), pp. 749-756.

[19] K.-J. Song, R.A. Demmin, C. Dong, E. Garfunkel and T.E. Madey, Surface Sci. 227 (1990) L79.

[20] K.-J. Song, C.-Z. Dong and T.E. Madey, Langmuir 7 (1991) 3019.

[21] J. Chevrier, G. Cappello, F. Comin and J.P. Palmari, in: Proceedings of the Conference, "New Horizons in Quasicrystals: Research and Applications"; A.I. Goldman, D.J. Sordelet, P.A. Thiel and J.M. Dubois, Eds.; (World Scientific, Singapore, 1997), pp. 144-151.

[22] T.M. Schaub, D.E. Bürgler, H.-J. Güntherodt and J.B. Suck, Phys. Rev. Lett. 73 (1994) 1255-1258.

[23] T.M. Schaub, D.E. Bürgler, H.-J. Güntherodt, J.B. Suck and M. Audier, Appl. Phys. A 61 (1995) 491-501.

[24] T.M. Schaub, D.E. Bürgler, H.-J. Güntherodt and J.-B. Suck, Z. Phys. B 96 (1994) 93-96.

[25] T.M. Schaub, D.E. Bürgler, H.-J. Güntherodt, J.B. Suck and M. Audier, in: Proceeding of the 5th International Conference on Quasicrystals, Avignon, France, May 22-26 1995.; C. Janot and R. Mosseri, Eds.; (World Scientific, Singapore, 1995), pp. 132-138.

[26] Z. Shen, C.J. Jenks, J. Anderegg, D.W. Delaney, T.A. Lograsso, P.A. Thiel and A.I. Goldman, Phys. Rev. Lett. 78 (1997) 1050-1053.

[27] W. Raberg, Ph.D. Dissertation, Universität Bonn, 1998.

[28] M. Boudard, M. dexxBoissieu, C. Janot, G. Heger, C. Beeli, H.U. Nissen, H. Vincent, R. Ibberson, M. Audier and J.M. Dubois, J. Phys. C 4 (1992) 10149.

[29] M. Gierer, M.A.V. Hove, A.I. Goldman, Z. Shen, S.-L. Chang, C.J. Jenks, C.-M. Zhang and P.A. Thiel, Phys. Rev. Lett. 78 (1997) 467-470.

[30] Z. Shen, P.J. Pinhero, T.A. Lograsso, D.W. Delaney, C.J. Jenks and P.A. Thiel, Surf. Sci. Lett. 385 (1997) L923-L929.

[31] M. Gierer, M.A. VanxxHove, A.I. Goldman, Z. Shen, S.-L. Chang, P.J. Pinhero, C.J. Jenks, J.W. Anderegg, C.-M. Zhang and P.A. Thiel, Phys. Rev. B 57 (1998) 7628-7641.

[32] M.J. Capitan, J. Alvarez, J.L. Joulaud and Y. Calvayrac, Phys. Rev. Lett. (1998) submitted.

[33] M. Quiquandon, A. Quivy, J. Devaud, F. Faudot, S. Lefèbvre, M. Bessière and Y. Calvayrac, J. Phys.: Condens. Matter 8 (1996) 2487.

[34] J. Chevrier, G. Cappello, F. Schmithüsen, A. Dechelette, F. Comin and A. Stierle, (1998) in preparation.

[35] E. Belin, Z. Dankházi, A. Sodac, Y. Calvayrac, T. Klein and J.-M. Dubois, J. Phys.: Condens. Matter 4 (1992) 4459.

[36] E. Belin, Z. Dankházi and A. Sadoc, Mat. Sci. and Engineering A: Structural Mat. Prop. Microstr. and Processing 182 (1994) 1994.

[37] E. Belin-Ferré, V. Fournée and J.-M. Dubois, in: New Horizons in Quasicrystals: Research and Applications; A.I. Goldman, D.J. Sordelet, P.A. Thiel and J.M. Dubois, Eds.; (World Scientific, Singapore, 1997), pp. 9-16.

[38] C. Janot and M. dexxBoissieu, Phys. Rev. Lett. 72 (1994) 1674-1677.

[39] C. Janot, Phys. Rev. B 53 (1996) 181-191.

[40] C. Janot and J.-M. Dubois, in: Introduction to Quasicrystals; J.B. Suck, Ed. (Springer Verlag, 1998), pp. in press.

[41] M. Gierer, M.A.V. Hove, Z. Shen, C.J. Jenks and P.A. Thiel, (1997) unpublished data.

[42] X. Wu, S.W. Kycia, C.G. Olson, P.J. Benning, A.I. Goldman and D.W. Lynch, Phys. Rev. Lett. 75 (1995) 4540.

Figure Captions.

Figure 1. Measured and calculated LEED patterns of quasicrystalline(-like) surfaces: (a) LEED pattern of Al-Pd-Mn twofold surface obtained by annealing at 900 K for 4 hours, E=60eV; (b) LEED pattern of Al-Pd-Mn threefold surface obtained by annealing at 700 K for 1 hour, E=40eV; (c) LEED pattern of Al-Pd-Mn fivefold surface obtained by annealing at 800 K for 2 hours, E=70eV; the calculated LEED patterns for (d) twofold surface; (e) threefold surface; (f) fivefold surface.

Figure 2. Comparison of high- and low-resolution LEED spot profiles on the i-Al-Pd-Mn fivefold surface, at an incident beam energy of 85 eV. In both experiments, the sample was ion sputtered for 15 minutes and annealed before the measurement. The annealing parameters were 800 K for 2 hours and 750 K for 0.5 hours, in the high- and low-resolution experiments, respectively. The real-space dimension that corresponds to the spot width is indicated.

Figure 3. LEED patterns of quasicrystalline(-like) threefold surface measured at: (a) 30 eV; (b) 65 eV; and (c) 110 eV.

Figure 4. X-ray photoelectron spectra of the Mn $2p_{3/2}$ transition for the threefold surface. Curve (a) is the spectrum immediately after sputtering, (b) follows annealing to 600 K, and (c) follows annealing to 800 K.

Table 1. Spot spacings, and ratios of spot spacings, for the three high-symmetry surfaces. The ideal ratios are determined from the x-ray scattering data (Fig. 1, lower panels). The values of kj at each individual energy were obtained by averaging over all equivalent spots that were accessible at that energy. (Some spots were always blocked by the sample manipulator.) Uncertainties are given as ± one standard deviation (67% confidence interval).

Al-Pd-Mn twofold:

	j=0	j=1	j=2	j=3
# of measurements at different energies		5	10	6
k_j	-	1.029±0.010	1.663±0.028	2.716±0.021
Bulk value		0.948		
k_j/k_1	-	1	1.616±0.043	$(1.624\pm0.014)^2$
Ideal ratio	-	1	$1.618 = \tau$	$1.618^2 = \tau^2$

Al-Pd-Mn threefold:

	j=0	j=1	j=2	j=3
# of measurements at different energies	3	8	8	4
k_j	0.699±0.012	1.123±0.014	1.826±0.018	2.992±0.028
Bulk value	0.677			
k_j/k_0	1	1.607±0.048	$(1.616\pm0.022)^2$	$(1.624\pm0.014)^3$
Ideal ratio	1	$1.618 = \tau$	$1.618^2 = \tau^2$	$1.618^3 = \tau^3$

Al-Pd-Mn fivefold:

	j=0	j=1	j=2	j=3
# of measurements at different energies	5	4	13	9
k_j	0.669±0.006	1.080±0.012	1.752±0.029	2.867±0.031
Bulk value	0.616			
k_j/k_0	1	1.617±0.032	$(1.619\pm0.021)^2$	$(1.624\pm0.012)^3$
Ideal ratio	1	$1.618 = \tau$	$1.618^2 = \tau^2$	$1.618^3 = \tau^3$

Table 2. Characteristics of terminations which maximize the density of intact PMI's, for the three high-symmetry surfaces. Single values are averages over 10 different self-similar planes. The ranges given in parentheses are the complete range of values.

Surface symmetry	5f	3f	2f
Number of Similar terminations Used in average, n	10	10	10
Density of topmost plane (atoms/Å^2)	0.0793 (0.0551-0.087)	0.0628 (0.0529-0.0704)	0.0632 (0.0411-0.0809)
Density of second plane (atoms/Å^2)	0.0558 (0.0435-0.0797)	0.0573 (0.0540-0.0584)	0.0821 (0.0683-0.0931)
Bulk interplanar separation (Å)	0.48	0.86	0.91
Combined lateral density (atoms/Å^2)	0.135	0.120	0.145
Density of intact PMI's touching the topmost plane (clusters/Å^2)	0.0066	0.0060	0.0073
Composition of topmost plane, Atomic % Al-Pd-Mn	95.3-0-4.7	93.7-0-6.3	77.5-20.3-1.2
Composition of two top planes combined, atomic % Al-Pd-Mn	71.8-20.4-7.8	62.7-21.1-16.1	71.8-23.4-4.8

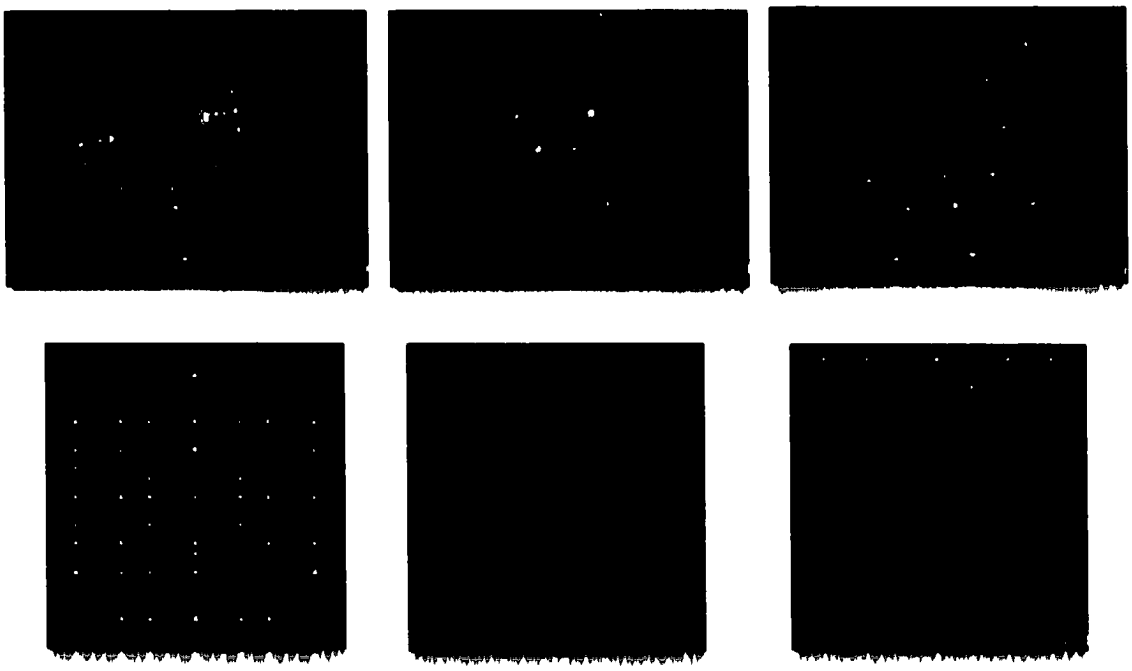

Fig. 1

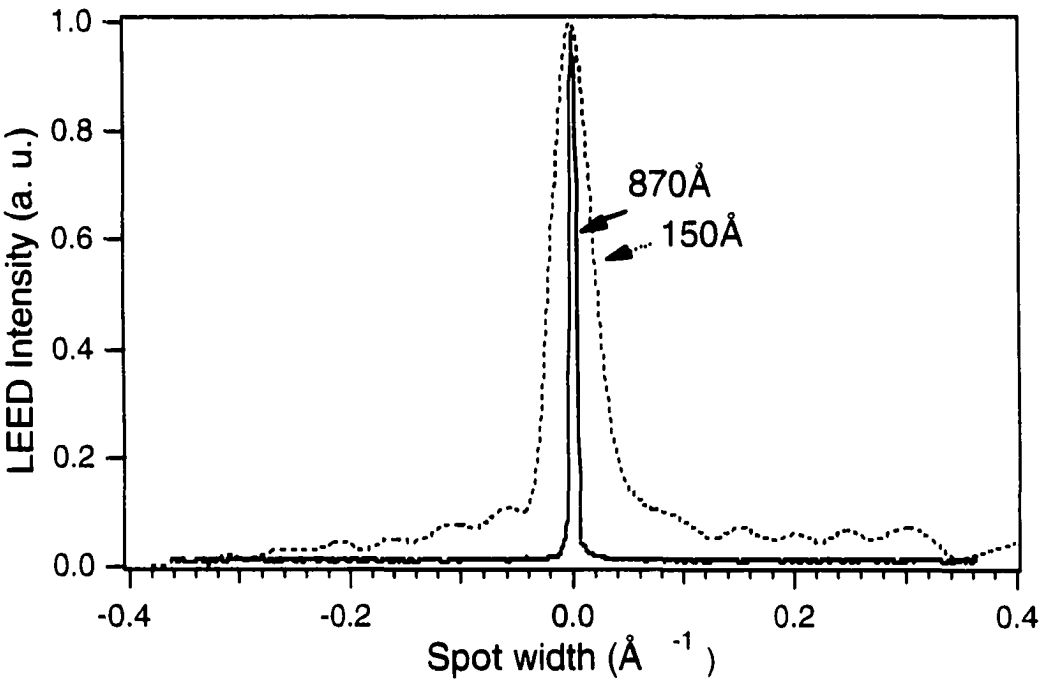
1.0
0.8
0.6
0.4
0.2
0.0
LEED Intensity (a. u.)
870Å
150Å
-0.4
-0.2
0.0
0.2
0.4
Spot width (Å -1)

Fig. 2

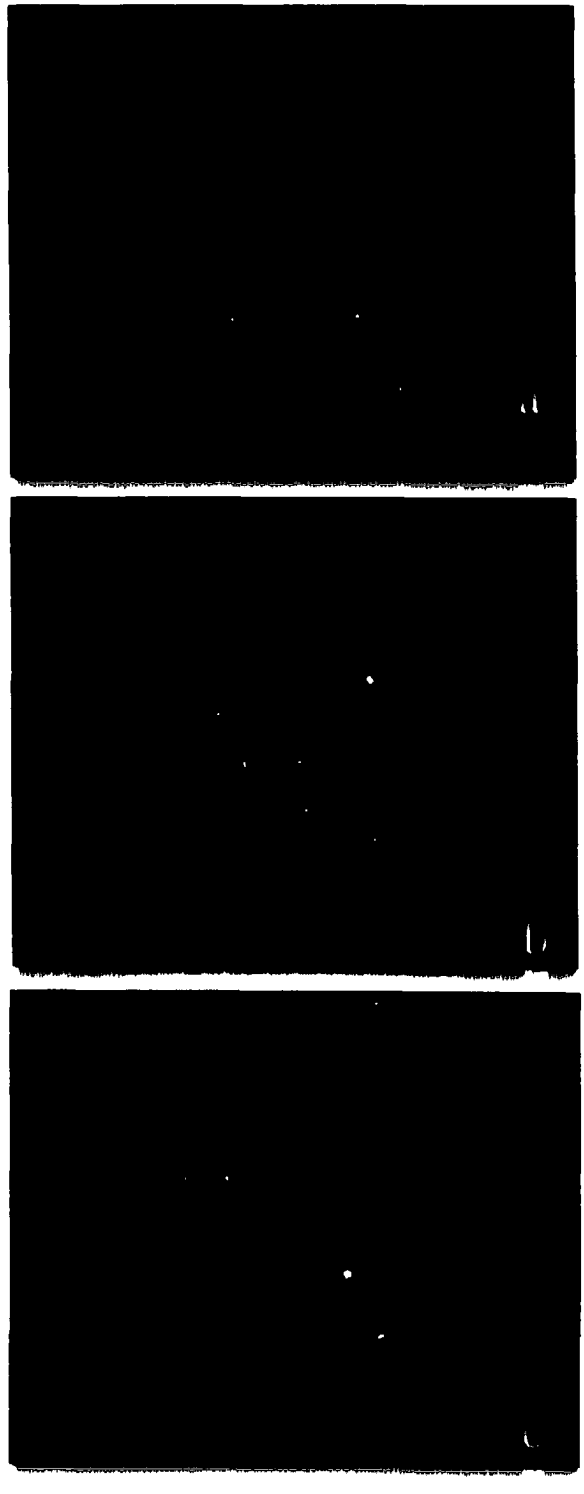

Fig 3

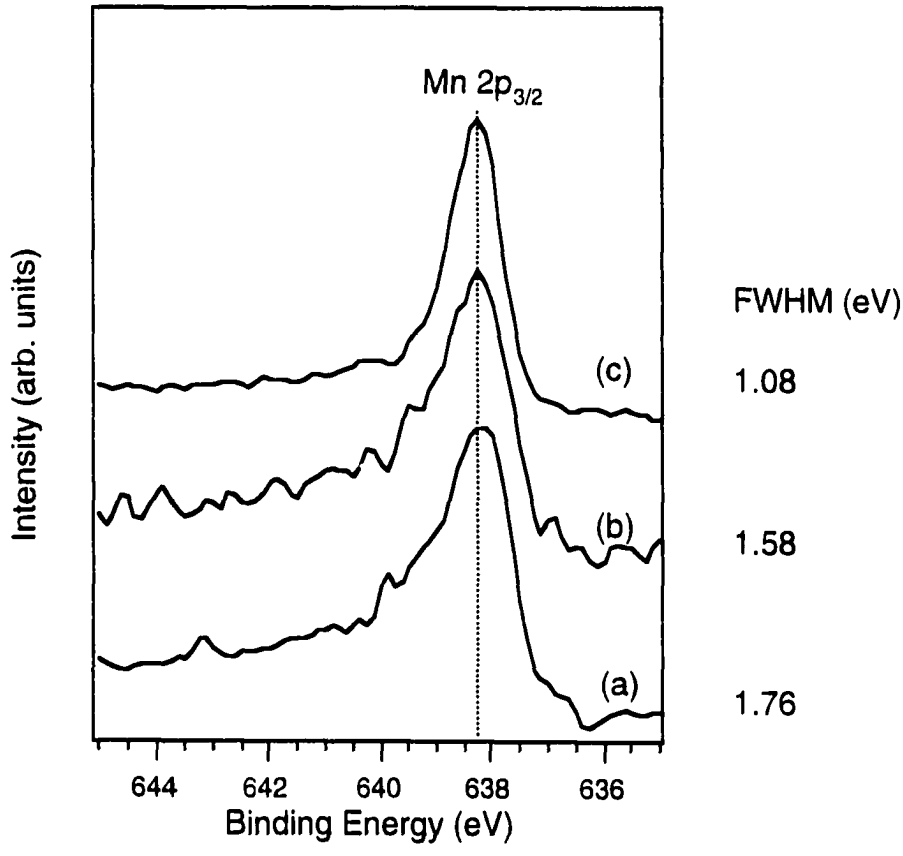
Mn 2p3/2
Intensity (arb. units)
(c)
(b)
(a)
FWHM (eV)
1.08
1.58
1.76
644
642
640
638
636
Binding Energy (eV)

Fig. 4

STM STUDY OF AN ICOSAHEDRAL Al-Pd-Mn FIVEFOLD SURFACE

A paper to be submitted to Physical Review Letters

Z. Shen, C. R. Stoldt, C. J. Jenks, and P. A. Thiel

Department of Chemistry and the Ames Laboratory

Iowa State University, Ames, IA 50011, USA

Abstract

We have used Scanning Tunneling Microscopy (STM) to investigate the structure of the fivefold surface of icosahedral Al-Pd-Mn in Ultra-High Vacuum (UHV). Terrace-step like structure starts to form after annealing the sputtered surface above 700K. After annealing the surface at 900K, large atomic flat terraces were formed all over the surface. On the terraces fine structures with fivefold symmetry are observed. Pattern analysis of the Auto-Correlation Function (ACF) of the STM images and the bulk structure model suggests that those fine structures may be intact Pseudo-Mackay Icosahedron (PMI) clusters. Step height analysis also shows that the surface terminations prefer to keep some PMI clusters intact.

PACS numbers: 61.44 Br, 68.35 Bs, 61.14 Hg

Quasicrystals exhibits unique structural features, [1-4] coupled with unusual combinations of physical properties. [5,6] Some of the interesting properties of quasicrystals, such as low surface energy and low friction, involve surface phenomena. With the availability of large single grains of quasicrystalline alloys, such as the icosahedral phase of Al-Pd-Mn, the study of surface structure and chemistry by techniques such as scanning tunneling microscopy (STM) [7-11] and low-energy electron diffraction (LEED) [10-14] has emerged as one of the most active areas in quasicrystal research.

Although the bulk structure of quasicrystals are known pretty well, especially for i-Al-Pd-Mn [15,16], the surface structures of quasicrystals are still unknown. In order to investigate the atomic structure of the quasicrystal surfaces, mainly two different types of experimental techniques have been applied. Diffraction experiments such as low energy electron diffraction (LEED) allows one to determine the reciprocal space structure of the surfaces. By analyzing the LEED intensity-voltage (IV) data, atomic-scale structure of quasicrystalline surfaces can be obtained. [13,17] The other type of techniques is direct imaging techniques such as scanning tunneling microscopy (STM) and atomic force microscopy (AFM). These microscopic methods image real space structure of surfaces and provide the direct information about surface structure.

STM experiments were performed in an ultrahigh vacuum chamber equipped with Omicron room temperature STM, Omicron HRLEED system, Auger electron spectroscopy, mass spectrometer, and ion bombardment gun. The base pressure of the chamber is $3\text{-}4\times10^{-11}$ Torr. The pressure during STM measurements is $4\text{-}6\times10^{-11}$ Torr. Other papers [18,19] describe our methods of quasicrystalline sample preparation outside UHV chamber. Our method of surface preparation in UHV involves ion bombardment at room temperature and

annealing. The sample is sputtered for 15 minutes each time (1keV, 12-15 uA sample current without bias). Annealing began at 400K, and went up in 50K increments whenever annealing at a given temperature no longer revealed significant surface segregation of carbon and oxygen.

Before any STM measurements, the sample was fresh cleaned by Ar^+ sputtering for 15 minutes and annealed at given temperature for 2 hours. Auger and SPA-LEED were done after STM measurements to make sure that STM measurements were done on a clean surface.

Our sample is a flat square wafer, approximately 8.5 x 8.5 mm^2 in area, and 1.5 mm thick. The bulk composition of our sample is $Al_{71.3}Pd_{19.1}Mn_{9.6}$. The surface normal was oriented to a fivefold axis within 0.2° by x-ray Laue. This sample was previously used for LEED study in another chamber [20]. The clean surface after annealing above 750K yields beautiful quasicrystalline fivefold LEED pattern. I-V analysis of the fivefold LEED pattern has been done by using the bulk structure of icosahedral AlPdMn determined by x-ray and neutron diffraction. [13,17] The best fits correspond to a mix of several relaxed bulklike terminations.

Figure 1a shows the STM image of the surface just after sputtering. The surface exhibits a rough surface with grain structure. After annealing the surface between 700-900K, the surface morphology changes dramatically with increasing annealing temperature. The grain or cluster structure starts to disappear and flat terraces start to develop. Figure 1b-c show the STM image of the surface after annealing at 700K and 800K, respectively. At this point, the terraces are still not atomic flat. We couldn't get atomic or near atomic resolution images on those terraces. After annealing the surface at 900K, the grain or cluster structure

completely disappeared. Large terraces with steps were formed all over the surface. The typical tunneling condition of our measurements is 0.5-2 V for tunneling voltage and 0.2-1 nA for tunneling current.

The LEED pattern of above annealed surface is fivefold patterns with quasi-periodicity, which is the same high temperature LEED pattern we observed in conventional LEED chamber [21]. After annealing at 800K for 2 hours, spot profile of high resolution LEED (SPA-LEED) shows that the average terrace size is about 870Å [21].

In order to precise measure the step heights, we calibrated the z-piezo by using the step heights on Ag (100) surface, and assuming that the step heights on Ag (100) have bulk value. Three distinct step heights were found on the surface: 6.49+0.2Å, 4.08+0.2Å, and 2.41+0.2Å. The first two step heights were reported already by T. Schaub et al. [9-11], and the 2.41Å step is reported here for the first time. The 6.49Å steps are found much more frequently than the other two steps on the surface.

Figure 2a shows a 500x500Å STM image of one of those terraces. The corrugation of the image is about 1Å, which means the terrace is atomically flat. The major feature of the image is the bright balls with 5-8Å diameter. Those balls seem randomly arranged if just examined by eye. But if we look at the image more carefully, we can see some lines which link some of those balls, and we can find some local arrangements of those balls with fivefold symmetry.

Figure 2b shows the Fourier transform of the STM image. It clearly shows two tenfold rings of spots, which implies that the STM image has fivefold or tenfold symmetry. Figure 2c is the two dimensional autocorrelation function (ACF) of the STM image (Fig. 2a). In the ACF image, correlation maxima appear as bright spots. Tenfold rings of bright spots

are clearly visible in the ACF image which also implies that the symmetry of our STM image is fivefold or tenfold. ACF is an even function which must have an extra inversion center, which would make the ACF image of a fivefold structure has tenfold symmetry. In our ACF pattern, we can see correlation maxima (bright spots) even close to the edges, which indicates the strong spatial correlation of the features in our STM image over distances of at least 250Å.

In the previous STM study of AlPdMn fivefold surface by Schaub et al. [9-11], they used a cleaning procedure similar to as what we used. They also observed flat terraces with fivefold symmetry. They found two distinctive step heights: 6.78Å and 4.22Å. The difference between their study and our study is that they started from a surface close to a twofold axis, and after annealing the surface at temperature close to the melting point (1020-1070K) they obtained fivefold facets which are 31.72° away from the twofold surface. Also their tunneling condition is different from ours: 2V for tunneling voltage, and 5 to 40 pA for tunneling current.

Another STM study of Al-Pd-Mn fivefold surface was done by Ebert et al. [8,22]. They prepared the clean surface by in-situ cleavage in UHV chamber. They observed rough surface (with a maximum corrugation of 10Å) with cluster-subcluster structure.

Both studies have been interpreted in terms of fundamental concepts of bulk quasicrystalline structure. In the structural model of the icosahedral Al-Pd-Mn quasicrystal [15,16] proposed by Janot and Boudard, the basic structure unit is a pseudo-Mackay icosahedron (PMI). The PMI consists of three centrosymmetric shells of atoms, with a total of 51 atoms, and with an overall diameter about 10Å. These PMI pack into large, self-similar icosahedra, and so on. Chemical bonds are strong within the PMI, and intercluster bonds are

weaker. According to this model, when a sample breaks or cleaves, it should do so in a way that leaves most of the PMI intact.

Figure 3a shows a bulk terminated Al-Pd-Mn fivefold surface using the structure model proposed by Boudard et al. This termination is one of the terminations which gives good Pendry R-factor in LEED I-V analysis [13,17]. Figure 3b is the two dimensional ACF of the atomic model. It has tenfold rings of bright spots which appear similar to the ACF of our STM image. But if we compare the radii of the corresponding rings and the distances between bright spots, the values are much (about two and half times) smaller than those of our STM image.

In order to quantitatively compare the ACF images from our STM data and from the structure model, we plot the histograms of distance between every two bright spots in the ACF images. Figure 4a and b show such histograms for the ACF images of STM image and structure model, respectively. One can clearly see that the distinctive distances in the STM images are much larger than in atomic structure model.

Figure 5a is the same termination as in Figure 3a but only shows the intact PMI clusters. (The tops of those PMI clusters just touch the topmost plane.) The ACF of Figure 5a is shown in Figure 5b. Again, rings of tenfold bright spots are clearly shown. But the radii of those rings and spacing between bright spots are much larger than those of atomic structure model. Actually, the ACF of PMI clusters is the τ^2 inflation of the ACF of atomic model. This can be seen more clearly in the histogram (Figure 4c). Now the distinctive distances agree with our STM data quite well.

The above discussion doesn't prove that the ball-like features in our STM images are PMI clusters. It only shows that the scale of those features is much larger than the atomic scale, and comparable to the scale of PMI clusters. Figure 6 shows the histograms of ACF of Mn atoms (Figure 6a) on topmost layer, Pd atoms (Figure 6b) on the second layer, and PMI clusters cut by the topmost layer (Figure 6c) respectively. Figure 6a and 6c are very similar to that of intact PMI clusters because the distance between those Mn atoms and between broken PMI clusters are on the same order of intact PMI clusters.

Another important observation is about the step heights in the STM images. In our experiments, three distinctive step heights are observed: 6.49±0.2Å, 4.08±0.2Å, and 2.41±0.2Å. Interestingly, if we look at the step heights produced by LEED I-V [17], we can also find three step heights between "good" terminations: 6.60Å, 4.08Å, and 2.52Å. The 6.60Å and 4.08Å are the step heights between "best" terminations, and the 2.52Å steps are between one of the "best" and one of the "good" terminations.

Figure 7 is the side view of the fivefold terminations, which is one of the twofold planes. It can be seen that PMI clusters also form layer structure just like atoms in structure model. According to the structure model [15], the PMI clusters are extremely stable. We can assume that in order to keep the surface energy low, we must keep as many intact PMI clusters as possible. The lines in Figure 7 are parallel to the fivefold planes and they are the "good" terminations according to above assumption. All of those "good" terminations keep some of the PMI clusters intact, although they also cut through some other clusters. The step heights between the "good" planes are either 6.60Å or 2.04Å. Interestingly, most of these "good" terminations are the same terminations found to give good Pendry R-factors in LEED IV analysis.

In summary, our STM data of Al-Pd-Mn fivefold surface shows that terrace-step-kink structures begin to form on the surface after Ar ion sputtering and annealing annealing above 700K. Large atomic flat terraces are formed after annealing at 900K. Fine structures with fivefold icosahedral symmetry were found on those terraces. Data analysis of our STM images and structure model of icosahedal Al-Pd-Mn suggest that the surface structure of i-Al-Pd-Mn fivefold surface is the unreconstructed quasicrystalline surface structure, and the fine structures in the STM images may be the pseudo Mackay clusters which are the structure units of the structure model.

Acknowledgments. M. Quiquandon and J. M. Dubois provided valuable comments and suggestions. We thank M. de Boissieu for supplying information about the stomic planes in AlPdMn as well as the software used to generate the three-dimensional atomic bulk positions. This work was supported by the Director, Office of Energy Research, Office of Basic Energy Sciences, Materials Sciences Division, of the U.S. Department of Energy under Contract No. W-405-Eng-82.

References.

[1] A.I. Goldman and M. Widom, Ann. Rev. Phys. Chem. 42 (1991) 685-729.

[2] P.W. Stephens and A.I. Goldman, Scientific American (April 1991) 24-31.

[3] C. Janot, Quasicrystals: A Primer (Clarendon Press, Oxford, 1992).

[4] A.I. Goldman and K.F. Kelton, Reviews of Modern Physics 65 (1993) 213-230.

[5] J.M. Dubois, in: Introduction to the Physics of Quasicrystals; J.B. Suck, Ed. (Springer Verlag, Berlin, 1998), pp. in press.

[6] J.M. Dubois and P. Weinland "Coating materials for metal alloys and metals and method," CNRS, Nancy, France, 1993.

[7] A.R. Kortan, R.S. Becker, F.A. Thiel and H.S. Chen, Phys. Rev. Letters 64 (1990) 200.

[8] P. Ebert, M. Feuerbacher, N. Tamura, M. Wollgarten and K. Urban, Phys. Rev. Lett. 77 (1996) 3827-3830.

[9] T.M. Schaub, D.E. Bürgler, H.-J. Güntherodt and J.B. Suck, Phys. Rev. Lett. 73 (1994) 1255-1258.

[10] T.M. Schaub, D.E. Bürgler, H.-J. Güntherodt and J.-B. Suck, Z. Phys. B 96 (1994) 93-96.

[11] T.M. Schaub, D.E. Bürgler, H.-J. Güntherodt, J.B. Suck and M. Audier, Appl. Phys. A 61 (1995) 491-501.

[12] E.G. McRae, R.A. Malic, T.H. Lalonde, F.A. Thiel, H.S. Chen and A.R. Kortan, Phys. Rev. Letters 65 (1990) 883.

[13] M. Gierer, M.A.Van Hove, A.I. Goldman, Z. Shen, S.-L. Chang, C.J. Jenks, C.-M. Zhang and P.A. Thiel, Phys. Rev. Lett. 78 (1997) 467-470.

[14] Z. Shen, C.J. Jenks, J. Anderegg, D.W. Delaney, T.A. Lograsso, P.A. Thiel and A.I. Goldman, Phys. Rev. Lett. 78 (1997) 1050-1053.

[15] C. Janot and M. dexxBoissieu, Phys. Rev. Lett. 72 (1994) 1674-1677.

[16] M. Boudard, E. Bourgeat-Lami, M. de Boissieu, C. Janot, M. Durand-Charré, H. Klein, M. Audier and B. Hennion, Phil. Mag. Lett. 71 (1995) 11.

[17] M. Gierer, M.A. Van Hove, A.I. Goldman, Z. Shen, S.-L. Chang, P.J. Pinhero, C.J. Jenks, J.W. Anderegg, C.-M. Zhang and P.A. Thiel, Phys. Rev. B 57 (1998) 7628-7641.

[18] S.-L. Chang, W.B. Chin, C.-M. Zhang, C.J. Jenks and P.A. Thiel, Surf. Sci. 337 (1995) 135-146.

[19] C.J. Jenks, D. Delaney, T. Bloomer, S.-L. Chang, T. Lograsso and P.A. Thiel, Appl. Surf. Sci. 103 (1996) 485-493.

[20] Z. Shen, M.J. Kramer, C.J. Jenks, A.I. Goldman, T. Lograsso, D. Delaney, M. Heinzig, W. Raberg and P.A. Thiel, Phys. Rev. B (1998) submitted.

[21] Z. Shen, W. Raberg, M. Heinzig, C.J. Jenks, P. J. Pinhero, T. Lograsso, D. Delaney and P.A. Thiel, (1998) in preparation: chapter IV of this thesis.

[22] P. Ebert, F. Yue and K. Urban, Phys. Rev. B 57 (1998) 2821-2825.

[23] P. Gardner, R. Martin, M. Tushaus and A.M. Bradshaw, J. Electron Spectroscopy and Rel. Phenom. 54/55 (1990) 619-628.

Figure Captions.

Figure 1. STM images of Al-Pd-Mn fivefold surface after sputtering for 15 minutes and annealing for 2 hours at different temperature. (a) just after sputtering, no annealing, 1000Åx1000Å, 1.0V, 0.5nA; (b) 700K annealing, 300Åx300Å, 2.0V, 0.2nA; (c) 800K annealing, 1000Å x 1000Å, 1.0V, 0.5nA; (d) 900K annealing, 1000Åx1000Å, 1.0V, 1.0nA.

Figure 2. (a) 500Å x 500Å STM image on a flat terrace after 900K annealing, 1.0V 0.5nA; (b) fast Fourier transform (FFT) of (a); (c) two dimension autocorrelation function (ACF) of (a), ±250Å x ±250Å.

Figure 3. (a) Structure model of Al-Pd-Mn fivefold surface based on LEED I-V analysis [23] and Boudard's model [16]. Top three layers are shown. (b) ACF image of (a), ±64Å x ±64Å.

Figure 4. Histograms of distance in ACF images of (a) atomic structure model (Figure 3); (b) only intact PMI clusters on surface (Figure 4); (c) STM image (Figure 2).

Figure 5. (a) Structure model of Al-Pd-Mn fivefold surface based on LEED I-V analysis [23] and Boudard's model [16]. Only intact PMI clusters are shown. (b) ACF image of (a), ±64Å x ±64Å.

Figure 6. Histograms of distance in ACF images of (a) Mn atoms on the topmost plane; (b) Pd atoms on the second topmost plane; (c) PMI clusters cut by the topmost plane

Figure 7. Structure of a twofold Al-Pd-Mn plane, which is parallel to a fivefold axis and can be considered as a side view of fivefold planes. The lines are parallel to fivefold planes. The circles are PMI clusters with equatorial sections in the twofold plane. Those lines are possible fivefold surface terminations which will keep some of the PMIs intact. The distance between lines are 6.60Å or 2.04Å.

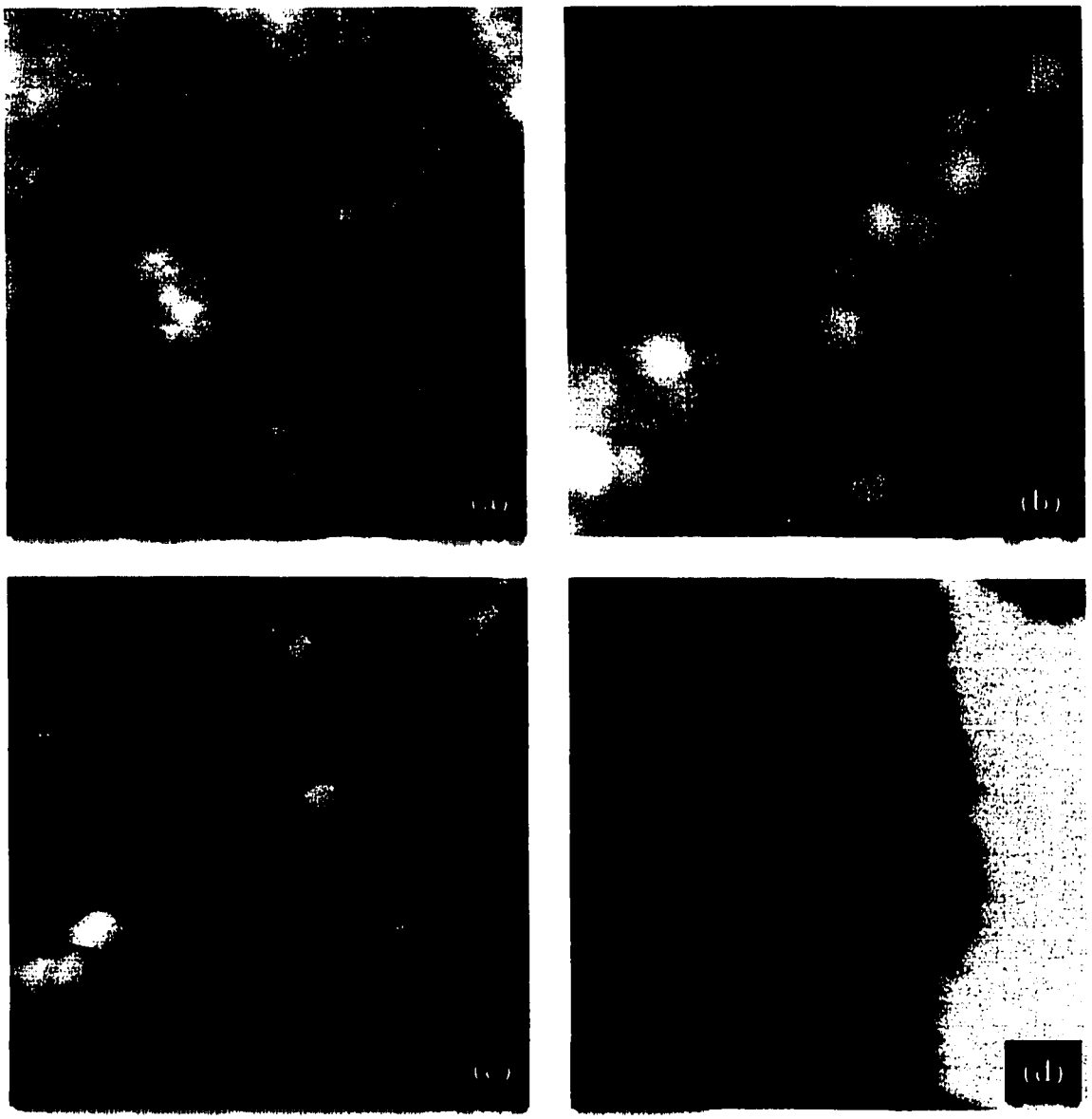

Fig. 1

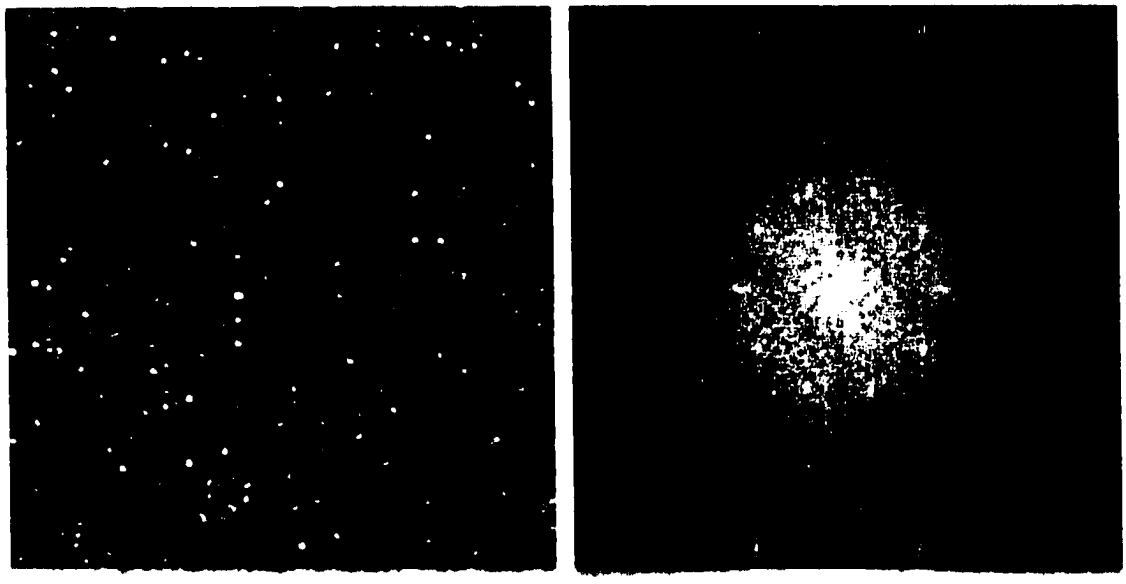

(a) (b)

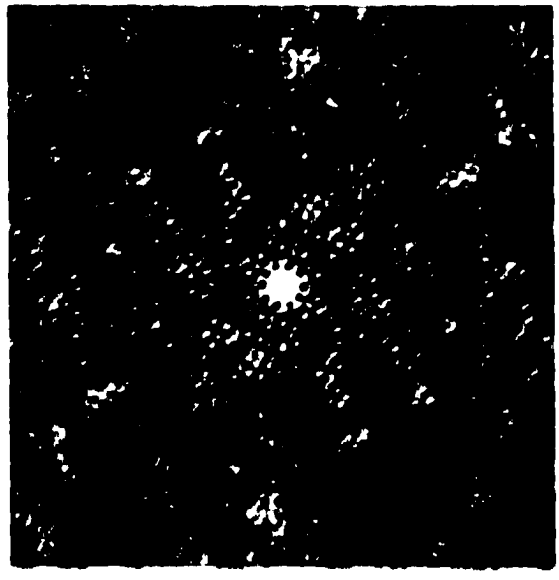

(c)

Fg. 2

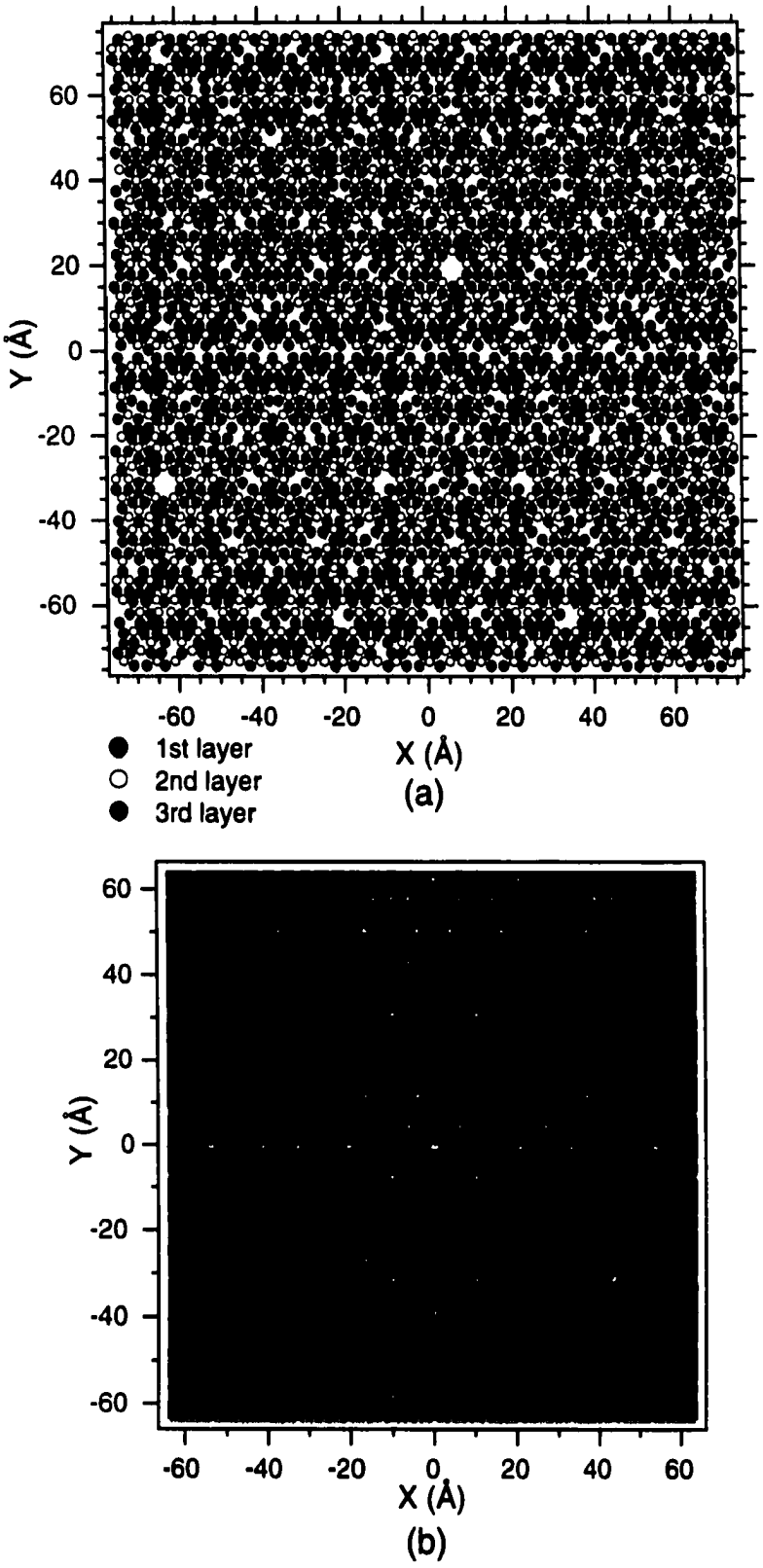
60
40
20
0
-20
-40
-60
Y (Å)
-60 -40 -20 0 20 40 60
X (Å)
1st layer
2nd layer
3rd layer
(a)
60
40
20
0
-20
-40
-60
Y (Å)
-60 -40 -20 0 20 40 60
X (Å)
(b)

Fig. 3

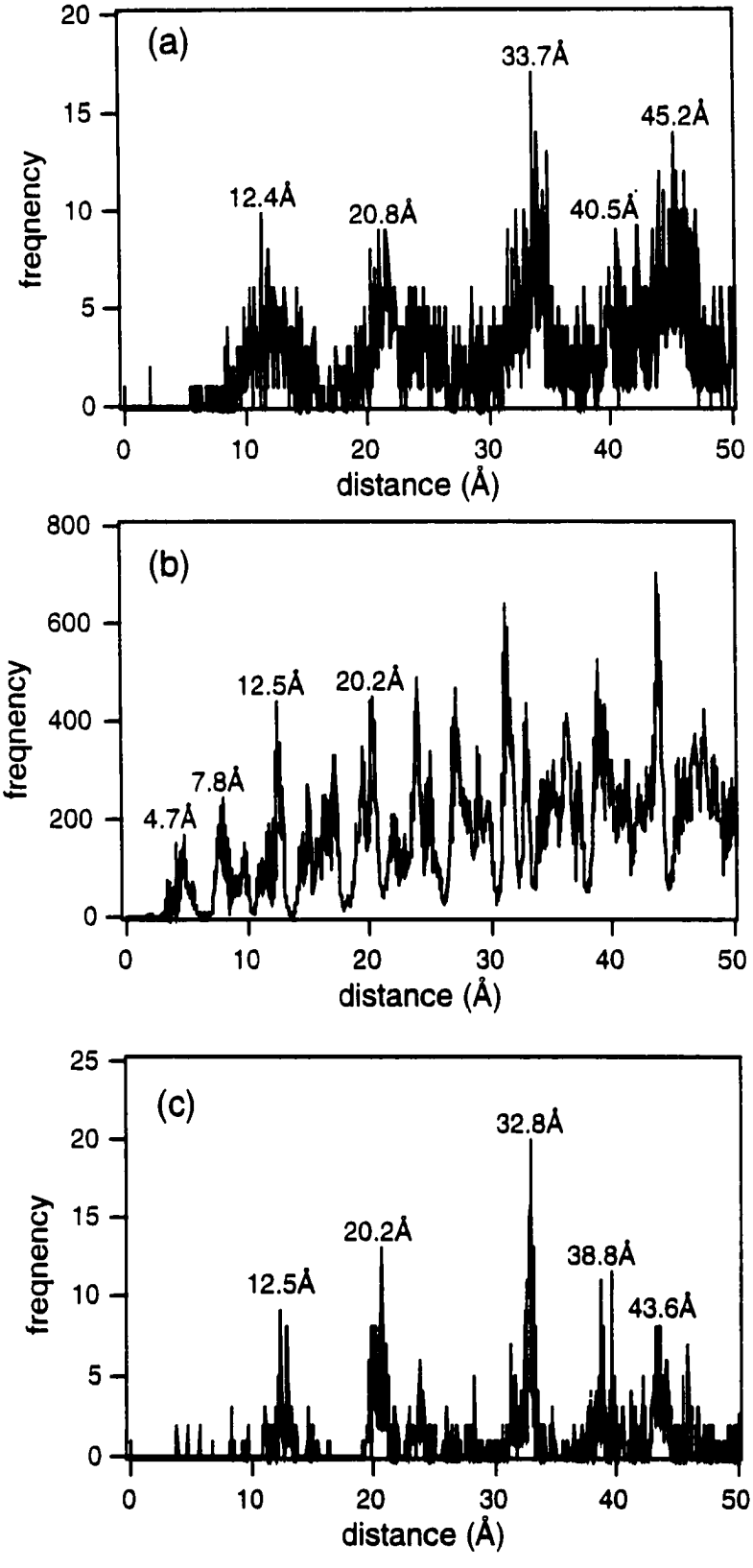
(a)
33.7Å
45.2Å
12.4Å
20.8Å
40.5Å
freqnency
distance (Å)
(b)
12.5Å
20.2Å
7.8Å
4.7Å
freqnency
distance (Å)
(c)
32.8Å
20.2Å
38.8Å
12.5Å
43.6Å
freqnency
distance (Å)

Fig. 4

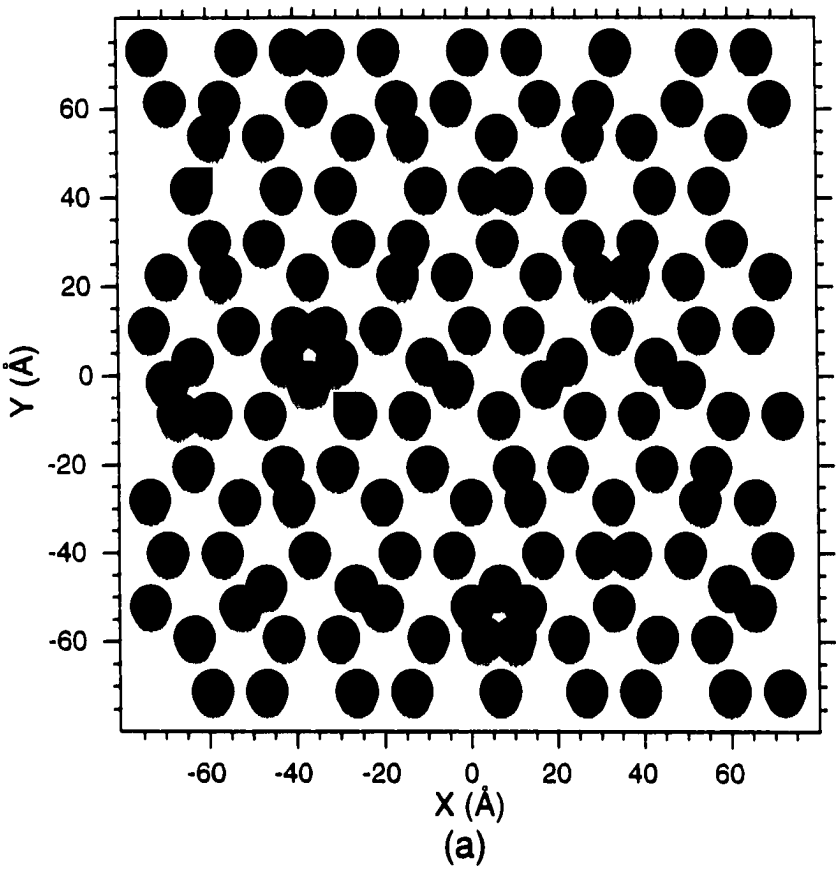
60
40
20
0
-20
-40
-60
Y (Å)
-60 -40 -20 0 20 40 60
X (Å)
(a)

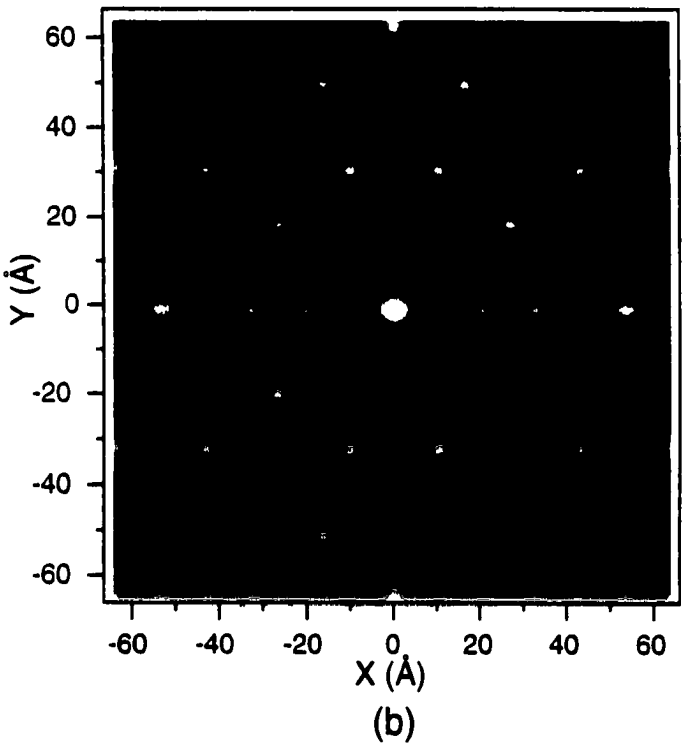
60
40
20
0
-20
-40
-60
Y (Å)
-60 -40 -20 0 20 40 60
X (Å)
(b)

Fig. 5

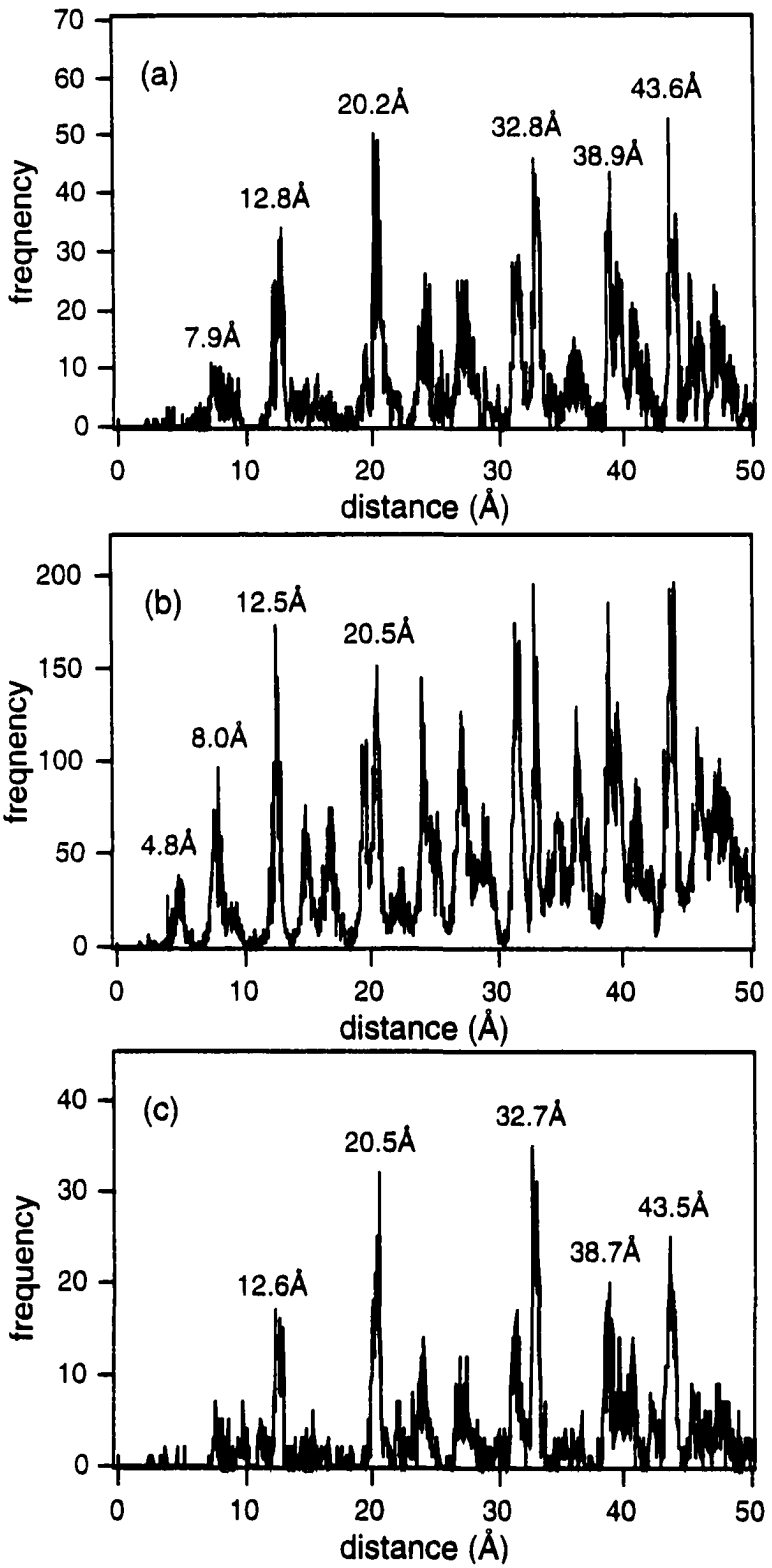
(a)
7.9Å
12.8Å
20.2Å
32.8Å
38.9Å
43.6Å
freqnency
distance (Å)
(b)
4.8Å
8.0Å
12.5Å
20.5Å
freqnency
distance (Å)
(c)
12.6Å
20.5Å
32.7Å
38.7Å
43.5Å
frequency
distance (Å)

Fig. 6

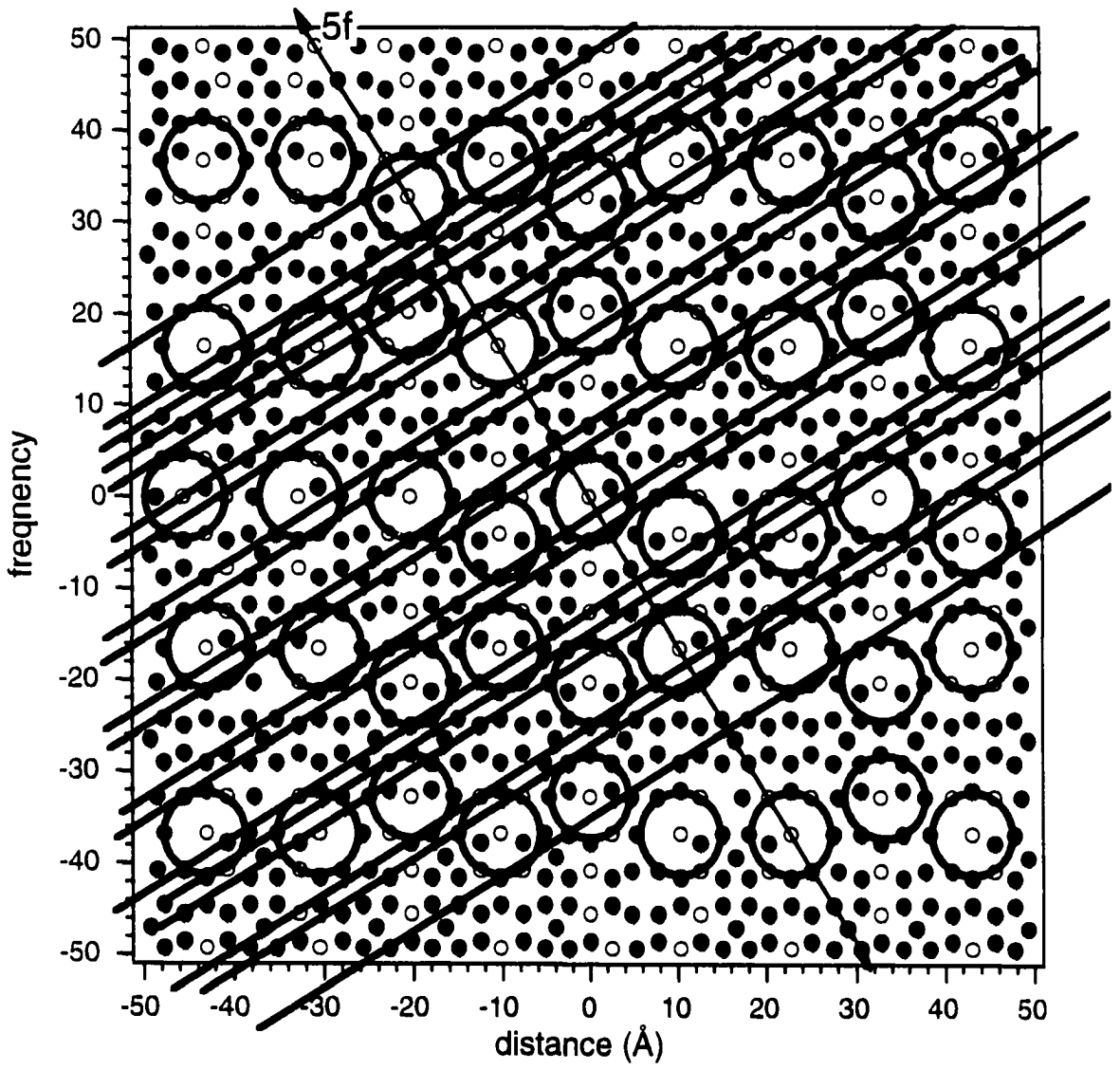
5f
freqnency
distance (Å)
50
40
30
20
10
0
-10
-20
-30
-40
-50
-50
-40
-30
-20
-10
0
10
20
30
40
50

Fig. 7

GENERAL CONCLUSIONS

The main conclusions that can be drawn from the work presented in this dissertation are given below:

a) Quasicrystalline – (like) structures are formed on i-Al-Pd-Mn twofold, threefold, fivefold surfaces and i-Al-Cu-Fe fivefold surface after Ar ion sputtering and annealing above 700K. The results from LEED studies agree very well with the unreconstructed quasicrystalline surfaces.

b) Crystalline cubic phases with CsCl structures are formed on i-Al-Pd-Mn and i-Al-Cu-Fe surfaces after Ar ion sputtering and annealing below 800K. There are multiple rotational domains on twofold and fivefold surfaces. The orientations of the cubic phases are [111] on threefold surface, [110] on twofold and fivefold surfaces.

c) There is a close structure relationship between cubic and corresponding icosahedral phases. A model based on the related symmetries of cubic close packing and icosahedral packing is proposed to explain the orientation and number of cubic domains.

d) STM study of Al-Pd-Mn fivefold surface shows that terrace-step-kink structure start to form on the surface after annealing above 700K. Large atomic flat terraces were formed after annealing at 900K. Fine structures with fivefold icosahedral symmetry were found on those terraces. Data analysis of our STM images and structure model of icosahedal Al-Pd-Mn suggest that the fine structures in our STM images may be the pseudo Mackay clusters which are the structure units of the structure model. STM study also supports unreconstructed quasicrystalline surface structure.

e) This database allows comparisons between different high-symmetry surfaces within a single alloy, and between different alloy surfaces having the same symmetry. We can assume that above conclusions may be general among Al-rich, icosahedral materials.

APPENDIX: AUGER INTERFACE

HARDWARE

The computerized Auger interface system consists of the following hardware components: Gateway 2000 E-3000 series Pentium 200/MMX computer, National Instruments PCI-MIO-16E-4 analog and digital I/O board, National Instruments SCB-68 68-pin shielded connector block, and a modified Auger Sweep Generator board.

The block diagram of the original Auger Cylindrical Mirror Analyzer (CMA) control unit is shown in Fig.1a. The sweep generator produces a ramp voltage of 0-10V amplitude. Then the ramp voltage is sent to modulator and operational amplifier to produce high voltage for CMA head. All the scan parameters are controlled in the sweep generator, e.g. scan start energy, scan range, and scan rate. The Auger signal from CMA head goes to the lock-in amplifier and then is plotted on an X-Y plotter. Because of the limitation of the resolution and signal input range of the plotter, the sensitivity of lock-in amplifier must be optimized for different elements (such as Pd and Al) in order to get good signal-to-noise ratio while measuring surface compositions. In conclusion, the manual operation of Auger spectrum acquisition is time consuming which may increase the surface contamination in ultra high vacuum.

In order to improve the efficiency, a computerized Auger interface is built to automatically collect Auger spectrum and calculate the surface composition. The block diagram of the revised CMA control unit is shown in Fig. 1b. The old sweep generator is replaced by the output from the analog and digital I/O board. And the X-Y plotter is replaced by the input to the analog and digital I/O board. The scan parameters now are controlled by

the software. And the Auger signal is digitized and then displayed and stored on computer. Because of the large input range of the I/O board, now we can use the highest sensitivity (10mV) of the lock-in amplifier for all Auger peaks.

Fig. 2a is the schematic diagram of the original Sweep Generator board. Please notice two connectors which are labeled by big arrows: Pin 13 "TO HV PWR SUPPLY" and J1 "OUTPUT". Fig. 2b is the schematic diagram of the modified Sweep Generator board. Now J1 becomes the output ramp signal from computer and connected to Pin 13 directly. By doing this, we by passed the whole board and use the board just as a connector from the computer to the high voltage power supply.

Fig. 3 is the diagram of the SCB-68 connector block. Three channels are used for input and output of Auger interface: A/D input channel 0 (pin 68 and 34, differential mode) is connected to the output (-1 to +1V) from lock-in amplifier (Auger signal); A/D input channel 1(pin 33 and 66, differential mode) is connected to the D/A output from computer to measure the output ramp signal (0 to 10V) which can be converted to the CMA energy; D/A output channel 0 (pin 22 and 55) is connected to the J1 connector on the modified Sweep Generator board as the output ramp signal (0 to 10V) from the computer.

SOFTWARE

The Auger data acquisition software is written in National Instruments LabView 4.1 programming language. Fig. 4 shows the front control panel of the main Auger program. The control panel consists of three major parts. The upper left frame controls the scan parameter: start energy, end energy, scan rate, and number of scans. The plots in the upper right and lower part of the panel display the Auger spectrum. The upper right plot displays the real

time Auger signal; and the big lower plot displays the averaged final Auger spectrum. The upper center frame contains the information needed to calculate the surface composition: peak position and sensitivity factors. The normalized peak intensities and the final composition are also displayed in this frame.

The upper left frame serves as the "Sweep generator" board of Auger electronics. You can define "start energy", "end energy", and "scan rate" for each scan. You can also change energy resolution. A resolution (smaller number) will produce a larger file and more memory will be used during acquisition. 0.10eV/point turns out to be a good setting.

The upper left plot is the real time display of the Auger spectrum. It plots Auger intensity vs. energy during acquisition. The x value is the energy during the first scan.

The lower large plot is the averaged Auger spectrum. It plots the averaged spectrum after all scans are finished. The x value is energy (eV).

The upper center frame contains the element information used for calculating composition. Emin and Emax define the energy ranges of peaks which you wanted to use for composition calculation. Be sure to use correct sensitivity factor for each peak. A list of common sensitivity factors is shown below the input table. (You can always add more elements by using the "text" tool.

Before you run the program, you need to setup the numbers in the upper left frame: start energy, end energy, energy resolution, scan rate, and number of scans. You need to also setup the peak information for calculation.

To run the program, press "run" button in the tool bar. You will be asked to enter the temporary file name. The default name is "AugerTmp.txt". If you already saved last measurement, you can always use the default name and replace the old temporary file.

When the data acquisition is finished, the averaged Auger spectrum will be displayed in the lower plot. And composition will be calculated according to the element information you provide in the upper center table. The program then will ask you to save the data. The data is saved as text format. You can use other programs such as Igor or Axum to read the data later.

If you want to recalculate the composition by using different peak and sensitivity, you can run the program again. Be sure to change the "# of scans" to 1 and other scan parameters to be the same as the saved data before running. When the program asks you to input the temporary filename, choose "CANCEL", then "OK". The program will ask you to choose a file to be opened. Choose the saved data file and press "OK". Then the program will ask you to choose a file to save. The data you are about to save is the same as the last file. So just enter a temporary file name such as "temp". You can always delete it afterwards. Then the new composition will be displayed in the upper center part. Use "Position/size" tool to add number of peaks. Use "Operate value" tool to change the values. If you don't want to include certain peaks (such as O, C) for composition, make the Emin=Emax and recalculate the composition.

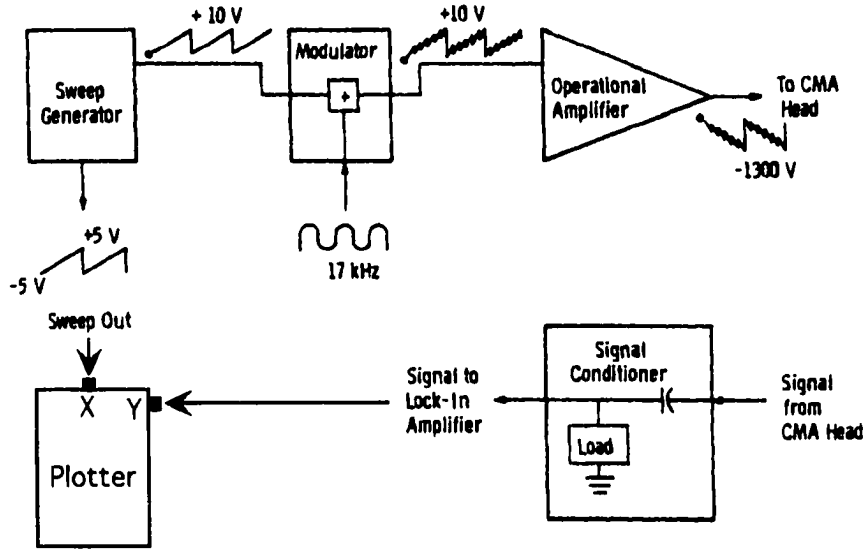

(a)

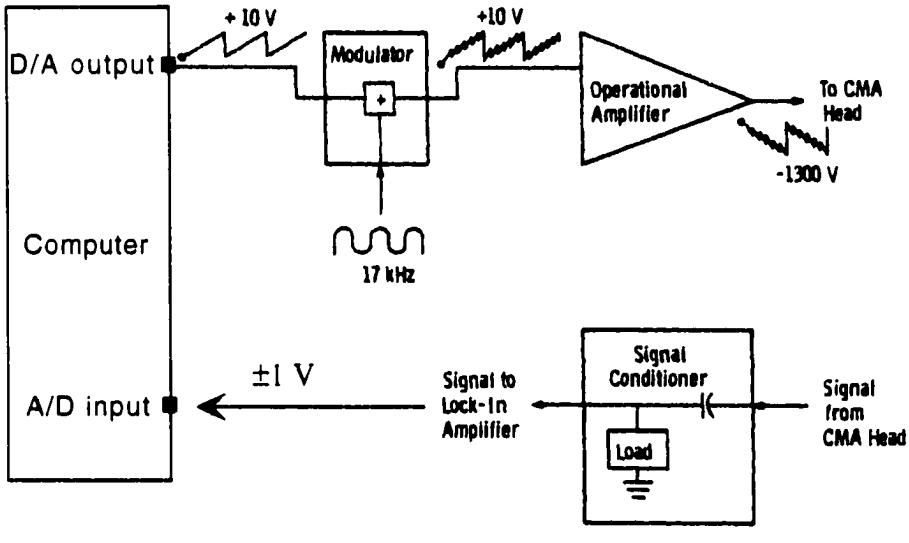

(b)

Fig. 1 Block diagrams of (a) original and (b) modified Auger Cylindrical Mirror Analyzer (CMA) control unit

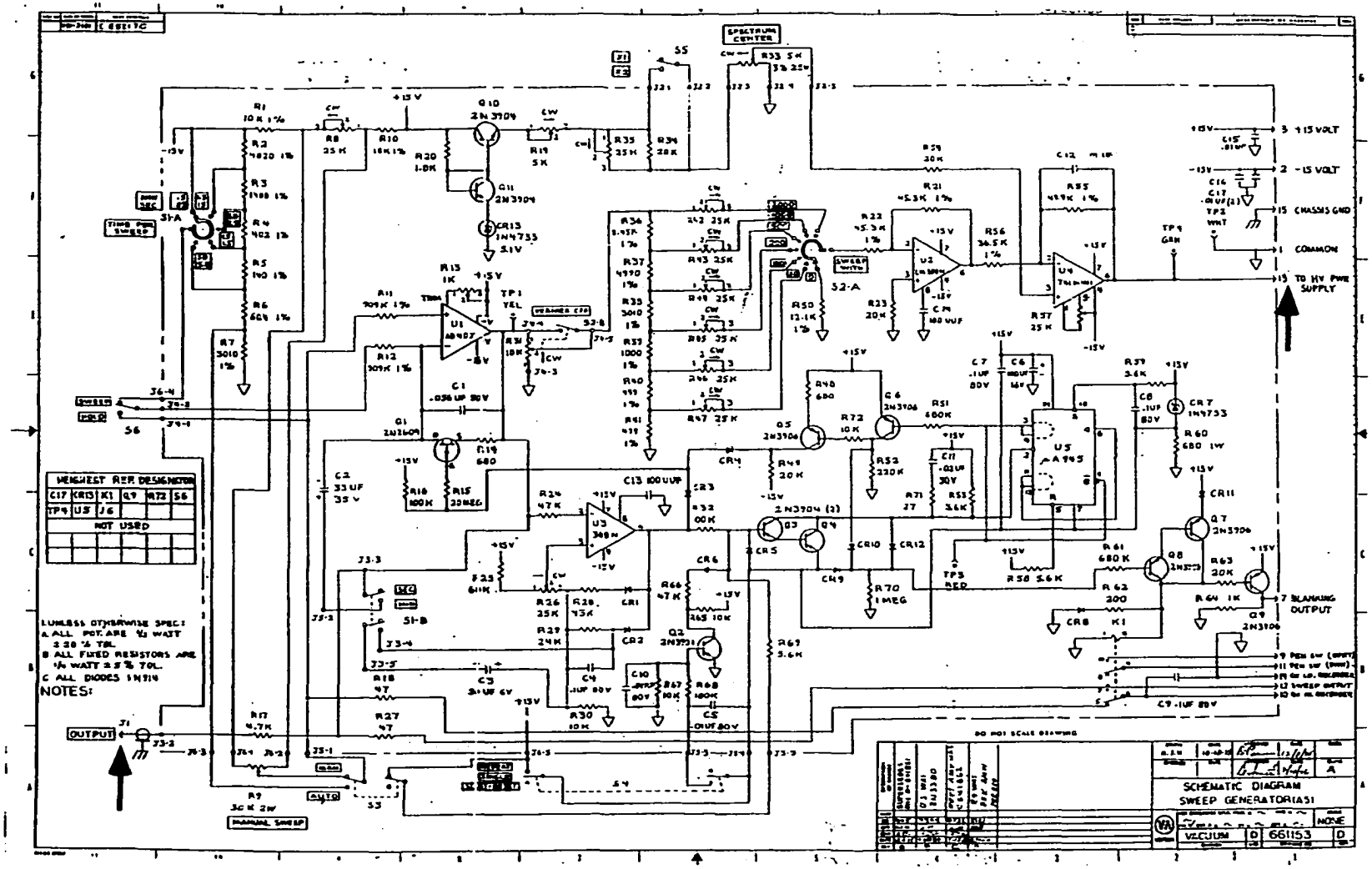

Fig. 2a Schematic diagram of original Sweep Generator

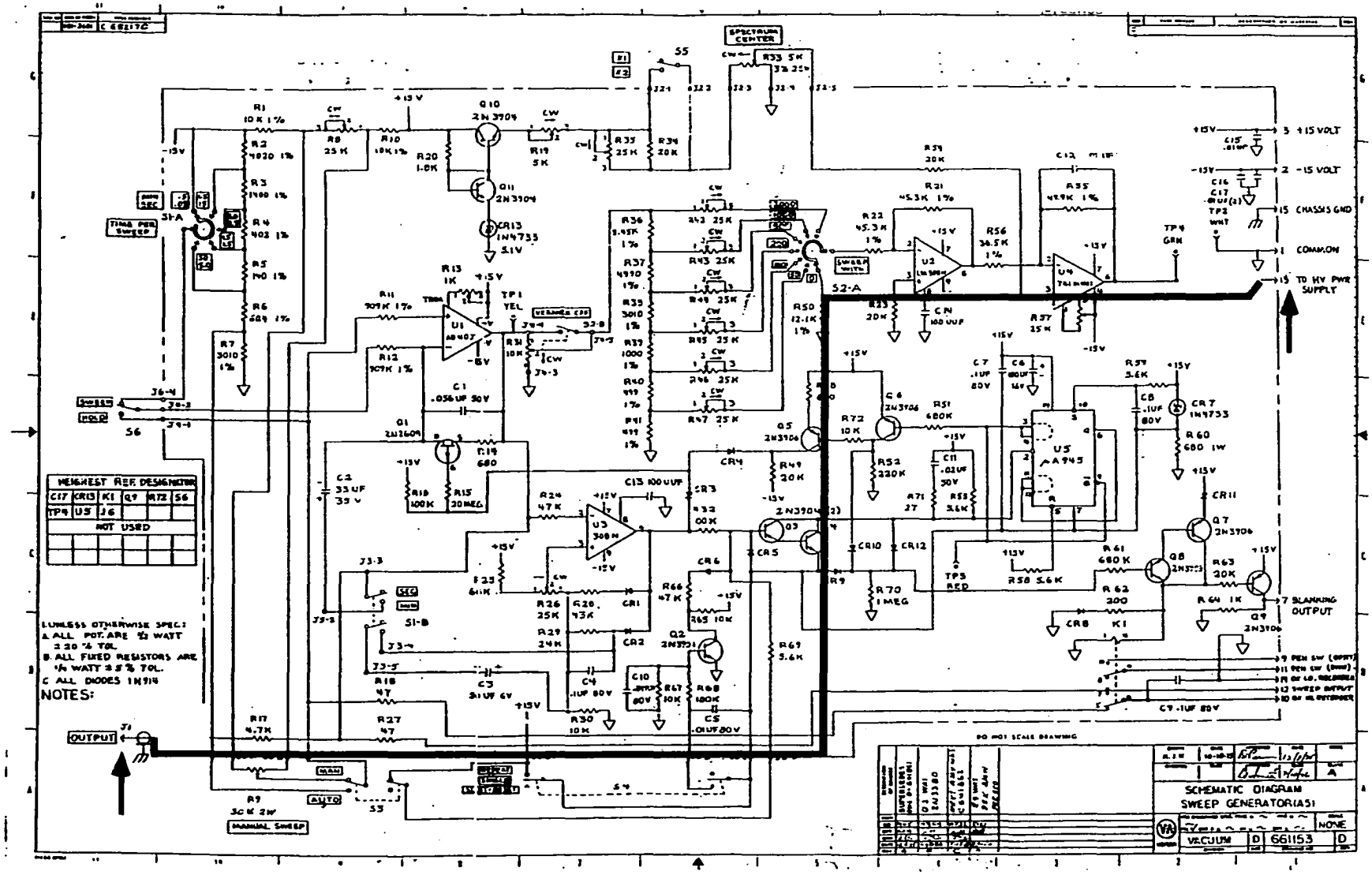

Fig. 2b Schematic diagram of modified Sweep Generator

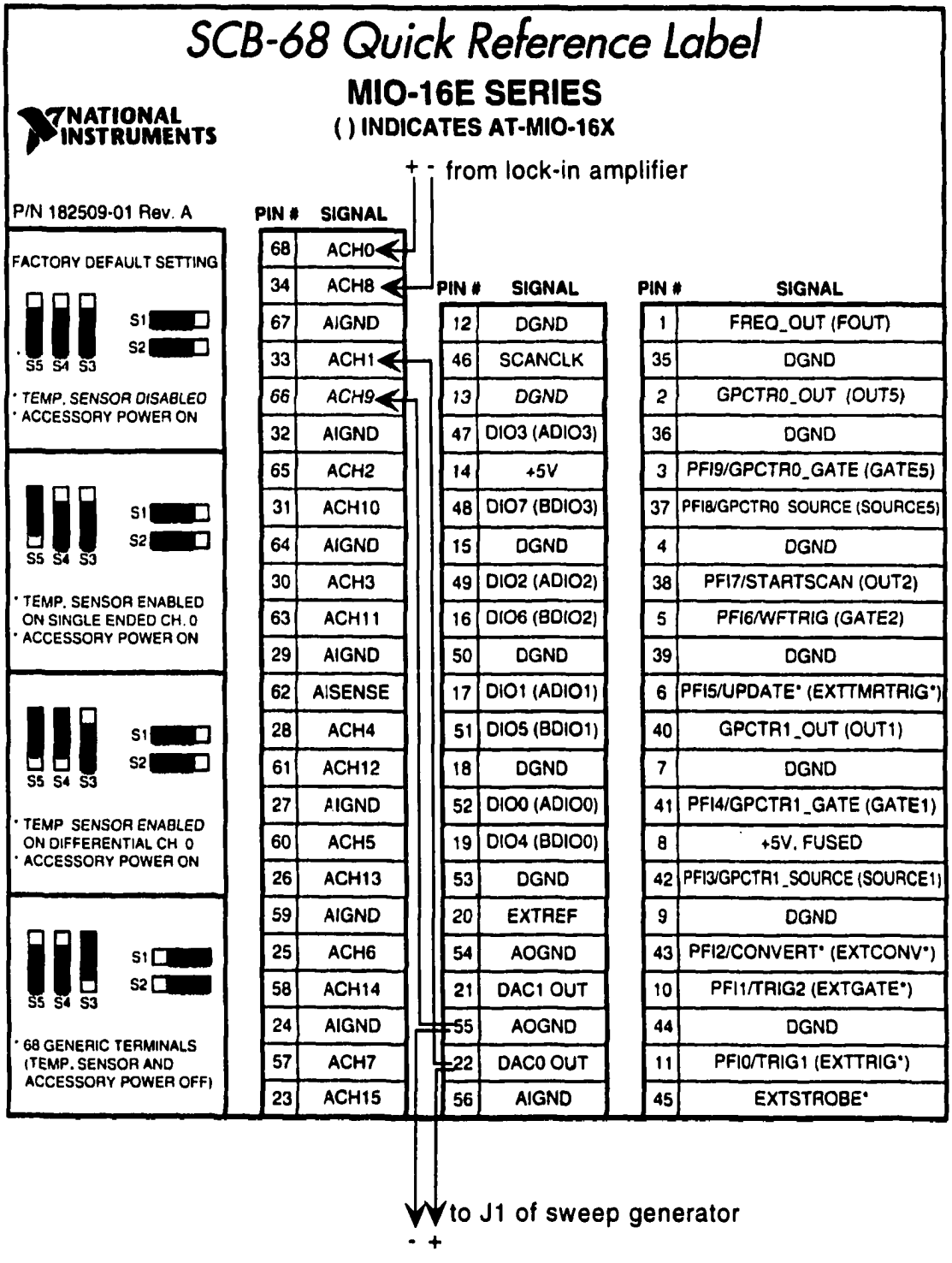

Fig. 3 Diagram of SCB-68 connector block

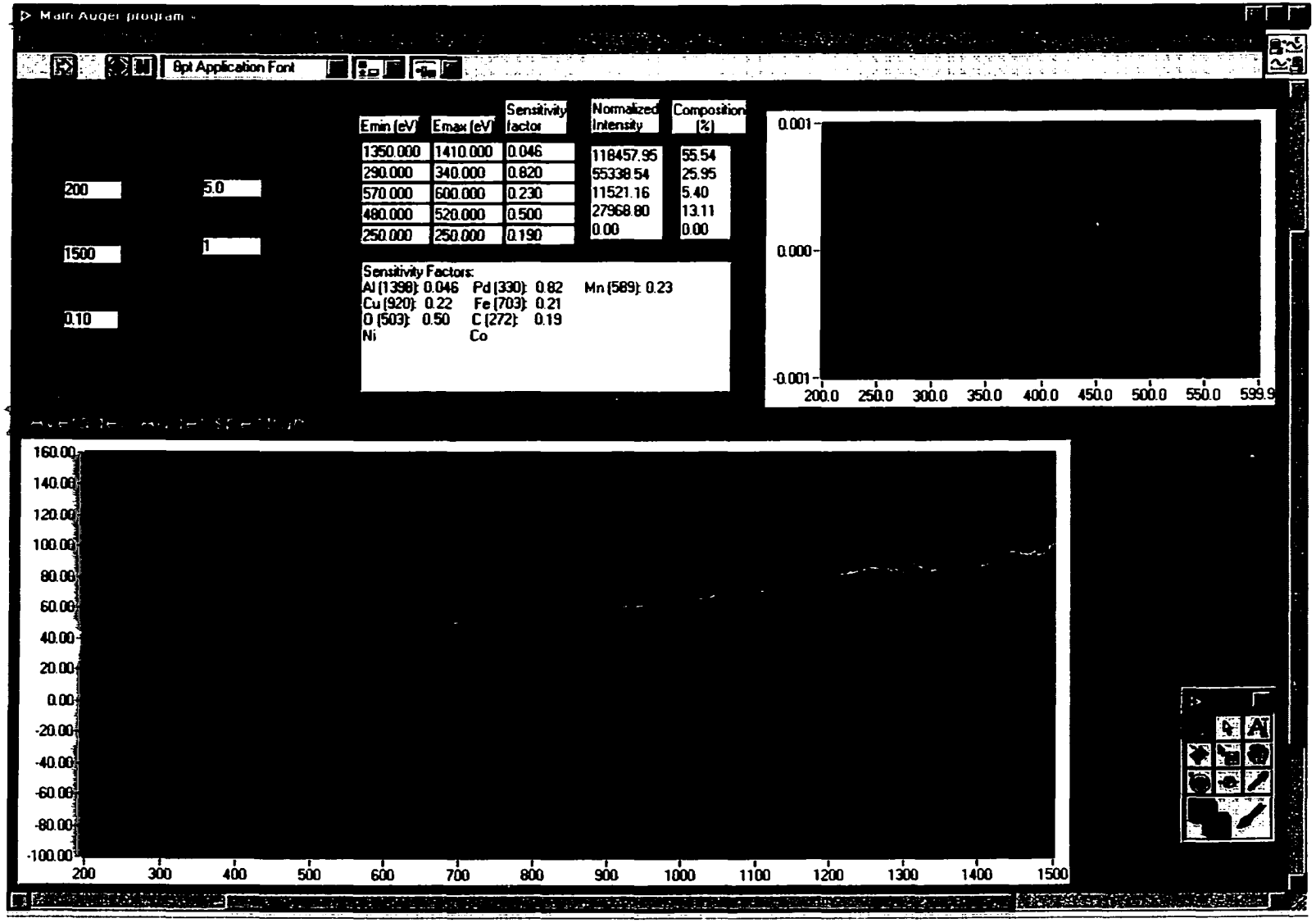

Fig. 4 Front panel of main Auger program

REFERENCES

[1] D. Shechtman, I. Blech, D. Gratias and J.W. Cahn, Phys. Rev. Lett. 53 (1984) 1951.

[2] D. Shechtman and I. Blech, Metall. Trans. A 16 (1985) 1005.

[3] IUCR, Acta Crystallographica A48 (1992) 922-946.

[4] M. Boudard, E. Bourgeat-Lami, M. de Boissieu, C. Janot, M. Durand-Charré, H. Klein, M. Audier and B. Hennion, Phil. Mag. Lett. 71 (1995) 11.

[5] C. Janot and M. dexxBoissieu, Phys. Rev. Lett. 72 (1994) 1674-1677.

[6] J.M. Dubois and P. Weinland "Coating materials for metal alloys and metals and method," CNRS, Nancy, France, 1993.

[7] U. Köster, W. Liu, H. Liebertz and M. Michel, J. Non-Cryst. Solids 153-154 (1993) 446-452.

[8] I.M. Hutchings, Tribology: Friction and Wear of Engineering Materials (CRC Press, Boca Raton, Florida, 1992).

[9] J.M. Dubois, in: Proceedings of the Conference "New Horizons in Quasicrystals: Research and Applications"; A.I. Goldman, D.J. Sordelet, P.A. Thiel and J.M. Dubois, Eds.; (World Scientific, Singapore, 1997), pp. 208-215.

[10] S.S. Kang, J.M. Dubois and J. vonxxStebut, J. Mater. Res. 8 (1993) 2471.

[11] J.-M. Dubois, S.S. Kang and Y. Massiani, J. Non-Crystalline Solids 153-4 (1993) 443-445.

[12] J.M. Dubois, Phys. Scripta T49A (1993) 17.

[13] J.-M. Dubois, S.S. Kang and A. Perrot, Mat. Sci. Eng. A179/A180 (1994) 122-126.

[14] J.M. Dubois, A. Proner, B. Bucaille, P. Cathonnet, C. Dong, V. Richard, A. Pianelli, Y. Massiani, S. Ait-Yaazza and E. Belin-Ferré, Ann. Chim. Materiaux 19 (1994) 3-25.

[15] J.M. Dubois, P. Plaindoux, E. Belin-Ferré, N. Tamura and D.J. Sordelet, in: Proceedings of the 6th International Conference on Quasicrystals (ICQ6); S. Takeuchi and T. Fujiwara, Eds.; (World Scientific, Singapore, 1998), pp. in press.

[16] A.R. Kortan, R.S. Becker, F.A. Thiel and H.S. Chen, Phys. Rev. Letters 64 (1990) 200.

[17] T.M. Schaub, D.E. Bürgler, H.-J. Güntherodt and J.B. Suck, Phys. Rev. Lett. 73 (1994) 1255-1258.

[18] T.M. Schaub, D.E. Bürgler, H.-J. Güntherodt and J.-B. Suck, Z. Phys. B 96 (1994) 93-96.

[19] T.M. Schaub, D.E. Bürgler, H.-J. Güntherodt, J.B. Suck and M. Audier, Appl. Phys. A 61 (1995) 491-501.

[20] P. Ebert, M. Feuerbacher, N. Tamura, M. Wollgarten and K. Urban, Phys. Rev. Lett. 77 (1996) 3827-3830.

[21] T.M. Schaub, D.E. Bürgler, H.-J. Güntherodt, J.B. Suck and M. Audier, in: Proceeding of the 5th International Conference on Quasicrystals, Avignon, France, May 22-26 1995.; C. Janot and R. Mosseri, Eds.; (World Scientific, Singapore, 1995), pp. 132-138.

[22] E.G. McRae, R.A. Malic, T.H. Lalonde, F.A. Thiel, H.S. Chen and A.R. Kortan, Phys. Rev. Letters 65 (1990) 883.

[23] M. Gierer, M.A. VanxxHove, A.I. Goldman, Z. Shen, S.-L. Chang, C.J. Jenks, C.-M. Zhang and P.A. Thiel, Phys. Rev. Lett. 78 (1997) 467-470.

[24] Z. Shen, C.J. Jenks, J. Anderegg, D.W. Delaney, T.A. Lograsso, P.A. Thiel and A.I. Goldman, Phys. Rev. Lett. 78 (1997) 1050-1053.

[25] X. Wu, S.W. Kycia, C.G. Olson, P.J. Benning, A.I. Goldman and D.W. Lynch, Phys. Rev. Lett. 75 (1995) 4540.

[26] C.J. Jenks, S.-L. Chang, J.W. Anderegg, P.A. Thiel and D.W. Lynch, Phys. Rev. B 54 (1996) 6301.

[27] S.-S. Kang and J.-M. Dubois, J. Mater. Res. 10 (1995) 1071-1074.

[28] S.-L. Chang, C.-M. Zhang, C.J. Jenks, J.W. Anderegg and P.A. Thiel, in: Proceedings of the 5th International Conference on Quasicrystals (ICQ5); C. Janot and R. Mosseri, Eds.; (World Scientific, Singapore, 1995), pp. 786-789.

[29] S.-L. Chang, J.W. Anderegg and P.A. Thiel, J. Noncryst. Solids 195 (1996) 95-101.

[30] C. Janot, Phys. Rev. B 53 (1996) 181-191.

[31] C.J. Jenks, D. Delaney, T. Bloomer, S.-L. Chang, T. Lograsso and P.A. Thiel, Appl. Surf. Sci. 103 (1996) 485-493.

ACKNOWLEDGMENTS

I would like to express my sincere appreciation to my advisor, Professor Patricia A. Thiel, for her support, guidance and encouragement throughout my graduate study.

Many former and present members of the Thiel group have made my time in Ames enjoyable. I am indebted to Dr. Sheng-Liang Chang and Dr. Cynthia Jenks for their skill in teaching me the essentials of ultrahigh-vacuum surface science during my first year in the lab. I have enjoyed the friendship of Dr. Patrick Pinhero, Conrad Stoldt and other group members.

I want to thank Professor Alan I. Goldman for leading me into the field of quasicrystal. I thank Professor Thomas A. Lograsso and Drew Delaney for supplying me the best quasicrystal samples in the world. I also want to thank all the people of the "quasicrystal cluster" at Ames.

Finally, I want to give my heartfelt appreciation to my family for their contribution of time, faith, passion, support, encouragement throughout the whole study: my wife Jing Wei, my parents Jichen Shen and Hexian Zhou, and my sister Zhouhu Shen.

This work was supported by the Ames Laboratory, which is operated for the U.S. Department of Energy by Iowa State University under Contract No. W-7405-Eng-82.

IMAGE EVALUATION
TEST TARGET (QA-3)

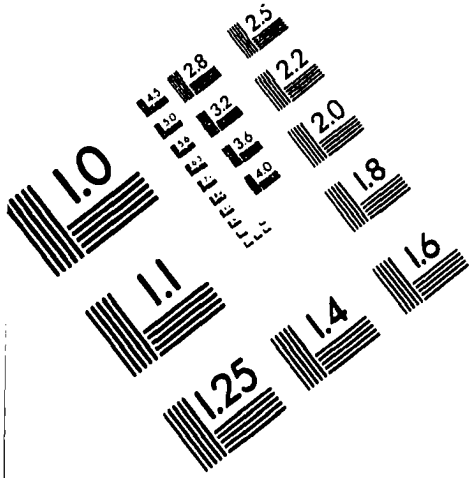

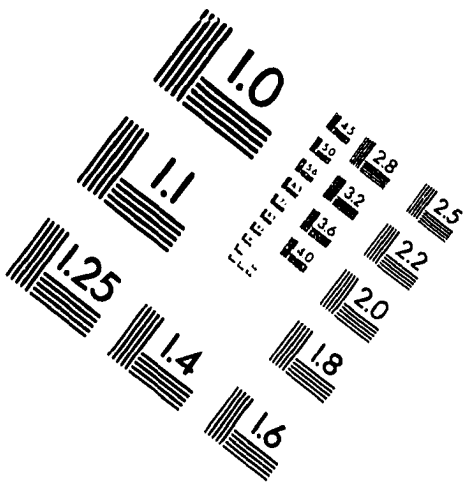

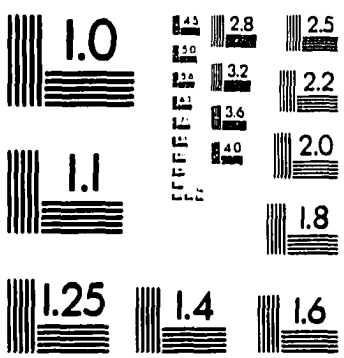

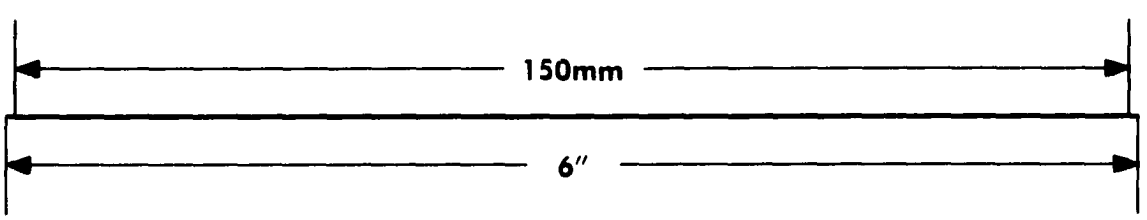

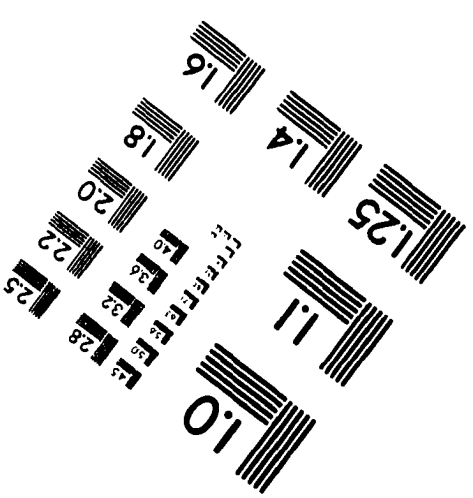

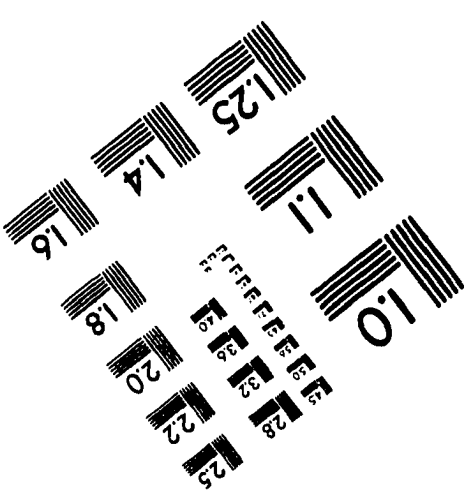

APPLIED IMAGE, Inc
1653 East Main Street
Rochester, NY 14609 USA
Phone: 716/482-0300
Fax: 716/288-5989